Earth-Science Reviews xxx (2014) xxx–xxx

Contents lists available at ScienceDirect

Earth-Science Reviews

journal homepage: www.elsevier.com/locate/earscirev

Environmental controls on marine ecosystem recovery following mass extinctions, with an example from the Early Triassic

Hengye Wei [a,b,*], Jun Shen [a,c], Shane D. Schoepfer [d], Leo Krystyn [e], Sylvain Richoz [f], Thomas J. Algeo [a,c,g,**]

[a] Department of Geology, University of Cincinnati, Cincinnati, OH 45221, USA
[b] College of Earth Science, East China Institute of Technology, Nanchang, Jiangxi 330013, PR China
[c] State Key Laboratory of Geological Processes and Mineral Resources, China University of Geosciences, Wuhan, Hubei 430074, PR China
[d] Department of Earth and Space Sciences, University of Washington, Seattle, WA 98195, USA
[e] Institute for Paleontology, Vienna University, Althanstrasse 14, 1090 Vienna, Austria
[f] Institute of Earth Sciences, Graz University, Heinrichstrasse 26, 8020 Graz, Austria
[g] State Key Laboratory of Biogeology and Environmental Geology, China University of Geosciences, Wuhan, Hubei 430074, PR China

ARTICLE INFO

Article history:
Received 25 April 2014
Accepted 21 October 2014
Available online xxxx

Keywords:
Productivity
Redox
Anoxia
Weathering
South China
India

ABSTRACT

The recovery of marine ecosystems following a mass extinction event involves an extended interval of increasing biotic diversity and ecosystem complexity. The pace of recovery may be controlled by intrinsic ecosystem or extrinsic environmental factors. Here, we present an analysis of changes in marine conditions following the end-Permian mass extinction with the objective of evaluating the role of environmental factors in the protracted (~5-Myr-long) recovery of marine ecosystems during the Early Triassic. Specifically, our study examines changes in weathering, productivity, and redox proxies in three sections in South China (Chaohu, Daxiakou, and Zuodeng) and one in northern India (Mud). Our results reveal: 1) recurrent environmental perturbations during the Early Triassic; 2) a general pattern of high terrestrial weathering rates and more intensely reducing marine redox conditions during the early Griesbachian, late Griesbachian, mid-Smithian, and (more weakly) the mid-Spathian; 3) increases in marine productivity during the aforementioned intervals except for the early Griesbachian; and 4) stronger and more temporally discrete intervals of environmental change in deepwater sections (Chaohu and Daxiakou) relative to shallow and intermediate sections (Zuodeng and Mud). Our analysis reveals a close relationship between episodes of marine environmental deterioration and a slowing or reversal of ecosystem recovery based on metrics of biodiversity, within-community (alpha) diversity, infaunal burrowing, and ecosystem tiering. We infer that the pattern and pace of marine ecosystem recovery was strongly modulated by recurrent environmental perturbations during the Early Triassic. These perturbations were associated with elevated weathering and productivity fluxes, implying that nutrient and energy flows were key influences on recovery. More regular secular variation in deepwater relative to shallow-water environmental conditions implies that perturbations originated at depth (i.e., within the oceanic thermocline) and influenced the ocean-surface layer irregularly. Finally, we compared patterns of environmental disturbance and ecosystem recovery following the other four "Big Five" Phanerozoic mass extinctions to evaluate whether commonalities exist. In general, the pace of ecosystem recovery depends on the degree of stability of the post-crisis marine environment.

Contents

* Correspondence to: H. Wei, College of Earth Science, East China Institute of Technology, Nanchang, Jiangxi 330013, PR China. Tel.: +86 18870073972.
** Correspondence to: T.J. Algeo, State Key Laboratory of Geological Processes and Mineral Resources, China University of Geosciences, Wuhan, Hubei 430074, PR China. Tel.: +86 513 5564195.
E-mail addresses: weihengye@163.com (H. Wei), Thomas.Algeo@uc.edu (T.J. Algeo).

http://dx.doi.org/10.1016/j.earscirev.2014.10.007
0012-8252/

1. Introduction

Each major mass extinction event in the geologic record has been followed by an interval of restructuring of marine ecosystems, reflected in changes in clade dominance, ecological niche partitioning, and community organization (e.g., Erwin, 1998). Increased productivity among primary producers and consumers can generate ecological niches higher in the marine trophic system (Kirchner and Weil, 2000), allowing a progressive rebuilding of a stable, complex ecosystem structure (Chen and Benton, 2012). Although lacking a specific quantitative definition, "ecosystem recovery" is generally regarded as the reappearance of marine communities with a high biotic diversity and an integrated and complex structure that is stable at multimillion-year timescales (Harries and Kauffman, 1990). The progress of post-extinction recovery commonly has been evaluated using metrics related to overall biodiversity and/or species origination rates (e.g., Jacobsen et al., 2011; Payne et al., 2011). However, "ecosystem recovery" is not simply a return to pre-extinction levels of biodiversity but, rather, the expansion and reintegration of entire marine ecosystems or communities (Erwin, 2008; Chen and Benton, 2012) as reflected by metrics such as alpha diversity (i.e., within-community species richness; Bambach, 1977; Clapham et al., 2006) and ecological tiering (Twitchett, 1999; Fraiser, 2011).

In the case of the Permian–Triassic (P–Tr) boundary mass extinction, an initial, aborted recovery occurred soon after the end-Permian crisis, during the Induan stage of the Early Triassic (Baud et al., 2008; Brayard et al., 2009; Stanley, 2009), and a more sustained recovery took place during the late Olenekian stage (Spathian substage) (Chen et al., 2011; Payne et al., 2011; Song et al., 2011), but full ecosystem recovery probably did not occur until the Middle Triassic (Erwin and Pan, 1996; Bottjer et al., 2008; Chen and Benton, 2012). The recovery of marine invertebrate ecosystems following the end-Permian crisis was apparently the most protracted of any major mass extinction (Bottjer et al., 2008), i.e., the "Big Five" Phanerozoic mass extinctions of Sepkoski (1984, 1986). An important unresolved issue is what controlled the long duration of the post-extinction recovery interval during the Early Triassic. At least three hypotheses have been advanced, linking the protracted recovery to: (1) the intensity of the mass extinction (Sepkoski, 1984; Solé et al., 2002), (2) the persistence of harsh environmental conditions (Hallam, 1991; Isozaki, 1997; Payne et al., 2004; Erwin, 2007), and (3) episodic occurrence of strong environmental disturbances during the recovery interval (Algeo et al., 2007, 2008; Orchard, 2007; Retallack et al., 2011) (Fig. 1).

Examination of long-term records of Early Triassic marine environmental conditions has the potential to provide information relevant to these hypotheses. In this study, we (1) review existing literature on the recovery of marine ecosystems following the end-Permian mass extinction, (2) analyze changes in marine productivity and redox conditions at four locales in China and India from the latest Permian through the Spathian substage of the Early Triassic, (3) evaluate the importance

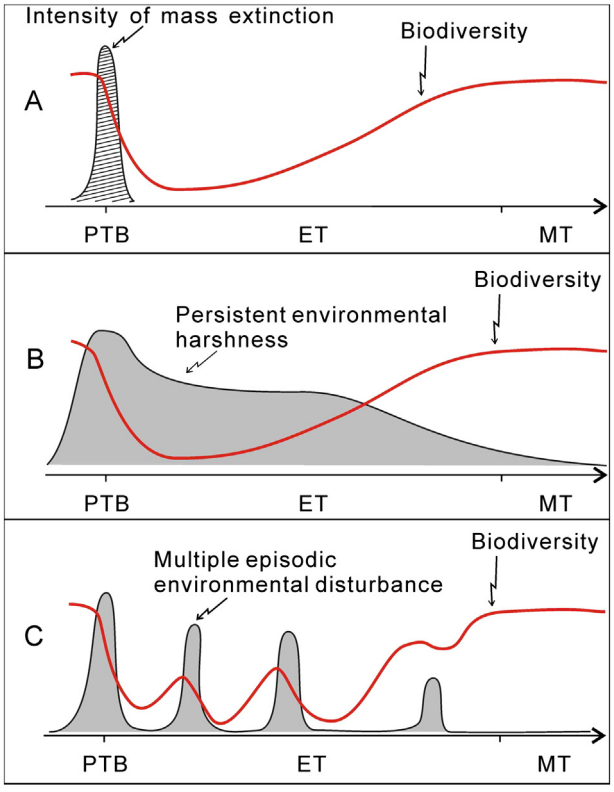

Fig. 1. Three hypotheses to account for the protracted recovery of Early Triassic marine ecosystems, linking it to (A) the intensity of the mass extinction (Solé et al., 2002); (B) the persistence of harsh environmental conditions (Hallam, 1991; Isozaki, 1997; Payne et al., 2004); and (C) the episodic recurrence of major environmental perturbations (Orchard, 2007; Stanley, 2009; Algeo et al., 2011a; Retallack et al., 2011). The heavy solid line represents a general biodiversity trend (cf. Tong et al., 2007b), and the shaded lines represent extinction intensity (A) or environmental stresses (B and C). PTB: Permian–Triassic boundary. ET: Early Triassic. MT: Middle Triassic.

Please cite this article as: Wei, H., et al., Environmental controls on marine ecosystem recovery following mass extinctions, with an example from the Early Triassic, Earth-Sci. Rev. (2014), http://dx.doi.org/10.1016/j.earscirev.2014.10.007

of marine environmental changes during the Early Triassic as controls on the marine ecosystem recovery, and (4) compare the Early Triassic marine ecosystem recovery with those following other Phanerozoic mass extinctions. Our comparative analysis of recoveries following each of the 'Big Five' Phanerozoic mass extinctions is intended to identify general features or patterns of marine ecosystem recovery and their relationships to contemporaneous environmental changes.

2. Background

2.1. The end-Permian biotic crisis

The end-Permian mass extinction was the most severe biocrisis of the Phanerozoic (Fig. 2; Erwin et al., 2002; Irmis and Whiteside, 2011). It killed ~80–96% of marine invertebrate species and ~70% of terrestrial vertebrate species (McKinney, 1995; Benton and Twitchett, 2003). There appear to have been two pulses of marine extinction (Yin et al., 2012; Song-HJ et al., 2013) and environmental disturbance (Xie et al., 2005, 2007), rather than a single event during this biocrisis (Rampino and Adler, 1998; Jin et al., 2000; Shen et al., 2011a). As an example, foram species in South China exhibit a ~57% extinction rate during the latest Permian pulse and a ~31% extinction rate during the earliest Triassic pulse (Song-HJ et al., 2013). According to high-precision U–Pb dating in South China sections, the interval between these extinction pulses was 60 ± 48 kyr (Burgess et al., 2014). The end-Permian mass extinction coincided with eruption of the Siberian Traps Large Igneous Province (Campbell et al., 1992; Renne et al., 1995; Reichow et al., 2009; Sobolev et al., 2011) as well as with major

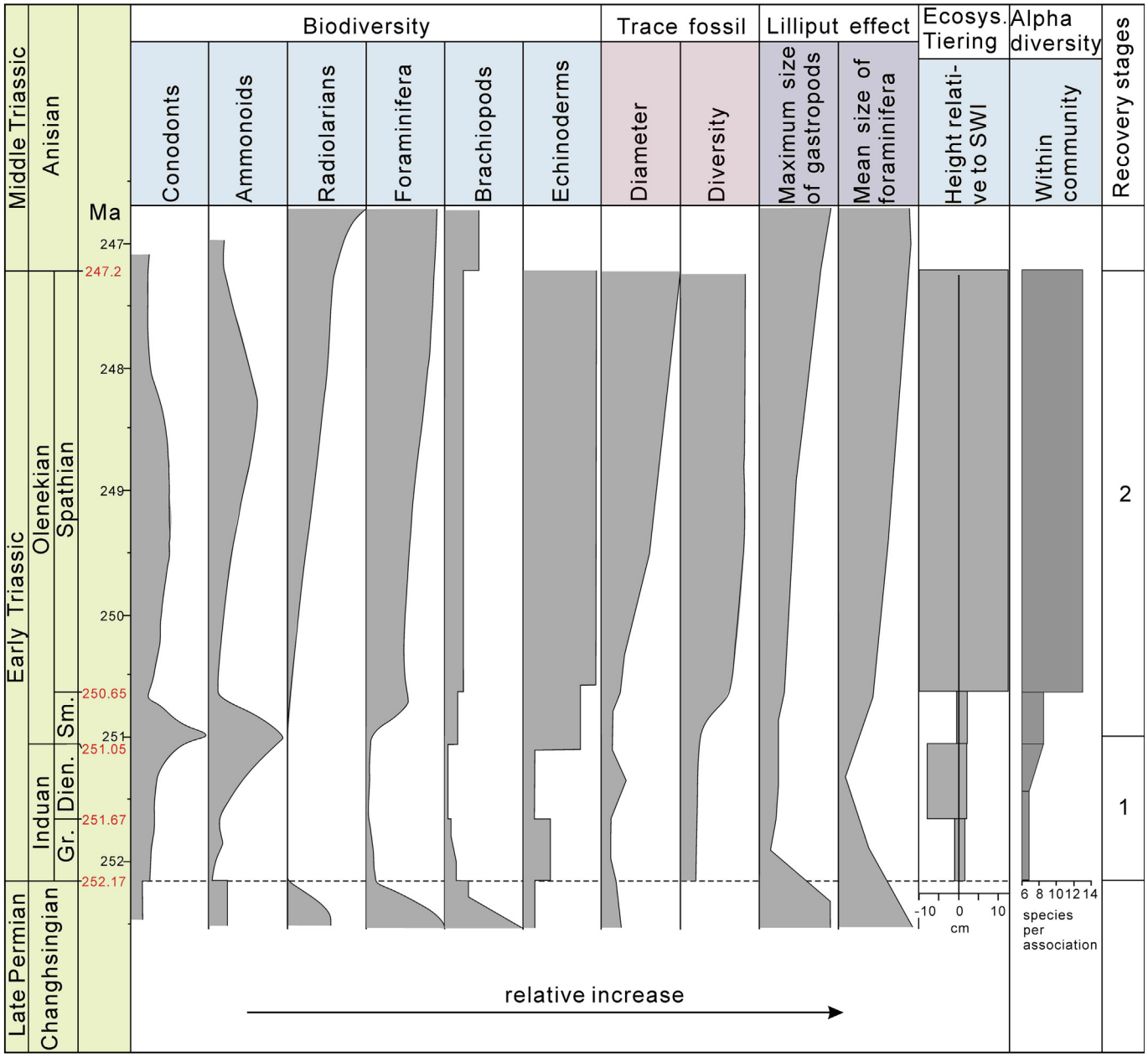

Fig. 2. General patterns of biodiversity and ecological change during the Permian–Triassic transition and Early Triassic. Gr. = Griesbachian; Dien. = Dienerian; Sm. = Smithian; SWI = sediment–water interface. For the tiering column, positive and negative values are elevations in centimeters relative to the sediment–water interface (SWI). Biodiversity data: conodont (Orchard, 2007; Stanley, 2009), ammonoid (Stanley, 2009; Zakharov and Abnavi, 2013), radiolarian (Racki and Cordey, 2000), foraminifera (Payne et al., 2011; Song et al., 2011), brachiopod (Chen et al., 2005a,b; Zakharov and Abnavi, 2013), and echinoderm (Chen and McNamara, 2006). Trace fossils: diameter (Twitchett, 1999; Chen et al., 2011) and ichnodiversity (Chen et al., 2011). Lilliput effect: maximum gastropod size (Payne, 2005) and mean foraminifer size (Payne et al., 2011; Rego et al., 2012). Tiering data (Twitchett, 1999) and alpha diversity data (Hofmann et al., 2013, 2014). Recovery stages 1 and 2 are defined in this study. The timescale is a modified version of that of Algeo et al. (2013) (see Supplementary Table 1).

environmental changes including global sea-level rise (Hallam and Wignall, 1999), ocean anoxia (Wignall and Twitchett, 1996; Isozaki, 1997), global warming (Joachimski et al., 2012; Sun et al., 2012; Romano et al., 2013), and, possibly, marine acidification (Payne et al., 2010; Hinojosa et al., 2012; Kershaw et al., 2012).

2.2. The Early Triassic marine ecosystem recovery

The recovery of marine ecosystems during the Early Triassic was a multi-step process. There were several phases of incomplete or aborted recovery during the Induan, and recovery from the P–Tr boundary mass extinction is generally regarded as not having been completed until the Middle Triassic, ~5 Myr after the end-Permian crisis (Mundil et al., 2004; Lehrmann et al., 2006; Ovtcharova et al., 2006; Shen et al., 2011a). Both benthic and planktonic cyanobacteria bloomed immediately after the end-Permian mass extinction (Fig. 2; Lehrmann, 1999; Wang et al., 2005; Xie et al., 2005; Luo et al., 2011). Cyanobacterial microbialites reappeared episodically in different regions throughout the Early Triassic but they largely disappeared by the early Middle Triassic (Baud et al., 2007; Xie et al., 2010). An Early Triassic "chert gap" (Beauchamp and Baud, 2002) was caused by the loss of biosilica deposits from radiolarians and siliceous sponges, although occurrences of thin chert beds in the late Griesbachian and Dienerian (Kakuwa, 1996; Takemura et al., 2007; Sano et al., 2010) document a temporary local early recovery of siliceous faunas.

Some secondary consumers such as conodonts and ammonoids rebounded rapidly from the end-Permian mass extinction (Orchard, 2007; Brayard et al., 2009; Stanley, 2009). Their rapid recovery may have been assisted by a microphagous habit (Fischer and Bottjer, 1995), allowing them to benefit directly from increased biomass among primary producers. These clades subsequently declined during biocrises at the end of Griesbachian, Smithian, and Spathian substages of the Early Triassic, although they tended to rediversify rapidly during the intervening intervals (Fig. 2; Brayard et al., 2009; Stanley, 2009). However, conodonts display a strong Lilliput effect during the Smithian/Spathian boundary crisis (Chen et al., 2013). Compared to conodonts and ammonoids, recovery rates for benthic primary consumers such as foraminifers, gastropods, bivalves, brachiopods and ostracods were more gradual (Fig. 2; Payne et al., 2011). Among foraminifers, a sustained diversity increase began in the early Smithian (early Olenekian) (Song et al., 2011) and accelerated during the Anisian (early Middle Triassic) (Payne et al., 2011). Similar recovery patterns are observed also among brachiopods (Chen et al., 2005a,b) and ostracods (Crasquin-Soleau et al., 2007). The sizes of gastropod and bivalve shells were reduced across the P–Tr boundary and during the Griesbachian but returned to pre-extinction dimensions by the Anisian (Fig. 2; Fraiser and Bottjer, 2004; Payne, 2005; Twitchett, 2007). However, the high diversity, low dominance, and ecological complexity of mollusc fauna during the late Griesbachian and early Dienerian at Shanggan, South China (Hautmann et al., 2011) and on the Wasit Block in Oman (Krystyn et al., 2003; Twitchett et al., 2004) may represent an early recovery phase of these faunas.

The meso-consumer trace-makers and reef-builders can shed light on the recovery of benthic marine ecosystems. Generally, trace-makers decreased during the end-Permian biocrisis and recovered slowly in the Early Triassic (Fig. 2; Pruss and Bottjer, 2004; Chen et al., 2011). Locally, trace-fossil diversity shows occasional peaks during the Griesbachian to Smithian (Twitchett and Wignall, 1996; Twitchett, 1999; Zonneveld et al., 2010; Chen et al., 2011). However, small trace-fossil burrow size, low tiering levels, and low ichnofabric indices (bioturbation) generally persisted until the end of the Smithian substage, and the early Spathian is marked by a strong increase in trace-fossil diversity and complexity (Pruss and Bottjer, 2004; Chen et al., 2011). Nonetheless, Spathian ichnofaunas are less diverse than those of the Middle Triassic (Knaust, 2007). This pattern may suggest a stepwise recovery of trace-makers during Early to Middle Triassic (Twitchett and Barras, 2004). Furthermore, the recovery of trace-makers may have been diachronous, with a more rapid increase in ichnodiversity at high northern paleolatitudes than in the equatorial region (Pruss and Bottjer, 2004; Twitchett and Barras, 2004). With regard to reef-builders, a new metazoan reef ecosystem formed by various sponges and serpulid worms associated with microbial carbonates and eukaryotic organisms developed in the early Smithian, latest Smithian, and early to middle Spathian on the eastern Panthalassic margin, in Utah and Nevada (Fig. 2; Brayard et al., 2011). These equatorial sponge-microbe reefs are found as early as 1.5 Myr after the P–Tr boundary and represent a temporary recovery at least regionally (Brayard et al., 2011; Chen and Benton, 2012). However, the "reef gap", as represented by the absence of heavily calcified corals, persisted through the Early Triassic (Payne et al., 2006).

As for the top trophic level in the marine ecosystem, predatory fish and reptiles displayed different recovery trajectories. Fishes were rare in the Griesbachian-to-Smithian equatorial ocean (Fig. 2; Fraiser et al., 2005; Tong et al., 2006; Zhao and Lu, 2007; Sun et al., 2012) but more common in the middle to late Spathian (Goto, 1994; Wang et al., 2001; Benton et al., 2013). High-latitude regions had a more abundant and diverse fish fauna in the Early Triassic than the equatorial ocean (Scheaffer et al., 1976; Stemmerik et al., 2001; Mutter and Neuman, 2006; Romano and Brinkmann, 2010; Benton et al., 2013). Globally, fish diversity recovered by the Middle Triassic (Jin, 2006; Zhang et al., 2010; Hu et al., 2011). Marine reptiles first reappeared in the Smithian in high-latitude regions (Cox and Smith, 1973; Callaway and Brinkman, 1989) but later, in the Spathian, in equatorial regions (Li et al., 2002; Zhao et al., 2008). A high level of diversity among marine reptiles was achieved by the Middle to Late Triassic (Zhang et al., 2009).

To summarize, animals that were low in the marine trophic system tended to recover faster than those at higher trophic levels (Fig. 2; cf. Chen and Benton, 2012). Pelagic and nektonic faunas recovered faster than benthos as shown by rapid increases to multiple biodiversity peaks for ammonoids and conodonts during the Early Triassic, versus a slow return to pre-crisis diversity levels by the Middle Triassic for most bottom-dwellers. In Olenekian time, offshore benthos like calcareous algae and *Tubiphytes* recovered faster than those in nearshore environments in South China (Song et al., 2011). High-latitude biotas recovered faster than equatorial marine biota (Pruss and Bottjer, 2004). These differentiated responses may suggest that the pattern and intensity of environmental changes during the Early Triassic had an important influence on the pathways and tempo of marine ecosystem recovery.

2.3. Environmental change during the Early Triassic recovery

During the recovery interval following the end-Permian mass extinction, major changes in the environment related to volcanism, sea level, and paleoceanographic conditions took place. The eruption of the Siberian Traps large igneous province (LIP), which had begun at ~252 Ma close to the P–Tr boundary, continued strongly for ~1.5 Myr and more weakly for several million years longer (Fig. 3). The eruption history of this LIP is delineated by U–Pb ages for gabbroic intrusive rocks of 252 ± 4 Ma (Kuzmichev and Pease, 2007) and silicic tuff ages of 251.7 ± 0.4 (Kamo et al., 2003), an Ar–Ar age of 250.3 ± 1.1 Ma for the final stages of extrusive volcanism (Reichow et al., 2009), and younger Ar–Ar ages of 242.2 ± 0.6 Ma for a basalt (Reichow et al., 2009). This range of dates documents activity of the Siberian Traps LIP from 252 Ma to 242 Ma with a main eruptive phase at ~252 to 250 Ma (Reichow et al., 2009). Altogether, the Siberian Traps degassed ~6300 to 7800 Gt sulfur, ~3400 to 8700 Gt chlorine, and ~7100 to 13,600 Gt fluorine (Black et al., 2012). The high volatile contents increased the likelihood that volatiles reached the stratosphere and, thus, caused a drastic deterioration of global environments through direct toxicity and acid rainfall (Devine et al., 1984), ozone depletion (Johnston, 1980), and rapid climatic changes that may have included both global cooling (Sigurdsson et al.,

Please cite this article as: Wei, H., et al., Environmental controls on marine ecosystem recovery following mass extinctions, with an example from the Early Triassic, Earth-Sci. Rev. (2014), http://dx.doi.org/10.1016/j.earscirev.2014.10.007

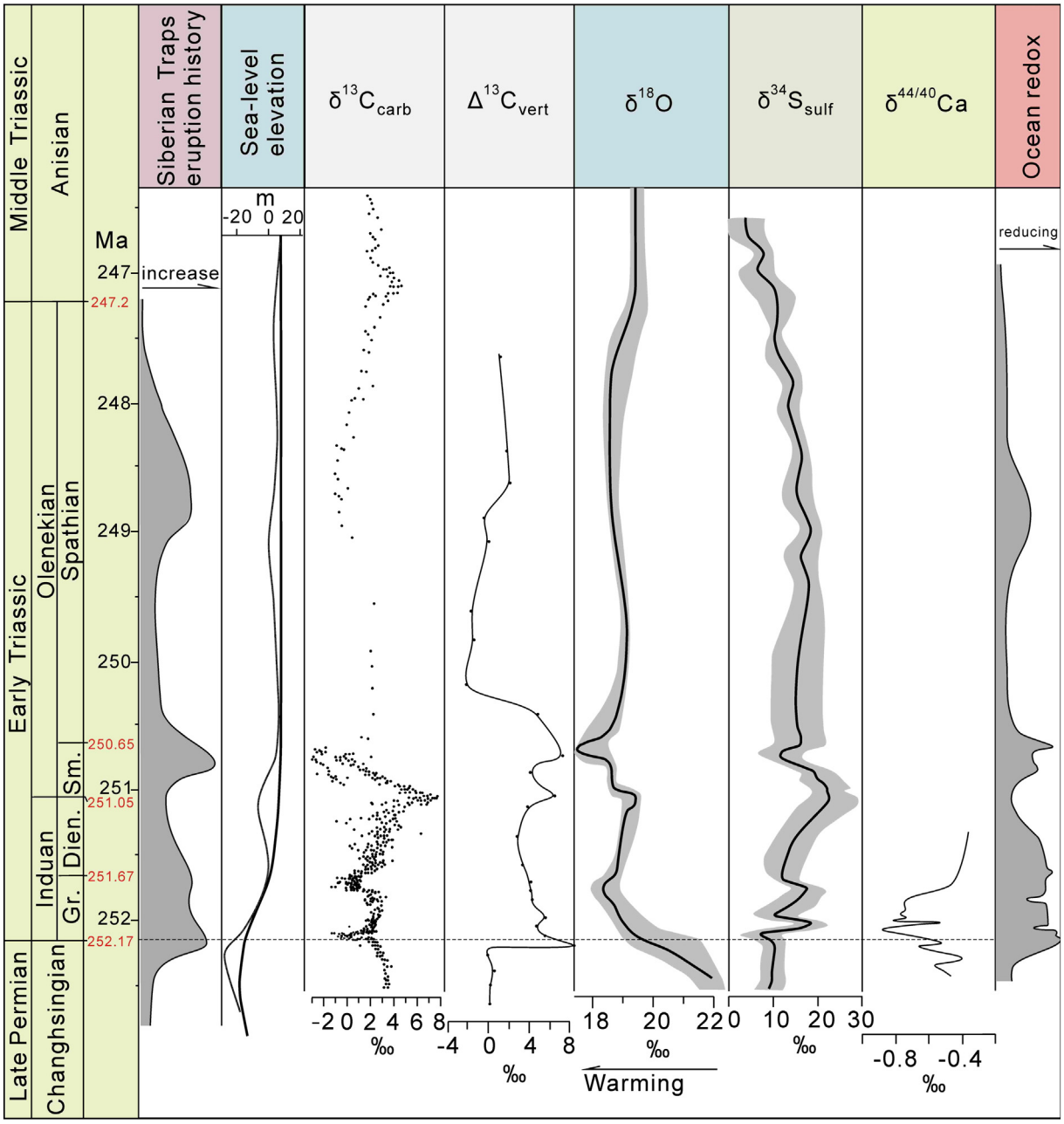

Fig. 3. Volcanic and oceanic environmental changes during the Permian–Triassic transition and Early Triassic. Abbreviations as in Fig. 2. Timing of Siberian Traps eruptions is interpretative. Data sources: $\delta^{13}C_{carb}$ (Payne et al., 2004), sea-level elevations (Haq et al., 1987; Haq and Schutter, 2008), vertical $\Delta^{13}C$ of DIC (Song et al., 2013a,b), bioapatite $\delta^{18}O$ (Sun et al., 2012; Romano et al., 2013), $\delta^{34}S_{sulf}$ (Song et al., 2014), $\delta^{44/40}Ca$ (Payne et al., 2010; Hinojosa et al., 2012), and ocean redox (Kakuwa, 2008; Wignall et al., 2010; Song et al., 2012; Grasby et al., 2013).

1992; Wignall, 2001; Timmreck et al., 2010) and global warming (Ganino and Arndt, 2009). This interval coincided with a long-term eustatic rise from the Late Permian until the middle Late Triassic, with the most rapid rise during the Early Triassic (Fig. 3; Haq et al., 1987; Haq and Schutter, 2008).

Major changes in tropical sea-surface temperatures accompanied the P–Tr boundary crisis. Temperatures increased gradually from ~60 kyr prior to the mass extinction event and then spiked rapidly at the time of this event (Joachimski et al., 2012; Burgess et al., 2014). During the Early Triassic, temperatures reached a maximum in the mid- to late Griesbachian (~36–40 °C), cooled slightly during the latest Griesbachian to the early Smithian, and then reached a second peak of extreme warmth in the late Smithian (Fig. 3; Sun et al., 2012; Romano et al., 2013). A pronounced retreat from peak temperatures occurred in the early Spathian, an event resulting in a major turnover and geographic displacement of marine invertebrate faunas (Galfetti et al., 2007a,b; Stanley, 2009). A weak warming episode in the mid-late Spathian was followed by a second large cooling step around the Early–Middle Triassic boundary, yielding distinctly more moderate temperatures during the Anisian although still warmer than in the pre-extinction Late Permian (Sun et al., 2012; Romano et al., 2013).

Ocean redox conditions exhibit pronounced geographic and secular variation during the latest Permian and Early Triassic. More reducing conditions developed widely at mid-water depths (i.e., with the oceanic thermocline) during the pre-extinction late Changhsingian (Algeo et al., 2012; Shen et al., 2013; Feng and Algeo, 2014). The end-Permian crisis was marked by a transient expansion of anoxia into shallow-marine settings, especially in the Tethyan Ocean (Fig. 3; Horacek et al., 2007; Grice et al., 2005; Algeo et al., 2007, 2008; Bond and Wignall, 2010; Brennecka et al., 2011; Shen et al., 2011b), although some places (e.g., Oman, Iran)

Please cite this article as: Wei, H., et al., Environmental controls on marine ecosystem recovery following mass extinctions, with an example from the Early Triassic, Earth-Sci. Rev. (2014), http://dx.doi.org/10.1016/j.earscirev.2014.10.007

remained oxic (Krystyn et al., 2003; Richoz et al., 2010). Thereafter, the Early Triassic is characterized by a complex pattern of redox variation (Song et al., 2012; Grasby et al., 2013). The intensity of anoxia appears to have declined during the Spathian, and episodes of marine anoxia seem to have terminated around the Early–Middle Triassic boundary (Hermann et al., 2011; Song et al., 2012).

Marine productivity can vary greatly during major biocrises (Kump and Arthur, 1999). Several factors during the P–Tr boundary crisis might have led to higher productivity: 1) phosphate liberated from sediments under anoxic conditions can stimulate productivity (Ingall and van Cappellen, 1990), and 2) intensified subaerial weathering can increase the flux of river-borne P to the oceans (Algeo and Twitchett, 2010; Algeo et al., 2011b). Variations in marine productivity can be reconstructed using carbon isotopes or elemental data (Kump and Arthur, 1999; Algeo et al., 2013; Schoepfer et al., 2014-this volume). The 'biological pump' removes ^{12}C-enriched carbon from the ocean-surface layer and transfers it to the ocean thermocline, producing a vertical gradient in the $\delta^{13}C$ of dissolved inorganic carbon ($\Delta^{13}C_{DIC}$). Changes in $\Delta^{13}C_{DIC}$ can thus provide information about the intensity of the organic carbon sinking flux and, indirectly, primary productivity (Hilting et al., 2008). A large vertical $\delta^{13}C_{DIC}$ gradient in the Nanpanjiang Basin of South China was interpreted as evidence of elevated marine productivity during the Early Triassic (Fig. 3; Meyer et al., 2011), although this gradient has also been attributed to intensified water-column stratification (Song-HY et al., 2013; Luo et al., 2014). However, an analysis of marine productivity changes based on organic carbon burial fluxes suggested a productivity crash in Early Triassic seas of the South China craton (Algeo et al., 2013). The large carbon-isotope excursions of the Early Triassic (Payne et al., 2004; Tong et al., 2007a,b; Clarkson et al., 2013) were hypothesized to have been due to marine productivity fluctuations (Algeo et al., 2011b), an inference supported by patterns of $\delta^{13}C$-$\delta^{34}S$ covariation (Song et al., 2014). The ultimate control on these fluctuations appears to have been temperature, with warm intervals associated with reduced productivity (Song et al., 2014).

Seawater pH values may have fluctuated during the P–Tr boundary crisis, as shown by analysis of calcium isotopes (Payne et al., 2010; Hinojosa et al., 2012). Calcium isotopic fractionation caused by the precipitation of carbonate minerals results in ^{40}Ca-rich marine sediments and ^{44}Ca-rich in seawater (Skulan et al., 1997; De La Rocha and DePaolo, 2000; Fantle and DePaolo, 2005; Tang et al., 2008). Abrupt negative excursions of $\delta^{44/40}Ca$ in both bulk carbonate and conodont apatite, representing a shift in seawater $\delta^{44/40}Ca$, occurred synchronously with the end-Permian biocrisis (Fig. 3; Payne et al., 2010; Hinojosa et al., 2012). The underlying cause of this change may have been eruption of the Siberian Traps, which injected a large amount of CO_2 into the atmosphere–ocean system, causing seawater acidification and increased riverine ^{40}Ca-rich calcium input owing to accelerated terrestrial weathering of carbonates (Payne et al., 2010; Blätter et al., 2011). Ocean acidification during Permian–Triassic transition may lead to the preferential extinction of heavily calcified marine organisms (Knoll et al., 2007; Clapham and Payne, 2011; Kiessling and Simpson, 2011) and could explain the abrupt transition on carbonate platforms from skeletal to microbial and abiotic carbonate factories described by Kershaw et al. (2011).

To summarize, eruption of the Siberian Traps during the Late Permian to Early Triassic resulted in a major perturbation of the atmosphere–ocean system. Environmental changes linked to early phases of the eruption appear began slowly during an interval of at least ~60 kyr preceding the main mass extinction, but accelerated sharply at the end of the Permian. Major environmental effects related to continuing eruption of Siberian Traps flood basalts persisted for ~1.5 to 2.0 million years during the Early Triassic, with some effects continuing until the Early–Middle Triassic boundary, nearly 5 million years after the end of the Permian. The main phase of the eruption, coinciding with the Induan Stage of the Early Triassic, coincided with highly disturbed marine ecosystems, sea-level rise, seawater acidification, and widespread oceanic anoxia. These relationships show that environmental instability coincided with, and probably caused or contributed to, the delayed recovery of marine ecosystems during the Early Triassic.

3. Study sections

Three of the sections chosen for this study are from the South China craton, which was located in the eastern Paleotethys Ocean during the Permian–Triassic transition. The Chaohu section was deposited in a deep ramp setting on the northeastern (paleo-northwestern) margin of this craton, Daxiakou on the mid-ramp of the same margin, and Zuodeng on a shallow carbonate platform within the Nanpanjiang Basin on the southwestern (paleo-southeastern) margin of this craton (Fig. 4A). These sections were widely separated, with a distance of ~650 km between Chaohu and Daxiakou, and a distance of ~950 km between the latter and Zuodeng. The fourth study section is Mud, from the Spiti Valley of northern India, which was located in the south-central Neotethys Ocean during the Permian–Triassic transition (Fig. 4B). We collected a total of 794 samples from 167 m of section at Chaohu, 302 samples from 71 m of section at Daxiakou, 351 samples from 109 m of section at Zuodeng, and 135 samples from 26.5 m of section at Mud. Average sample spacing thus ranges from 20 to 31 cm for the four study sections, which equates to an average temporal interval of ~4 to 10 kyr between samples (see Supplementary Table 1 for the geologic timescale used in this study, and the Supplementary Information for age–depth models of the study sections).

3.1. Chaohu, Anhui Province, China

The Chaohu section is located in proximity to Chaohu city in Anhui Province (Fig. 4A). It is a composite section comprising sections at West Majiashan, West Pingdingshan, and South Majiashan, all of which are located within a ~1-km^2 area (Tong et al., 2003). These sections contain, respectively, the narrow P–Tr boundary interval, the Griesbachian to Smithian, and the Spathian (Fig. 5), according to conodont biostratigraphic data (Zhao et al., 2007). The top of the South Majiashan section coincides approximately with the Spathian–Anisian (Early–Middle Triassic) boundary (Zhao et al., 2007). During the Early Triassic, the Chaohu area was on the deep lower margin of a ramp about 300 km to the north (paleo-west) of the Cathaysia Oldland (Fig. 4A; Tong et al., 2003). Estimated depositional water depths in the Chaohu area were ~300–500 m (Song-HY et al., 2013). However, relative sea-level elevations began to decrease during the Spathian (Tong et al., 2001, 2007b; Chen et al., 2011) as a consequence of a collision between the North China and South China blocks that culminated in the late Middle Triassic (Li, 2001).

This section has been subject to detailed analysis of conodont and ammonoid biostratigraphy (Zhao et al., 2007), sequence stratigraphy (Tong, 1997; Li et al., 2007), carbon isotopes (Tong et al., 2007a), and paleomagnetic polarity (Tong et al., 2003), permitting development of a high-resolution geochronological framework for this study. The West Pingdingshan section is a candidate for the Global Stratotype Section and Point (GSSP) of the Induan–Olenekian boundary (Tong et al., 2003). Conodonts are found in abundance in the upper Griesbachian through Dienerian–Smithian boundary, the middle Smithian, and lower Spathian but are rarer in other stratigraphic intervals (Tong et al., 2003; Zhao et al., 2007). Foraminifers are found in the Induan stage (Song et al., 2011), ammonoids are particularly abundant around the Smithian–Spathian boundary, and some marine vertebrate fossils are found in the Olenekian (Tong et al., 2003).

The carbonate fraction of the sediment shows an increase upsection at Chaohu, from ~30% around the P–Tr boundary to ~40–70% in the Griesbachian and Dienerian, ~75% in the Smithian (except for a local decline to ~20% in the mid-Smithian), and ~87% in the Spathian (Fig. 5, Supplementary Table 2). Chert, which is probably mainly of biogenic origin, decreases upsection, from ~28% around the P–Tr boundary to ~5%

Please cite this article as: Wei, H., et al., Environmental controls on marine ecosystem recovery following mass extinctions, with an example from the Early Triassic, Earth-Sci. Rev. (2014), http://dx.doi.org/10.1016/j.earscirev.2014.10.007

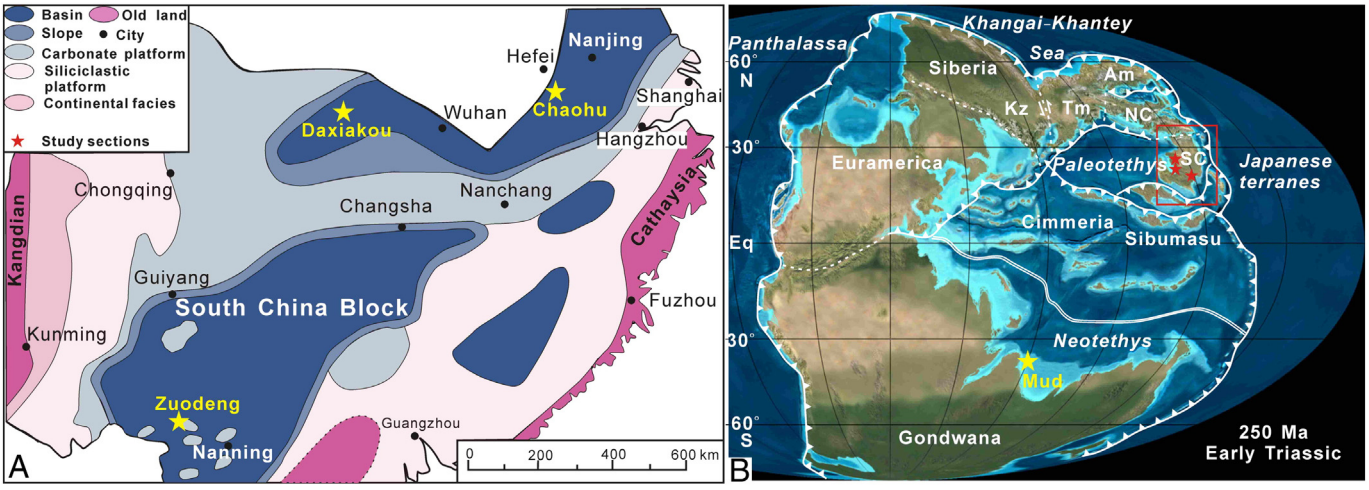

Fig. 4. Permian–Triassic paleogeography of (A) South China (modified from Tong et al., 2007a), and (B) the world (modified from Algeo et al., 2013). Am = Amuria; Kz = Kazakhstan; NC = North China; SC = South China; Tm = Tarim. Present-day east in panel A is approximately the same as paleo-north in panel B owing to a ~90° clockwise rotation of the South China craton after the Early Triassic.

in the Spathian. Clay-mineral content shows a similar upsection decrease, from ~50% around the P–Tr boundary to ~8% in the Spathian. These mineralogic changes are reflected in an upsection shift in lithology from cherty mudrock with minor limestone interbeds around the P–Tr boundary to thin-bedded marls with mudrock interbeds in the Griesbachian and Dienerian, dominant mudrock with marlstone interbeds in the Smithian, and thick-bedded limestone with marlstone interbeds in the Spathian (Fig. 5; Tong et al., 2003, 2007a; Guo et al., 2008).

3.2. Daxiakou, Hubei Province, China

The Daxiakou section is located in Xingshan county, Yichang city, in the Yangtze Gorge area of Hubei Province (Fig. 4A). During the Early Triassic, it was located in a deep-ramp setting on the northern margin of the South China Block (Tong and Yin, 2002; Zhao et al., 2005), ~850 km from the Kangdian Oldland (Fig. 4A). Conodont biostratigraphy shows that the section spans the early Changhsingian through mid-Smithian interval (Zhao et al., 2005). Fossils of ammonoids, conodonts, and bivalves, among others are found in particular abundance in upper Dienerian to lowermost Smithian strata (Li et al., 2009), implying relatively high primary productivity at that time (Tong, 1997). Estimated depositional water depths in the Daxiakou area were ~200–300 m (Song-HY et al., 2013).

The carbonate component is high (>80%) throughout the section except for the P–Tr boundary interval and in Dienerian to lower Smithian strata (Fig. 5, Supplementary Table 3). In the P–Tr transition, average carbonate, chert, and clay-mineral contents are ~30%, ~20%, and 50%, respectively, and strata consist of thin-bedded, dark-gray to black cherty shales (cf. Wu et al., 2012). In the Dienerian to lower Smithian, average carbonate, chert, and clay-mineral contents are ~60%, ~10%, and ~30%, respectively, and strata consist of marlstones with mudrock intercalations.

3.3. Zuodeng, Guangxi Province, China

The Zuodeng section is located in Zuodeng county, Tiandong city, in Guangxi Province. During the Early Triassic, this section was located on a carbonate platform (the Debao Platform) within the Nanpanjiang Basin (Fig. 4A), a deep-marine embayment on the southwestern (paleo-southeastern) margin of the South China Block that existed from the Late Paleozoic to the Late Triassic (Enos et al., 1997). The Debao Platform was one of many isolated, shallow carbonate platforms within this basin, the largest being the Great Bank of Guizhou (Lehrmann et al., 2007). The Nanpanjiang Basin was adjacent to a subduction-zone volcanic arc along the South China–Indochina plate margin (Cai and Zhang, 2009), where volcanism was more intense than on the northern margin of the South China Block (e.g., Xie et al., 2010). This section ranges from the upper Changhsingian through the lower Spathian, as shown by conodont biostratigraphy (Yang et al., 1986; Tong et al., 2007a). Abundant gastropods and ostracods are found in the upper Griesbachian (Wang et al., 2001) and prolific ammonoids, conodonts, and fishes in the lowermost Smithian (Yang et al., 1986). Estimated depositional water depths in the Zuodeng area were ~30–50 m based on the energy subtidal feature of the Lower Triassic limestones for the Debao isolated platform (next to the Pingguo isolated platform, Lehrmann et al., 2007).

Carbonate content at Zuodeng is much higher than for the other study sections, averaging ~95% in upper Changhsingian to Spathian strata with a small decrease to ~80% in the upper Smithian (Fig. 5, Supplementary Table 4). This section consists mainly of thin- to thick-bedded lime mudstone (cf. Wang et al., 2001). The lack of data around the P–Tr boundary is due to this interval being covered at the time of sample collection.

3.4. Mud, Spiti Valley, India

The Mud section is located in the Spiti Valley, which is part of the district of Lahul and Spiti, a central area of the western Himalaya in northern India. Lower Triassic strata are well exposed in this area. During the Early Triassic, the study area was located at mid-southern latitudes (~30–35°S) on the northern Gondwanan margin (Fig. 4B; Krystyn et al., 2007). Middle Permian rifting (Stampfli et al., 1991; Garzanti et al., 1996) resulted in the formation of the Neo-Tethys Ocean (Stampfli et al., 1991; Garzanti et al., 1996), and the surface uplift of the rift shoulders resulted in widespread non-deposition, erosion and the unconformities in the stratigraphic record (Stampfli et al., 1991; Garzanti et al., 1996). The study section was deposited in a mid-shelf setting having a gentle slope, as implied by the modest water depths of deposition (~50–70 m) despite the distal location of the section (Krystyn et al., 2007).

The base of this section consists of Wuchiapingian to lower Changhsingian strata that are overlain by an unconformity (or highly condensed interval) spanning the upper Changhsingian and lower Griesbachian (Bhargava et al., 2004). The main part of the study section consists of a conformable succession of mid-Griesbachian to lowermost Spathian strata. Ammonoids are common in the upper Griesbachian to

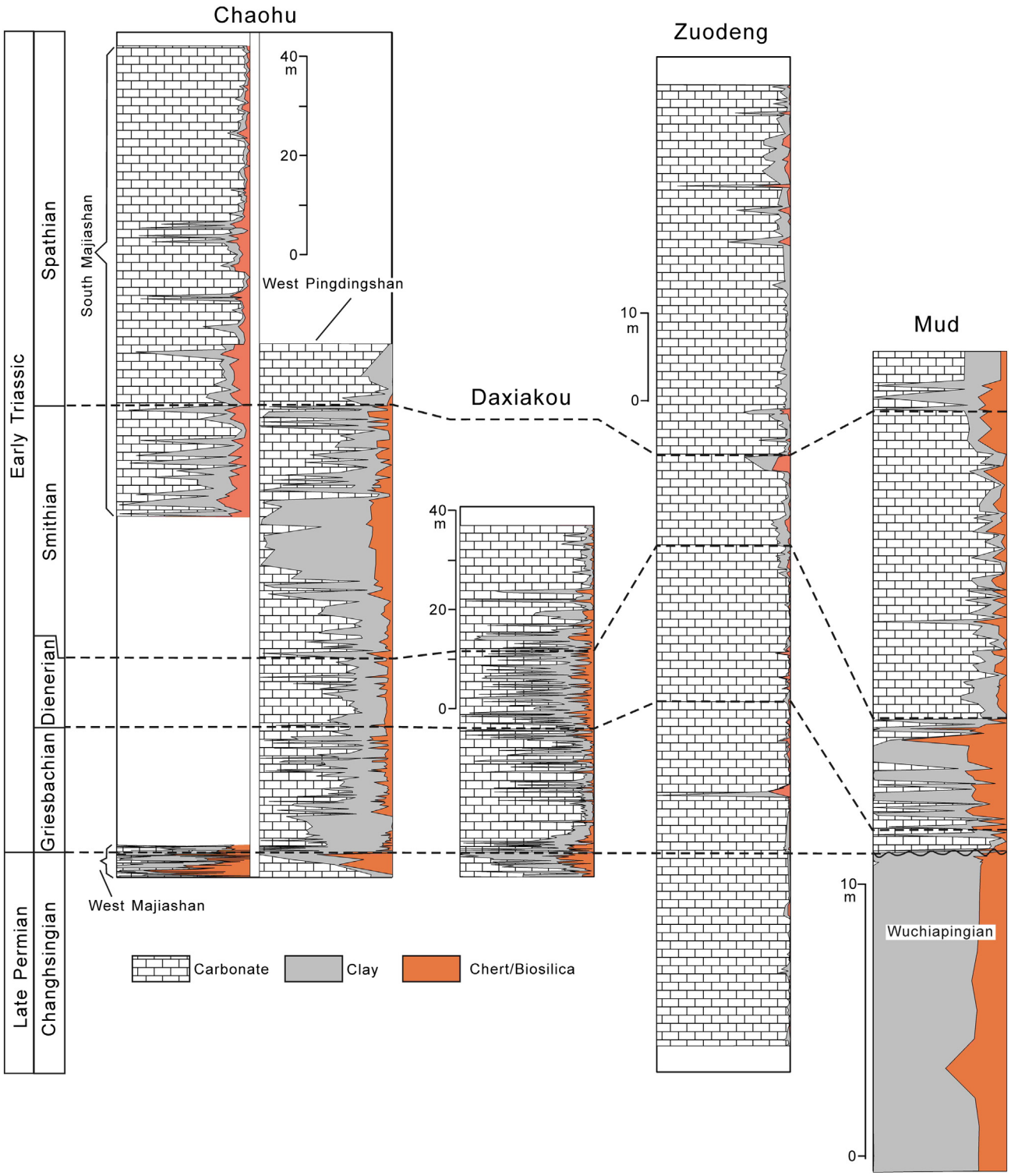

Fig. 5. Stratigraphic variation in lithology of the four study sections. Lithologies calculated per Eqs. (1–3) in Supplementary Information. The timescale at left is plotted relative to thickness in the Chaohu section and is non-linear; note the different thickness scales for the four sections.

lower Smithian interval (Krystyn and Orchard, 1996; Krystyn et al., 2007). Average ammonoid shell size decreases from large in the lower Smithian to small in the middle Smithian (Krystyn et al., 2007), suggesting the development of more hostile environmental conditions at that time. Current bedforms are consistent with a well-oxygenated watermass during the earliest Smithian (Krystyn et al., 2007). The Mud section is a candidate GSSP for the Induan–Olenekian boundary, which was formerly placed at the Bed 12/13 contact (Krystyn et al., 2007) but has been revised downward to approximately the Bed 9/10 contact (Brühwiler et al., 2010).

The Wuchiapingian to lower Changhsingian strata are composed of siliceous shale, with a ~25% chert fraction (Fig. 5, Supplementary Table 5). A sharp change in lithology occurs at the P–Tr unconformity, with Lower Triassic strata consisting dominantly of carbonates. However, low carbonate content is found in limited intervals of the Dienerian and lower Spathian, which consist mainly of marlstones (cf. Krystyn

et al., 2007). For most of Lower Triassic strata, it consists of thin-bedded argillaceous limestone with shale intercalation (e.g., Krystyn et al., 2007) and the average carbonate, shale and chert are ~78%, ~16% and ~6%, respectively (Fig. 5).

4. Results

We report raw values for geochemical proxies for terrestrial chemical weathering, marine productivity, and marine redox conditions in Sections 4.1 to 4.3. We then used an age-thickness model for each study section (see Supplementary Information for details) in order to calculate fluxes for the same proxies (Sections 4.4 to 4.6). All raw chemostratigraphic data and calculated flux values for the four study sections are given in Supplementary Tables 2 to 5.

4.1. Weathering proxies

We used Al and Fe concentrations as well as the chemical index of alteration (CIA) to evaluate terrestrial weathering changes during the Early Triassic. In predominantly carbonate successions such as those of the present study, increases in Al and Fe (which are present mainly in clay minerals) can be due to climatically controlled fluctuations in subaerial weathering rates (cf. Sageman et al., 1997). CIA was calculated as $Al_2O_3 / (Al_2O_3 + K_2O + Na_2O)$ (see Supplementary Information for details). It is a widely used proxy in reconstructing paleoclimate since it is interpreted as a measure of the extent of conversion of feldspars related to the weathering (Young and Nesbitt, 1998; Price and Velbel, 2003). Note that the CIA results for each study section are described in conjunction with weathering fluxes (Section 4.4).

At Chaohu, Al ranges from <0.1 to 15.0%, with an average value of 4.6% (Fig. 6A). It shows generally high values from the P–Tr boundary to the Smithian, followed by generally lower values in the Spathian. Fe ranges from <0.1 to 14.9%, with an average value of 2.7%. Fe shows a similar pattern to Al throughout the study section.

At Daxiakou, Al ranges from <0.1 to 18.1%, with an average value of 2.3% (Fig. 6B). It shows lower values in the early Griesbachian and the early Smithian and higher values from the late Griesbachian through the Dienerian with a short interlude of relatively low values in the early Dienerian. Fe ranges from <0.1 to 9.0%, with an average value of 1.5%. Fe shows a similar pattern to Al within the Induan stage.

At Zuodeng, Al ranges from <0.1% to 14.3%, with an average value of 0.8% (Fig. 6C). It shows relatively higher values from the late Dienerian to the early Smithian, in the late Smithian, and in the middle Spathian but very low values in other intervals. Fe ranges from <0.1 to 5.0%, with an average value of 0.6%. Fe shows a similar pattern to Al throughout the study section except for the late Griesbachian, where the Al profile shows several peaks that the Fe profile does not.

At Mud, Al ranges from <0.1 to 11.4%, with an average value of 3.5% (Fig. 6D). It shows high values from the end of the Griesbachian to earliest Smithian and at the end of the Smithian but low values during most of the Smithian. Fe ranges from 0.4 to 20.7%, with an average value of 2.8%. Fe shows high values from the late Griesbachian to earliest Dienerian and in the early Smithian but low values during most of the Dienerian and Smithian. The Fe and Al profiles show rather different patterns in this section.

4.2. Productivity proxies

We used TOC, phosphorus (P), and excess barium (Ba_{xs}) concentrations to evaluate marine productivity fluxes during the Early Triassic. Ba_{xs} was calculated as the amount of non-detrital barium (see Supplementary Information for details). These are widely used proxies for paleomarine productivity since their accumulation depends on organic matter abundance and preservation (Tribovillard et al., 2006; Calvert and Pedersen, 2007). A method to estimate actual paleomarine productivity values was developed by Schoepfer et al. (2014-this volume), who established regression equations to evaluate primary and export production as a function of TOC and P mass accumulation rates (MARs) using published data from Cenozoic sediment cores.

At Chaohu, TOC ranges from 0.02 to 5.17%, with an average value of 0.28% (Fig. 7A). It shows high values at the P–Tr boundary and in the mid Spathian, and moderately high values from the late Griesbachian to early Dienerian, the late Dienerian to earliest Smithian, and the mid to late Smithian. In contrast, it shows low values in the mid-Griesbachian, early Smithian, and most of the Spathian. P ranges from ~0 to 0.52%, with an average value of 0.03%. Ba_{xs} ranges from 0.29 to 2992 ppm, with an average value of 176 ppm. Both P and Ba_{xs} show patterns of variation that are similar to that of TOC, although Ba_{xs} exhibits relatively higher values in the late Griesbachian and mid to late Smithian.

At Daxiakou, TOC ranges from 0.06 to 4.65%, with an average value of 0.30% (Fig. 7B). It shows high values at the P–Tr boundary but relatively low values from the Griesbachian to early Smithian. P ranges from ~0 to 2.23%, with an average value of 0.03%. It exhibits a different pattern from TOC, showing relatively high values at the P–Tr boundary and in the late Griesbachian to early Smithian and low values in the mid-Griesbachian and early to mid-Smithian. Ba_{xs} ranges from 1.51 to 895 ppm, with an average value of 78 ppm. It shows a slightly different pattern, with high values at the P–Tr boundary and from the end-Griesbachian to the early Smithian and relatively lower values in the mid-Griesbachian and mid-Dienerian.

At Zuodeng, TOC ranges from 0.06 to 1.52%, with an average value of 0.15% (Fig. 7C). It shows generally low values for the entire Early Triassic, although with a small increase during the late Griesbachian–early Dienerian and the early Smithian. P ranges from ~0 to 0.30%, with an average value of 0.01%. It exhibits a different pattern from TOC, with generally high values during the late Smithian and Spathian (punctuated by peaks in the end-Smithian and mid-Spathian) and low values from the Griesbachian to mid-Smithian. Ba_{xs} ranges from 0.39 to 920 ppm, with an average value of 40 ppm. It shows low values (<30 ppm) through most of the Early Triassic but two peaks in the mid-Dienerian and mid-Spathian.

At Mud, TOC ranges from 0.07 to 2.71%, with an average value of 0.49% (Fig. 7D). It shows high values in the Dienerian and low values in the late Griesbachian, Smithian, and early Spathian. P ranges from 0.01 to 0.85%, with an average value of 0.07%. It shows a gradual upsection decrease. Ba_{xs} ranges from 0.1 ppm to 1723 ppm, with an average value of 166 ppm. It shows high values in the Dienerian and late Griesbachian, and low values in the Smithian and early Spathian.

4.3. Redox proxies

We used Mo, U, and V concentrations to evaluate ocean redox changes during the Early Triassic. Redox-sensitive trace elements typically become enriched in marine sediments under reducing conditions (Algeo and Maynard, 2004; Algeo and Lyons, 2006; Tribovillard et al., 2006; Algeo and Tribovillard, 2009). Reducing conditions, characterized by low O_2 and/or high H_2S concentrations in bottomwaters, are produced by some combination of decreased ventilation, commonly due to sluggish watermass circulation, and high respiratory oxygen demand, commonly due to a high sinking flux of organic matter (Pedersen and Calvert, 1990).

At Chaohu, Mo ranges from ~0 to 149 ppm, with an average of 3.4 ppm (Fig. 8A). U ranges from ~0 to 52 ppm, with an average of 3.5 ppm. V ranges from <1 to 2892 ppm, with an average of 110 ppm. For all three proxies, high values are observed at the P–Tr boundary and in the late Griesbachian, Dienerian, and late Smithian. In addition, the V profile exhibits enrichment in the mid-Smithian, and both the Mo and V profiles show a short episode of somewhat higher values in the early Spathian.

At Daxiakou, Mo ranges from ~0 to 604 ppm, with an average of 7.3 ppm (Fig. 8B). U ranges from ~0 to 39 ppm, with an average of

Please cite this article as: Wei, H., et al., Environmental controls on marine ecosystem recovery following mass extinctions, with an example from the Early Triassic, Earth-Sci. Rev. (2014), http://dx.doi.org/10.1016/j.earscirev.2014.10.007

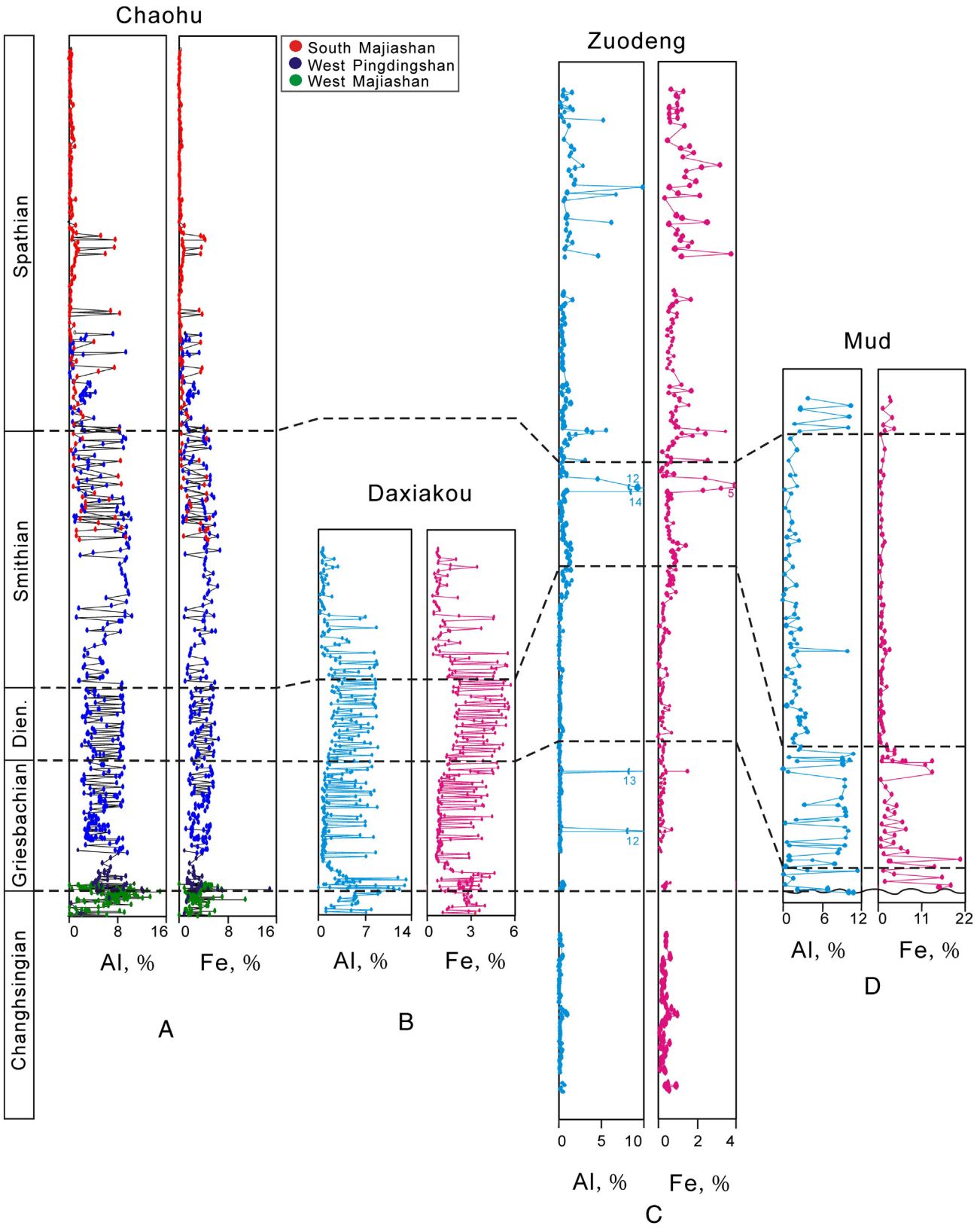

Fig. 6. Chemostratigraphic profiles of weathering proxies (Al and Fe) for the four study sections. Vertical scales are identical to those in Fig. 5.

2.9 ppm. V ranges from <1 to 1326 ppm, with an average of 53 ppm. For all three proxies, high values are observed at the P–Tr boundary and in the Dienerian, and V shows an additional peak in the late Griesbachian that is not seen in the Mo and U profiles.

At Zuodeng, Mo ranges from ~0 to 102 ppm, with an average of 3.8 ppm (Fig. 8C). U ranges from ~0 to 68 ppm, with an average of 6.8 ppm. V ranges from ~0 to 162 ppm, with an average of 14.0 ppm. For all three proxies, high values are observed in the late

Please cite this article as: Wei, H., et al., Environmental controls on marine ecosystem recovery following mass extinctions, with an example from the Early Triassic, Earth-Sci. Rev. (2014), http://dx.doi.org/10.1016/j.earscirev.2014.10.007

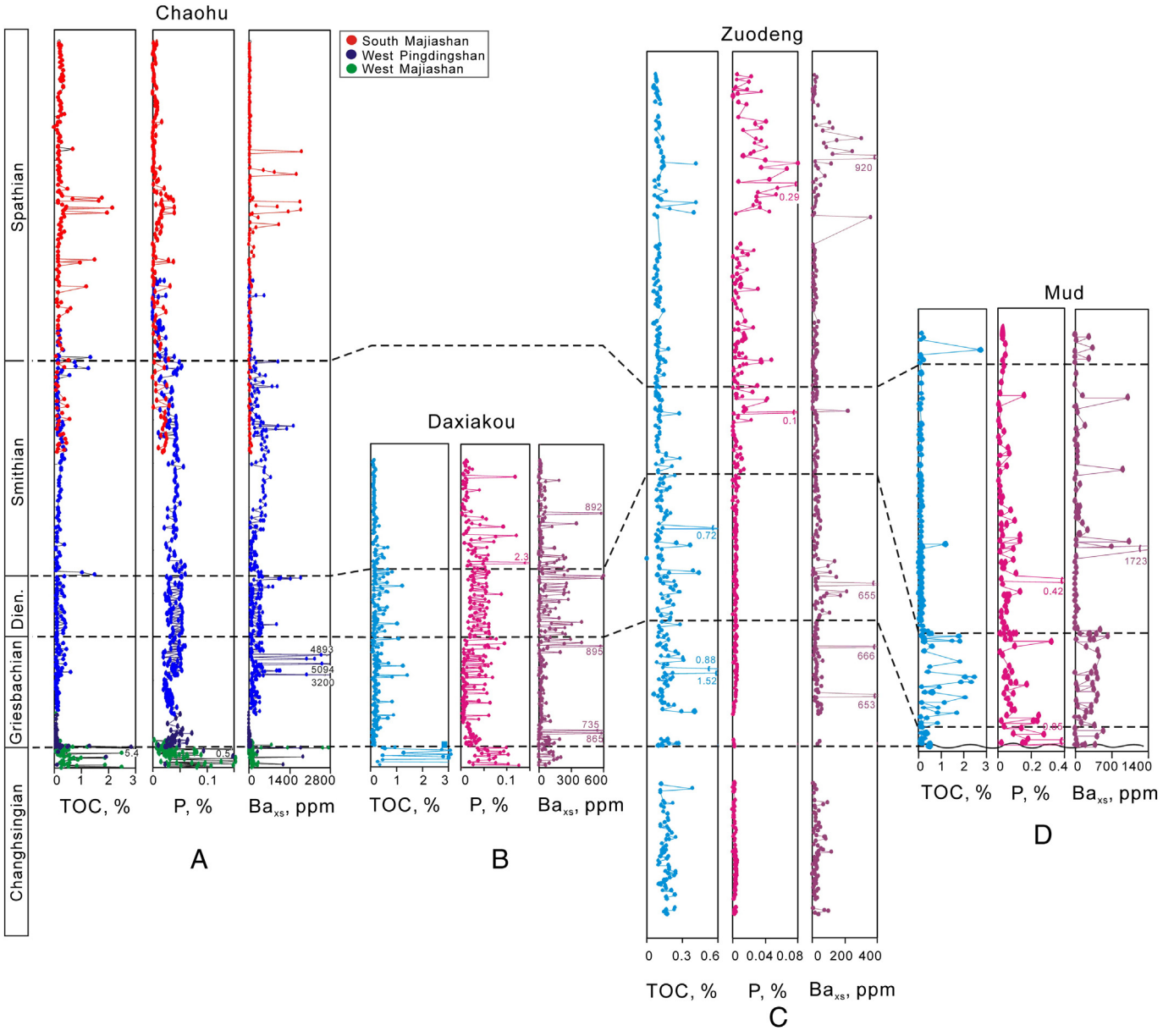

Fig. 7. Chemostratigraphic profiles of productivity proxies (TOC, P, and Ba_{xs}) for the four study sections. Vertical scales are identical to those in Fig. 5.

Dienerian and Smithian, with additional enrichment of V in the early Spathian.

At Mud, Mo ranges from <1 to 24 ppm, with an average of 2.4 ppm (Fig. 8D). U ranges from 0.3 to 7.3 ppm, with an average of 2.0 ppm. V ranges from 10 to 528 ppm, with an average of 132 ppm. For all three proxies, high values are observed in the Dienerian.

4.4. Weathering fluxes

At Chaohu, the Al flux ranges from <0.1 to 36 g m^{-2} y^{-1}, with an average of 6.4 g m^{-2} y^{-1} (Fig. 9A). The Fe flux ranges from <0.1 to 25 g m^{-2} y^{-1}, with an average of 3.9 g m^{-2} y^{-1}. Both fluxes increase sharply at the P–Tr boundary and show peak values during the Griesbachian and Smithian, with a smaller increase in the early Spathian. The CIA ranges from 0.47 to 0.99, with an average of 0.75. High CIA values are found at the P–Tr boundary and in the Griesbachian and Smithian.

At Daxiakou, the Al flux ranges from <0.1 to 33 g m^{-2} y^{-1}, with an average of 3.8 g m^{-2} y^{-1} (Fig. 9B). The Fe flux ranges from <0.1 to 18 g m^{-2} y^{-1}, with an average of 2.7 g m^{-2} y^{-1}. Both fluxes increase sharply at the P–Tr boundary and show peak values during the Griesbachian and Smithian. The CIA ranges from 0.50 to 0.96, with an average of 0.80. High CIA values are found at the P–Tr boundary and in the late Griesbachian and Smithian, with significantly lower values in the mid-Griesbachian and Dienerian.

At Zuodeng, the Al flux ranges from <0.1 to 11.7 g m^{-2} y^{-1}, with an average of 0.46 g m^{-2} y^{-1} (Fig. 9C). The Fe flux ranges from <0.1 to 3.7 g m^{-2} y^{-1}, with an average of 0.37 g m^{-2} y^{-1}. The Fe flux is relatively larger during the late Griesbachian, whereas the Al flux is greater during the late Dienerian; both fluxes exhibit higher values during the Smithian and early Spathian. The CIA ranges from 0.39 to 0.99, with an average of 0.81. Relatively higher CIA values are observed in the Griesbachian and Smithian.

At Mud, the Al flux ranges from <0.1 to 6.2 g m^{-2} y^{-1}, with an average of 1.1 g m^{-2} y^{-1} (Fig. 9D). The Fe flux ranges from <0.1 to

Please cite this article as: Wei, H., et al., Environmental controls on marine ecosystem recovery following mass extinctions, with an example from the Early Triassic, Earth-Sci. Rev. (2014), http://dx.doi.org/10.1016/j.earscirev.2014.10.007

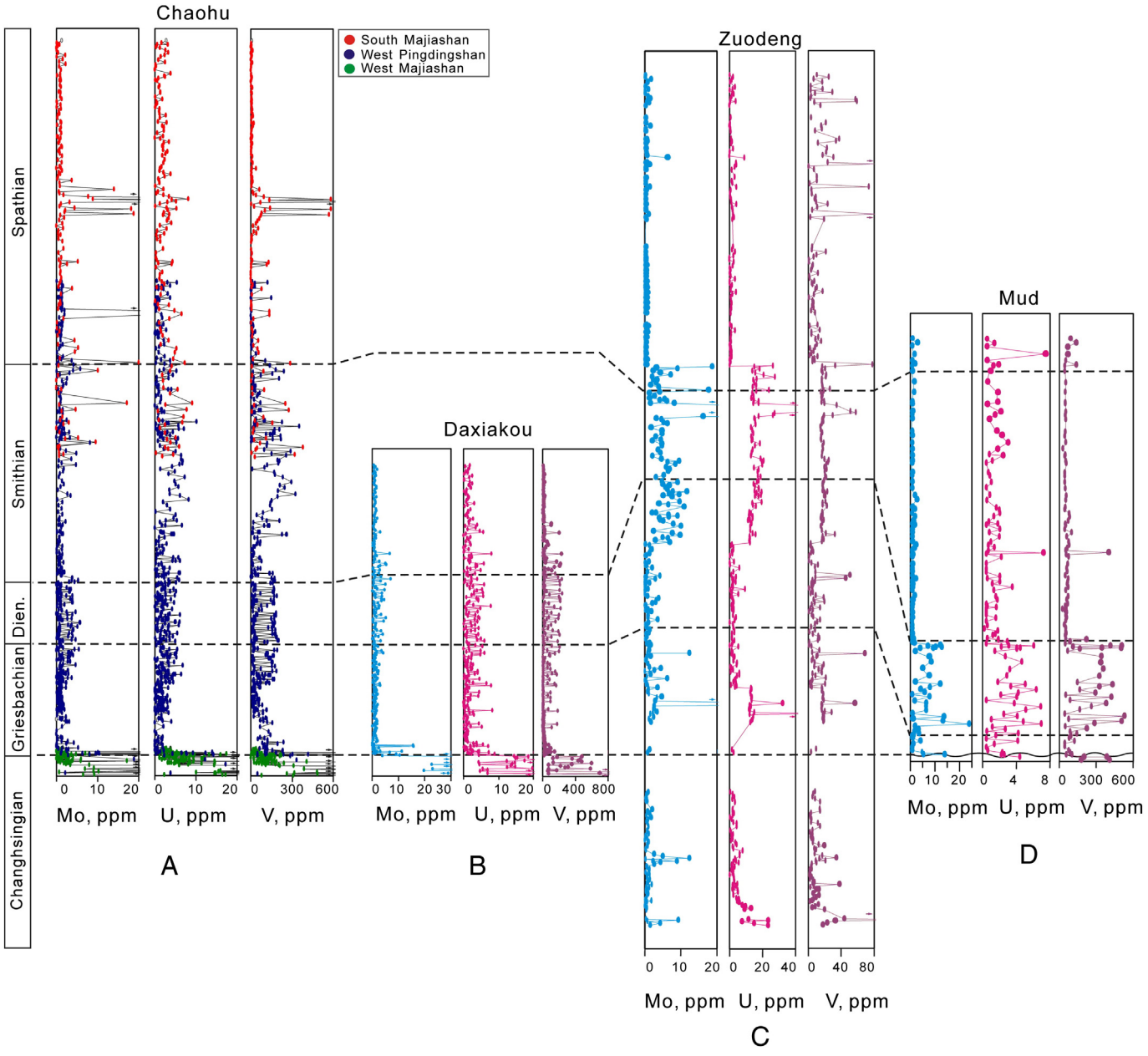

Fig. 8. Chemostratigraphic profiles of redox proxies (Mo, U, and V) for the four study sections. Vertical scales are identical to those in Fig. 5.

3.7 g m^{-2} y^{-1}, with an average of 0.8 g m^{-2} y^{-1}. Both fluxes are large during the late Griesbachian and late Smithian, and Fe additionally shows a peak around the Dienerian–Smithian boundary. The CIA ranges from 0.40 to 0.98, with an average of 0.72. High CIA values are observed in the late Griesbachian and Smithian.

Summarizing patterns of variation in the weathering proxies, high Al and Fe concentrations are observed mainly at the P–Tr boundary and in the late Griesbachian, Dienerian, and mid to late Smithian (Fig. 6). With regard to fluxes, the main peaks in the Al and Fe profiles are at the P–Tr boundary and in the late Griesbachian and mid to late Smithian (Fig. 9). Thus, these intervals were probably associated with enhanced inputs of terrestrial detrital material to the marine study areas. The similar trends of these geochemical proxies despite differences in lithology among the four study sections suggest that lithologic variation did not exert a strong influence on these proxies. CIA values show essentially the same patterns of secular variation as the Al and Fe fluxes. This is a significant observation because CIA is independent of secular variation in bulk–sediment fluxes and, thus, serves to confirm patterns of secular variation in the other weathering proxies.

4.5. Productivity fluxes

At Chaohu, the TOC flux ranges from 0.01 to 3.9 g m^{-2} y^{-1}, with an average of 0.36 g m^{-2} y^{-1} (Fig. 10A). The P flux ranges from 0.1 to 658 mg m^{-2} y^{-1}, with an average of 48.5 mg m^{-2} y^{-1}. The Ba_{xs} flux ranges from ~0 to 451 mg m^{-2} y^{-1}, with an average of 27 mg m^{-2} y^{-1}. All three proxies show a similar pattern of secular variation, with peak fluxes in the mid to late Griesbachian and the Smithian, and smaller increases around the P–Tr boundary and in the early Spathian.

At Daxiakou, the TOC flux ranges from <0.01 to 2.1 g m^{-2} y^{-1}, with an average of 0.32 g m^{-2} y^{-1} (Fig. 10B). The P flux ranges from 0.5 to 6395 mg m^{-2} y^{-1}, with an average of 64.6 mg m^{-2} y^{-1}. The Ba_{xs} flux

Please cite this article as: Wei, H., et al., Environmental controls on marine ecosystem recovery following mass extinctions, with an example from the Early Triassic, Earth-Sci. Rev. (2014), http://dx.doi.org/10.1016/j.earscirev.2014.10.007

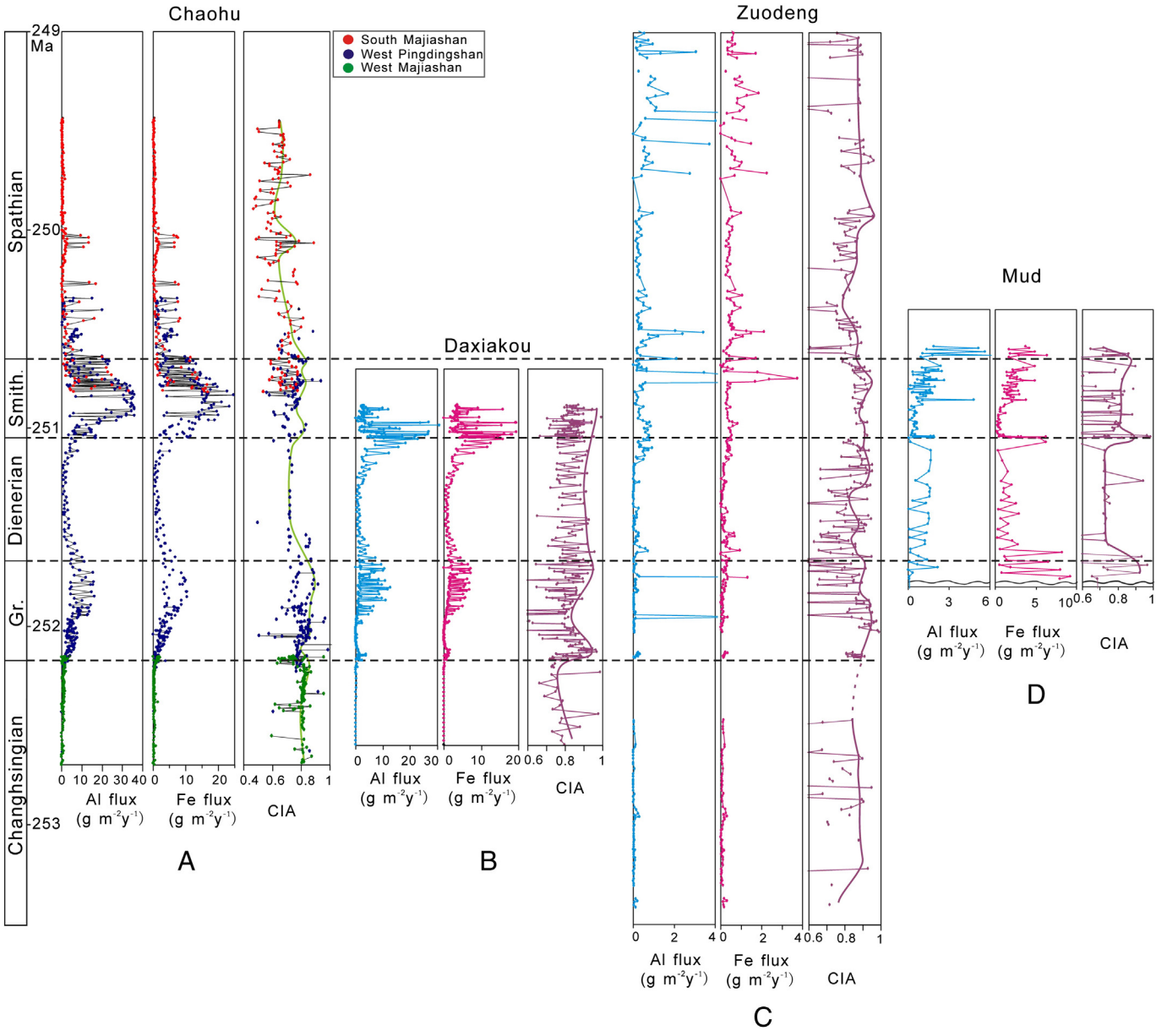

Fig. 9. Profiles of weathering fluxes and CIA (chemical index of alteration) for the four study sections.

ranges from 0 to 350 mg m^{-2} y^{-1}, with an average of 10 mg m^{-2} y^{-1}. All three proxies show a similar pattern of secular variation, with peak fluxes in the Griesbachian and Smithian.

At Zuodeng, the TOC flux ranges from 0.03 to 0.93 g m^{-2} y^{-1}, with an average of 0.09 g m^{-2} y^{-1} (Fig. 10C). The P flux ranges from 0.1 to 169.5 mg m^{-2} y^{-1}, with an average of 5.7 mg m^{-2} y^{-1}. The Ba_{xs} flux ranges from ~0 to 61 mg m^{-2} y^{-1}, with an average of 2 mg m^{-2} y^{-1}. The TOC and Ba_{xs} profiles show similar patterns of secular variation characterized by peak values in the late Griesbachian to early Dienerian, with low values through the remainder of the section. In contrast, the P profile shows peak values in the late Smithian to early Spathian, with low values through the remainder of the section.

At Mud, the TOC flux ranges from 0.01 to 1.5 g m^{-2} y^{-1}, with an average of 1.1 g m^{-2} y^{-1} (Fig. 10D). The P flux ranges from 1.9 to 183 mg m^{-2} y^{-1}, with an average of 20.3 mg m^{-2} y^{-1}. The Ba_{xs} flux ranges from ~0 to 115 mg m^{-2} y^{-1}, with an average of 6 mg m^{-2} y^{-1}. Patterns of secular variation differ among the three productivity-proxy fluxes. The P flux profile most closely matches secular variation in the South China sections, with high values in the late Griesbachian and Smithian, and low values in the Dienerian. In contrast, the TOC flux profile for Mud peaks in the Dienerian and shows low values in the Griesbachian and Smithian, and the Ba_{xs} flux profile peaks in the mid to late Smithian and shows low values through the remainder of the section.

Summarizing patterns of variation in the productivity proxies, high TOC, P and Ba_{xs} concentrations are found mainly at the P–Tr boundary and in the late Griesbachian, Dienerian, and mid to late Smithian, with a smaller peak in the early Spathian (Fig. 7). With regard to fluxes, the main peaks in the TOC, P and Ba_{xs} profiles are in the late Griesbachian and mid to late Smithian (Fig. 10). Thus, these intervals were probably associated with elevated rates of marine productivity relative to the remainder of the Early Triassic. In contrast to the weathering proxies, the productivity proxies exhibit low values around the P–Tr boundary, suggesting a decline in marine productivity during the end-Permian crisis interval.

4.6. Redox fluxes

At Chaohu, the Mo flux ranges from 0.01 to 11 mg m^{-2} y^{-1}, with an average of 0.29 mg m^{-2} y^{-1} (Fig. 11A). The U flux ranges from 0.01 to

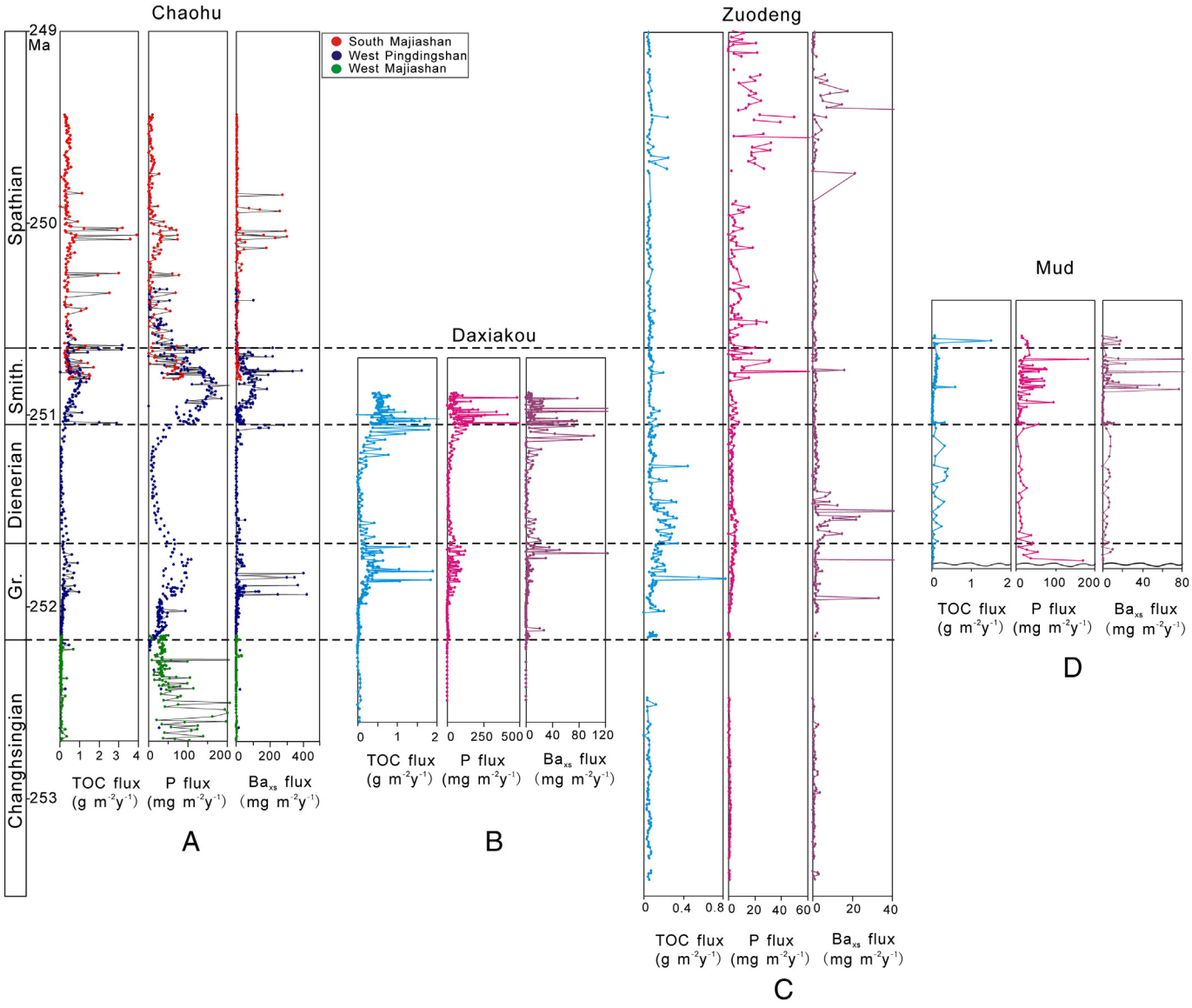

Fig. 10. Profiles of productivity proxy fluxes for the four study sections.

3.0 mg m^{-2} y^{-1}, with an average of 0.38 mg m^{-2} y^{-1}. The V flux ranges from the 0.1 to 174 mg m^{-2} y^{-1}, with an average of 11 mg m^{-2} y^{-1}. All three proxies show similar patterns of secular variation, with peak fluxes in the Griesbachian and Smithian. The Mo and U profiles also show a peak around the P–Tr boundary, and the Mo and V profiles show another peak in the early Spathian.

At Daxiakou, the Mo flux ranges from 0.01 to 2.1 mg m^{-2} y^{-1}, with an average of 0.19 mg m^{-2} y^{-1} (Fig. 11B). The U flux ranges from 0.01 to 2.6 mg m^{-2} y^{-1}, with an average of 0.27 mg m^{-2} y^{-1}. The V flux ranges from 0.01 to 73 mg m^{-2} y^{-1}, with an average of 5.9 mg m^{-2} y^{-1}. All three proxies show similar patterns of secular variation, with peak fluxes in the Griesbachian and Smithian. The Mo and U profiles also show a peak around the P–Tr boundary.

At Zuodeng, the Mo flux ranges from 0.01 to 7.4 mg m^{-2} y^{-1}, with an average of 0.24 mg m^{-2} y^{-1} (Fig. 11C). The U flux ranges from 0.01 to 3.7 mg m^{-2} y^{-1}, with an average of 0.41 mg m^{-2} y^{-1}. The V flux ranges from 0.01 to 6.4 mg m^{-2} y^{-1}, with an average of 0.83 mg m^{-2} y^{-1}. The three proxies show similar patterns of secular variation, although with minor differences. Peak values are in the late Dienerian and Smithian for the Mo flux profile, in the mid-Griesbachian, late Dienerian, and Smithian for the U flux profile, and in the Griesbachian, early Dienerian, late Dienerian, and Smithian for the V flux profile.

At Mud, the Mo flux ranges from 0.01 to 0.35 mg m^{-2} y^{-1}, with an average of 0.06 mg m^{-2} y^{-1} (Fig. 11D). The U flux ranges from 0.01 to 0.41 mg m^{-2} y^{-1}, with an average of 0.07 mg m^{-2} y^{-1}. The V flux ranges from 0.49 to 20 mg m^{-2} y^{-1}, with an average of 3.5 mg m^{-2} y^{-1}. The three proxies show similar patterns of secular variation, with peak values in the late Smithian. The Mo and V profiles exhibit a second, but somewhat smaller, peak in the Dienerian.

Summarizing patterns of variation in the redox proxies, high Mo, U and V concentrations are found mainly at the P–Tr boundary and in the late Griesbachian, Dienerian, and mid to late Smithian (Fig. 8). With regard to fluxes, the main peaks are in the Griesbachian and Smithian, although modest increases are found also at the P–Tr boundary and in the early Spathian (Fig. 11) and at Mud during the Dienerian. Thus, these intervals were probably associated with more reducing conditions in marine environments than the remainder of the Early Triassic.

Please cite this article as: Wei, H., et al., Environmental controls on marine ecosystem recovery following mass extinctions, with an example from the Early Triassic, Earth-Sci. Rev. (2014), http://dx.doi.org/10.1016/j.earscirev.2014.10.007

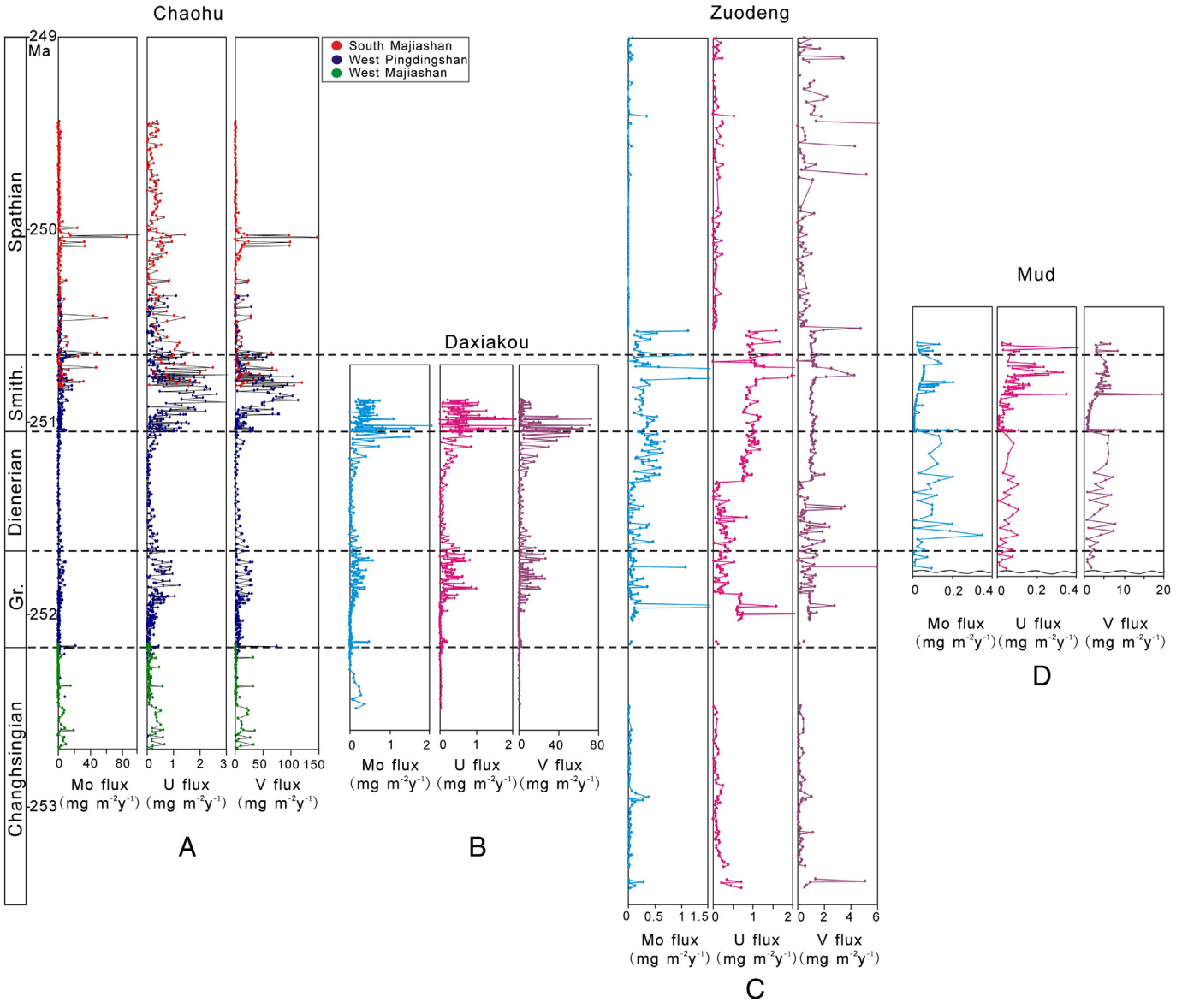

Fig. 11. Profiles of redox proxy fluxes for the four study sections.

Secular variation in the redox proxies broadly mirrors that seen for the weathering and productivity proxies, suggesting close connections between all three environmental parameters.

5. Discussion

5.1. Relationship of weathering, productivity, and redox variation to Early Triassic global events

The results above document major secular changes in weathering, productivity, and redox fluxes during the Early Triassic. In the following discussion, we consider relationships of these environmental proxies to coeval global events, in order to explore potential controls on the protracted recovery of Early Triassic marine ecosystems. Our analysis begins with the end-Permian mass extinction and proceeds through the Spathian, thus covering the full Early Triassic recovery interval.

The end-Permian crisis is generally regarded as having been triggered by the onset of massive eruptions of the Siberian Traps Large Igneous Province (Renne et al., 1995; Korte et al., 2010). It was marked by a general collapse of marine ecosystems, as reflected in biodiversity, trace fossil, and ecological tiering data (Erwin et al., 2002; Erwin, 2005; Fig. 12). This event was accompanied by an extreme climatic warming of >10 °C (Joachimski et al., 2012; Sun et al., 2012), a major expansion of oceanic anoxia globally (Brennecka et al., 2011), an abrupt incursion of sulfidic waters into the ocean-surface layer (Grice et al., 2005; Algeo et al., 2007, 2008), and large inputs of terrestrial material to shallow-marine areas (Ward et al., 2000; Sephton et al., 2005; Xie et al., 2007; Algeo and Twitchett, 2010), all of which are likely to have contributed to the biocrisis. Strong warming led to intensified stratification of the oceanic water-column, as reflected in a large vertical gradient of $\delta^{13}C_{DIC}$ (Song-HY et al., 2013), and thus to a strongly reduced nutrient supply via upwelling, contributing to a sharp decline in marine productivity. The study sections exhibit only limited evidence for these major environmental changes, however, as the end-Permian and P–Tr boundary are characterized by, at most, a small increase in terrestrial weathering fluxes (Fig. 9) and a transient shift toward more reducing conditions (Fig. 11; cf. Grice et al., 2005; Cao et al., 2009). The muted response of the terrestrial weathering and marine redox proxies in the study sections may be due to their distance from continental sources of siliciclastics and locations in areas with only limited local redox changes. Marine productivity exhibits a more visible change, declining sharply particularly across the South China craton (Fig. 10), a pattern

Please cite this article as: Wei, H., et al., Environmental controls on marine ecosystem recovery following mass extinctions, with an example from the Early Triassic, Earth-Sci. Rev. (2014), http://dx.doi.org/10.1016/j.earscirev.2014.10.007

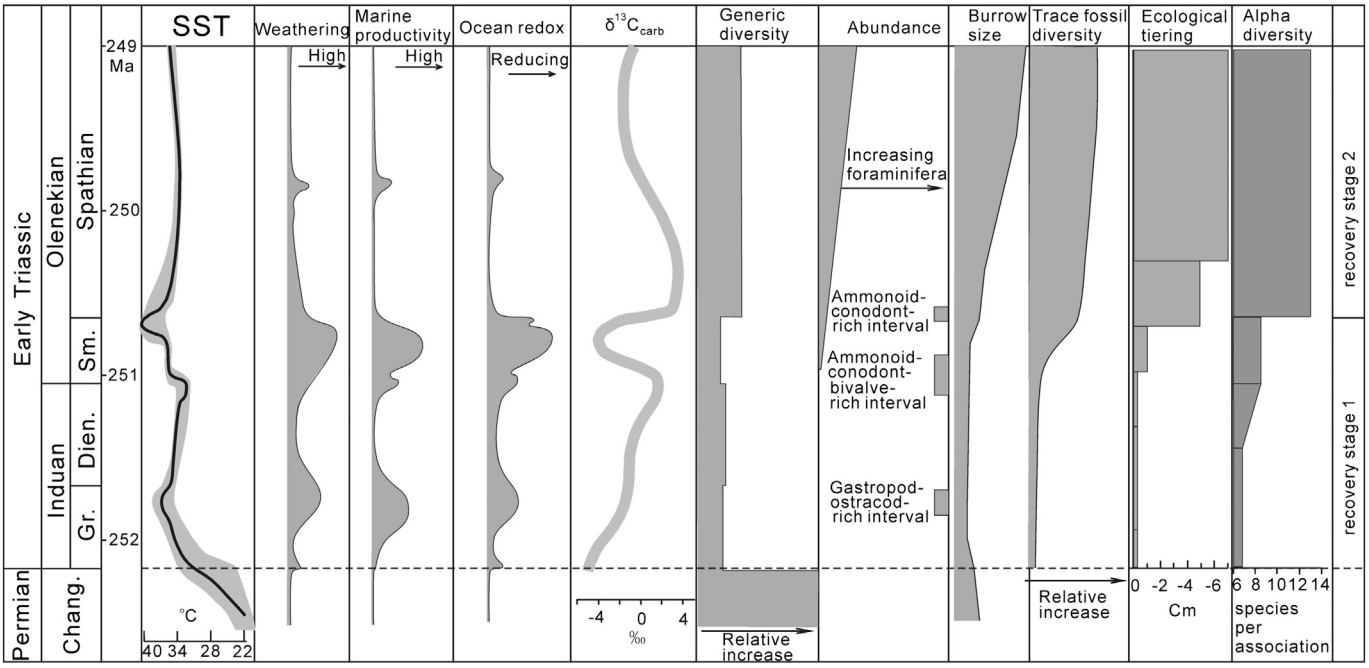

Fig. 12. Generalized patterns of marine environmental, biodiversity, and ecosystem change in the four study sections during the Early Triassic. The weathering, productivity, and redox profiles are based on Figs. 9–11. Data sources: sea-surface temperatures (SST) (Sun et al., 2012); $\delta^{13}C_{carb}$ and generic diversity (Tong et al., 2007a); fossil abundance (Yang et al., 1986; Wang et al., 2001; Tong et al., 2003; Krystyn et al., 2007; Zhao et al., 2007; Li et al., 2009; Song et al., 2011); trace fossil burrow size, ichnodiversity, and tiering (Chen et al., 2011); and alpha diversity (Hofmann et al., 2013, 2014).

possibly related to a productivity crash (Algeo et al., 2013) or to a shift in dominance from eukaryotic algae to bacterioplankton (Luo et al., 2014).

During the Griesbachian, the development of a hyper-greenhouse climate resulted in tropical sea-surface temperatures that were persistently >35 °C (Fig. 12; Sun et al., 2012). This warming contributed to expansion of marine anoxia (Fig. 11) through lowering of the solubility of dissolved oxygen in seawater and increasing the flux of river-borne nutrients to shallow-marine areas via enhanced chemical weathering (Fig. 9; Algeo and Twitchett, 2010). A consistently positive relationship is seen between redox conditions and marine productivity (Fig. 12), suggesting that organic carbon sinking fluxes controlled the expansion of oceanic oxygen-minimum zones (Algeo et al., 2011a). High seawater temperatures and widespread reducing conditions probably operated in tandem to keep benthic biotas under stress and to delay marine ecosystem recovery. As a result, benthic biotas were dominated by opportunistic lineages of eurytopic bivalves, gastropods, and ostracods (Erwin, 1998). Relatively high productivity levels during the Griesbachian (Fig. 10) offered adequate food resources for nekton, resulting in a transient diversification among conodonts and ammonoids (Stanley, 2009). High productivity may reflect dominance of bacterioplankton (Xie et al., 2010; Luo et al., 2014), which would have enhanced recycling of nutrients in the ocean-surface layer and reduced the organic carbon sinking flux (D'Hondt et al., 1998) and, thus, account for a decrease in the vertical gradient of $\delta^{13}C_{DIC}$ (Song-HY et al., 2013). However, at the end of Griesbachian, extreme warmth (Sun et al., 2012) and more widespread oceanic anoxia (Fig. 11) destroyed this surface-ocean ecosystem, resulting in a second-order mass extinction among conodonts and ammonoids (Brayard et al., 2006; Orchard, 2007; Stanley, 2009) and further depressing the benthic ecosystem. Expansion of the oceanic oxygen-minimum zone at this time would have resulted in a contraction of the ecospace available to planktic and nektic organisms (Fig. 13A).

The Dienerian was characterized by a warm climate, although one that was slightly cooler (~32–35 °C) than that of the late Griesbachian (Fig. 12; Sun et al., 2012). As a consequence of this relative cooling, terrestrial weathering fluxes were reduced (Fig. 9). In the marine environment, the Dienerian was characterized by lower marine productivity (Fig. 10) and a shift toward more oxidizing (or less reducing) conditions (Fig. 11). This substage was associated with a small negative excursion of $\delta^{13}C_{carb}$ (Tong et al., 2007a) and intermediate and relatively stable vertical $\delta^{13}C_{DIC}$ gradients (Song et al., 2013a,b), which are consistent with reduced marine productivity as well as a modest weakening of oceanic water-column stratification. With regard to marine biotas, the Dienerian exhibits increasing diversity among conodonts and ammonoids (Stanley, 2009) and other marine fauna (Tong et al., 2007a) and an increase in trace-fossil size (Twitchett, 1999; Chen et al., 2011; Fig. 2). Lower levels of oceanic productivity were probably associated with a greater proportion of eukaryotic plankton relative to bacterioplankton, which favored relatively greater export of organic carbon and nutrients from the ocean-surface layer (cf. D'Hondt et al., 1998). Comparatively cooler climatic conditions and contraction of the oceanic oxygen-minimum zone would have resulted in an expansion of the ecospace available to conodonts and ammonoids in the surface ocean (Fig. 13B). Thus, somewhat less severe environmental conditions in the Dienerian (relative to the Griesbachian) triggered a limited marine ecosystem recovery, although the brief interval since the end-Permian mass extinction (~0.5 Myr) may have insufficient for a complete recovery of marine ecosystems (e.g., Kirchner and Weil, 2000).

The Dienerian–Smithian boundary was characterized by a transient temperature minimum (~30–32°; Sun et al., 2012) and a large positive excursion (ca. +6‰) of $\delta^{13}C_{carb}$ globally (Payne et al., 2004; Tong et al., 2007a; Fig. 12). Positive $\delta^{13}C$ excursions are commonly associated with elevated marine productivity (Kump and Arthur, 1999). All four study sections show a substantial increase in terrestrial weathering fluxes at this time (Fig. 9), with two (Chaohu and Daxiakou) also showing evidence of increased marine productivity (Fig. 10). This pattern suggests that the increase in marine productivity may have been driven by

Please cite this article as: Wei, H., et al., Environmental controls on marine ecosystem recovery following mass extinctions, with an example from the Early Triassic, Earth-Sci. Rev. (2014), http://dx.doi.org/10.1016/j.earscirev.2014.10.007

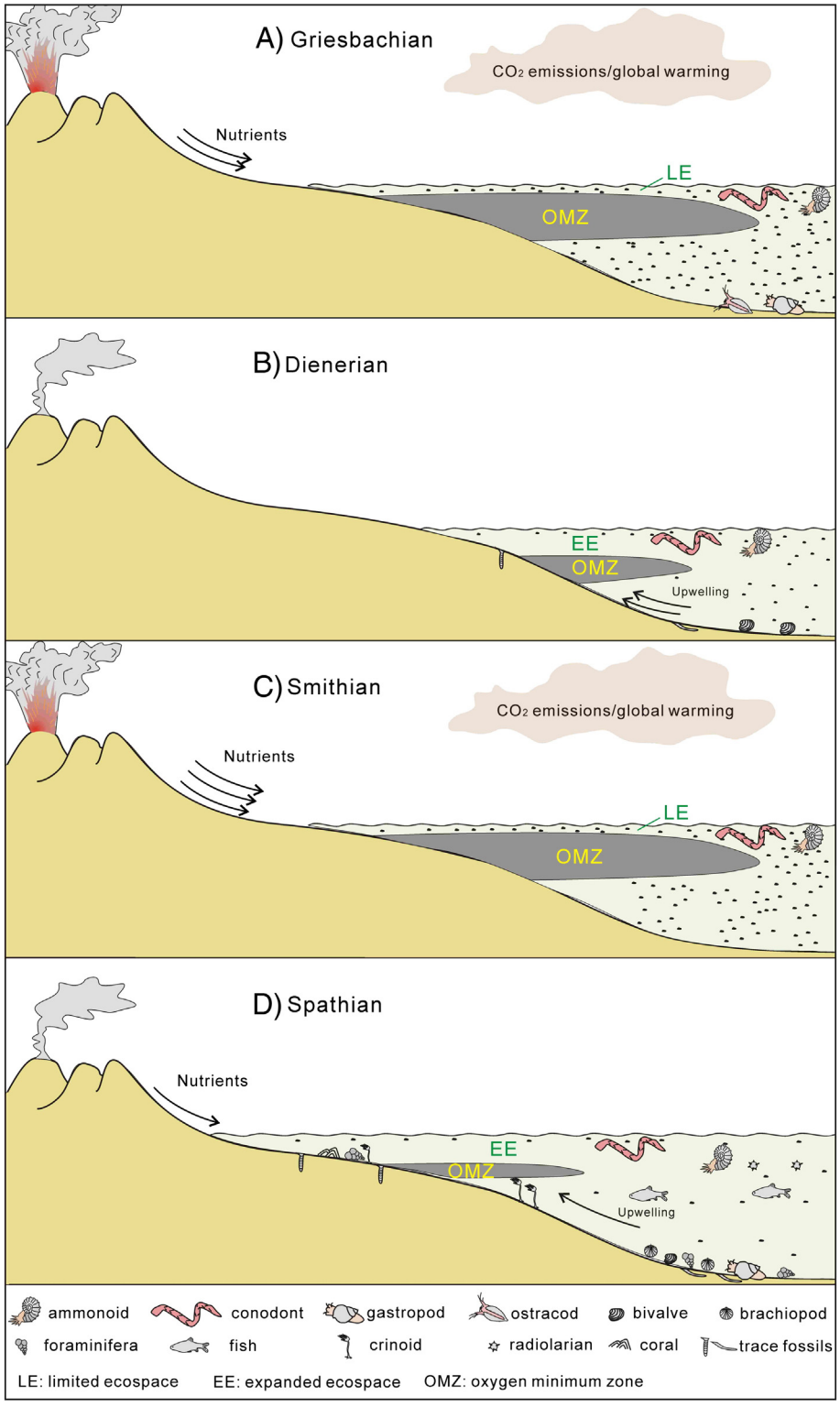

Fig. 13. Integrated model showing relationships between environmental change, shallow-marine ecospace, and marine ecosystem recovery during the Early Triassic. The Griesbachian (A) and Smithian (C) are generally characterized by stronger volcanism, enhanced weathering and riverine nutrient fluxes, an expanded OMZ, more intense water-column stratification, weaker upwelling, and limited ecospace. In contrast, the Dienerian (B) and Spathian (D) are generally characterized by weaker volcanism, decreased weathering and riverine nutrient fluxes, a contracted OMZ, less intense water-column stratification, stronger upwelling, and expanded ecospace.

enhanced riverine nutrient fluxes, possibly with an additional stimulus from upwelling of nutrient-rich deep waters owing to more vigorous thermohaline circulation as a consequence of climatic cooling and a steeper latitudinal temperature gradient. A concurrent shift toward somewhat more reducing conditions (Fig. 11) may have been driven by high O_2 demand associated with an enhanced sinking flux of organic matter. With regard to marine biotas, this interval witnessed the maximum diversification of conodonts and ammonoids during the

Please cite this article as: Wei, H., et al., Environmental controls on marine ecosystem recovery following mass extinctions, with an example from the Early Triassic, Earth-Sci. Rev. (2014), http://dx.doi.org/10.1016/j.earscirev.2014.10.007

Early Triassic (Stanley, 2009; Fig. 12), and a limited increase in the diversity of echinoderms, brachiopods, and forams (Chen et al., 2005a,b; Chen and McNamara, 2006; Song et al., 2011), suggesting improvements in both the ocean-surface and benthic ecosystems. Cooler temperatures and a contraction of oceanic oxygen-minimum zones resulted in an expansion of the ecospace available to marine faunas, and high productivity offered rich food resources for this ecosystem (Brayard et al., 2006; Orchard, 2007; Stanley, 2009). Enhanced oceanic overturning circulation generally results in improved ventilation of the global ocean (resulting in more ecospace availability), while simultaneously intensifying anoxia in limited areas of active upwelling (owing to greater nutrient fluxes to the ocean surface layer). The Dienerian–Smithian boundary thus represents an episode of significantly ameliorated marine environmental conditions prior to the onset of the Smithian crisis, and it may have laid a foundation for more rapid ecosystem recovery at the beginning of the Spathian, ~0.5 Myr later (e.g., Erwin, 2008; Chen and Benton, 2012).

The Smithian coincided with a major environmental and biotic crisis within the Early Triassic. It was characterized by development of a second hyper-greenhouse, with peak temperatures >38 °C (Sun et al., 2012; Romano et al., 2013), a large negative excursion of $\delta^{13}C_{carb}$ (Payne et al., 2004; Tong et al., 2007a,b), and a maximum vertical gradient in the $\delta^{13}C$ of DIC (Song et al., 2013a,b; Fig. 12). The negative shift in $\delta^{13}C_{carb}$ is likely to reflect a strong decline in marine productivity, and the large vertical $\delta^{13}C$ gradient an intensification of oceanic water-column stratification, both in response to extreme warming of the ocean-surface layer. In the study sections, the Smithian exhibits a large increase in terrestrial weathering fluxes (Fig. 9), reflecting stronger chemical weathering due to warming, and intensified marine anoxia (Fig. 11), due to a combination of riverine nutrient inputs and stronger water-column stratification. Productivity levels appear to have increased at this time in two of the study sections (Chaohu and Daxiakou; Fig. 10), although it is possible that these deep-water sections are recording enhanced organic matter preservation as a consequence of OMZ expansion rather than actual increases in surface-water productivity. Warming and other environmental stresses resulted in a major extinction event among conodonts and ammonoids at the end of the Smithian (Brayard et al., 2006; Orchard, 2007; Stanley, 2009; Fig. 12). Expansion of the oceanic oxygen-minimum zone at this time would have resulted in a contraction of the ecospace available to planktic and nektic organisms (Fig. 13C).

The Spathian marks the onset of a sustained recovery of marine ecosystems that was completed in the Middle Triassic (Bottjer et al., 2008; Chen and Benton, 2012). It was characterized by a pronounced climatic cooling from the hyper-greenhouse conditions of the preceding ~2 Myr, with tropical sea-surface temperatures falling to ~30–32 °C (Sun et al., 2012; Romano et al., 2013; Fig. 12). In the study sections, it is marked by large declines in terrestrial weathering fluxes, marine productivity, and the intensity of marine anoxia (Figs. 9–11). The decline in productivity can be attributed to a reduced supply of nutrients from riverine sources following climatic cooling and stabilization of terrestrial landscapes (Looy et al., 1999, 2001; Hermann et al., 2011) and from upwelling sources following a flushing out of the deep-ocean nutrient inventory as a result of re-invigorated thermohaline circulation at the Smithian–Spathian boundary (Zhang et al., 2014). Improved ocean ventilation and reduced organic carbon sinking fluxes were responsible for a shift toward less reducing conditions globally (Fig. 12). These environmental changes coincided with a gradual rediversification of pelagic organisms, rapid rediversification among benthic organisms and trace-makers, and higher-level integration of marine trophic systems (Chen et al., 2005a,b; Orchard, 2007; Stanley, 2009; Chen et al., 2011; Song et al., 2011; Chen and Benton, 2012). The more sustained ecosystem recovery of the Spathian relative to the Dienerian can be attributed to several factors, including a longer time interval, a cooler climate, less widespread marine anoxia, and generally more stable environmental conditions (Fig. 13D).

5.2. Spatial variation in Early Triassic marine environmental conditions

Although the four study sections generally show similar patterns of secular variation in weathering, productivity, and redox proxies, some differences exist among the sections that are probably controlled by paleogeographic location, water depth, and local bathymetry. First, the deep-ramp sections (Chaohu and Daxiakou) show peak weathering fluxes that are ~3× greater than for the mid-shelf section (Mud) and ~10× greater than for the shallow-platform section (Zuodeng; Fig. 9). These differences reflect relative proximity to sources of detrital siliciclastics and local bathymetry (e.g., the relative isolation of the shallow-platform section from detrital influx). Second, average CIA values are somewhat higher in the peri-equatorial South China sections (~0.75–0.80) relative to the mid-latitude Mud section (0.72), a difference that is attributable to variations in weathering intensity as a function of climate. Third, productivity proxy fluxes show some variation among the study sections (Fig. 10). Fluxes are similar for Chaohu, Daxiakou, and Mud but lower for Zuodeng, suggesting diminished marine productivity on shallow-platform tops relative to open-marine ramp and shelf settings. Fourth, redox proxy fluxes differ significantly among the study sections, with Chaohu exhibiting comparatively large fluxes, Daxiakou and Zuodeng intermediate fluxes, and Mud small fluxes (Fig. 11). These differences appear to be related to both water depth and paleogeographic location. Chaohu was the deepest section, with water depths of ~300–500 m putting it within the ocean thermocline and, thus, subject to influence by an expanding oxygen-minimum zone. However, the higher redox proxy fluxes for all South China sections relative to Mud suggest that the eastern Paleo-Tethys Ocean was subject to generally more strongly reducing conditions than the southern Neo-Tethys Ocean during the Early Triassic (Fig. 4B). Finally, all types of proxies exhibit a better-defined pattern of secular variation in the deep-ramp sections (Chaohu and Daxiakou) than elsewhere (Figs. 9–11). We attribute this relationship to differences in depositional water depth, which was >200 m for the deep-ramp sections but <100 m for the mid-shelf and shallow-platform sections (Section 3). With increasing water depths, sections were under greater influence by the oceanic oxygen-minimum zone, expansion of which occurred over discrete time intervals (Feng and Algeo, 2014). In contrast, the study sections located within the ocean-surface layer (<100 m) may have experienced more irregular secular variation in environmental conditions.

5.3. Influences on weathering, productivity, and redox fluxes

Modeling of geochemical proxy fluxes suggests a close relationship of changes in terrestrial weathering intensity, marine productivity rates, and ocean redox conditions throughout the Early Triassic (Figs. 9–11). Our interpretation, as presented above, is that this covariation reflects real relationships among these environmental parameters. Specifically, higher weathering intensities tend to result in increased riverine nutrient fluxes, leading to enhanced marine productivity (at least in coastal areas), and thus to intensified marine anoxia (again, possibly focused in coastal areas) (cf. Algeo et al., 1995, 2011a). These relationships are natural consequences of strong climate warming, as occurred repeatedly during the Early Triassic (Fig. 12; Joachimski et al., 2012; Sun et al., 2012; Romano et al., 2013). We recognize, however, that the relationships among these environmental parameters may vary in detail and can have alternative linkages. For example, expansion of marine anoxia can potentially lead to enhanced organic carbon burial fluxes in the absence of any change in marine productivity. We also recognize that the patterns exhibited by the four study sections inherently represent local marine environmental conditions (Fig. 13) that may or may not mirror contemporaneous global oceanographic changes. However, the strong similarities among some of the study sections, particularly those deposited at deeper water depths (i.e., Chaohu and Daxiakou), suggest that our results have

Please cite this article as: Wei, H., et al., Environmental controls on marine ecosystem recovery following mass extinctions, with an example from the Early Triassic, Earth-Sci. Rev. (2014), http://dx.doi.org/10.1016/j.earscirev.2014.10.007

probably captured some aspect of global marine environmental changes during the Early Triassic.

An additional important influence on the proxy fluxes is sediment bulk accumulation rate (BAR). These fluxes represent the multiplicative product of raw proxy concentrations and BAR (Supplementary Information), so an increase in either input variable can lead to higher calculated fluxes. The observation that, for each study section, the concentration profiles (Figs. 6–8) and flux profiles (Figs. 9–11) tend to exhibit similar features reflects the influence of raw concentrations on calculated fluxes. However, a degree of auto-correlation among the various proxy fluxes results from the use of a common age-thickness model for each study section and is unavoidable in studies of this type. The analysis of four widely separated sections (note that the three Chinese sections cover >1500 km of the South China craton) helps to compensate for this situation and serves as a test of the validity of results because each study section makes use of an independent, site-specific age-thickness model (e.g., Section 5.2). Moreover, our use of CIA also provides a check on the degree of procedural auto-correlation of results because CIA is a proxy that is completely independent of BAR. CIA shows unambiguous positive covariation with BAR-based weathering proxies (i.e., Al and Fe) in the Chaohu, Daxiakou, and Mud sections (Fig. 9), in which CIA exhibits maxima at the PTB or early Griesbachian, the late Griesbachian, the Dienerian–Smithian boundary or early Smithian, and the Smithian–Spathian boundary. The weathering proxies in general do not show a coherent pattern of secular variation in the third study section (Zuodeng), possibly because its paleodepositional setting (i.e., a shallow-marine carbonate platform) was not conducive to recording weathering fluxes.

5.4. Recovery patterns following other Phanerozoic mass extinctions

The marine ecosystem recovery following the end-Permian mass extinction is regarded as having been longer than those following other major Phanerozoic biocrises (Bottjer et al., 2008; Chen and Benton, 2012), although a detailed comparison with other recovery events has been lacking to date. In the following analysis, we examine patterns of marine ecosystem recovery following the other four "Big Five" Phanerozoic mass extinctions and consider their relationship to contemporaneous environmental conditions. This analysis reveals both commonalities and dissimilarities in the ecosystem recoveries following different mass extinction events.

The Cretaceous–Paleogene (K–Pg; formerly the Cretaceous–Tertiary, or K–T) boundary mass extinction at 66.0 Ma (Renne et al., 2013) is the most thoroughly investigated to date. It killed off ~50% of marine genera and ~70% of species (Jablonski and Chaloner, 1994; Sepkoski, 1998; Alroy et al., 2008), with high extinction rates among marine reptiles, ammonoids, rudist bivalves, planktonic foraminifera, and calcareous nanofossils (Pospichal, 1994; Marshall and Ward, 1996; Arenillas et al., 2000; Bown, 2005; Fastovsky and Sheehan, 2005; Fig. 14A). The coincidence in timing between the Chicxulub bolide impact and the K–Pg boundary extinction suggests that the impactor was the major cause of this mass extinction (Jolley et al., 2010; Renne et al., 2013), although the lethality of the impact may have been enhanced by long-term environmental stresses associated with the Deccan Traps eruptions (Courtillot et al., 1986; Courtillot et al., 1988; White and Saunders, 2005; Chenet et al., 2007).

Algal primary productivity may have recovered very rapidly, in less than a century following the K–Pg boundary impact (Fig. 14A, Sepúlveda et al., 2009). However, redevelopment of an integrated marine ecosystem with extended trophic chains took longer and proceeded in two stages: a rapid initial phase and a delayed second phase (Coxall et al., 2006). The initial phase took about 1 Myr (Sepúlveda et al., 2009; Hull et al., 2011; Alegret et al., 2012) and involved recovery of planktonic organisms such as dinoflagellates (Brinkhuis et al., 1998; Hildebrand-Habel and Streng, 2003), planktic foraminifera (Coccioni and Luciani, 2006; Hull et al., 2011), and radiolarians (Hollis et al., 2003), as well as coralline red algae (Aguirre et al., 2007). The delayed second phase of recovery lasted for ~4 Myr following the boundary crisis (Coxall et al., 2006) and culminated in a new diversity peak among planktic foraminifera (Olsson et al., 1999) and re-establishment of reef communities (Baceta et al., 2005).

The nutrient status of the early Danian ocean remains controversial, with some studies inferring high nutrient levels (Alegret and Thomas, 2009; Alegret et al., 2012) and others low nutrient levels (Coxall et al., 2006; Fuqua et al., 2008). Warmer conditions (as documented by a $\delta^{18}O$ shift; Fig. 14A) caused the oceanic oxygen-minimum zone to expand, decreasing the ecospace available to pelagic organisms. These adverse conditions abated 3–4 Myr after the K–Pg boundary crisis, stimulating an increase in pelagic biodiversity and full redevelopment of the marine food web (Coxall et al., 2006; Yamamoto et al., 2010). The post-K–Pg-boundary recovery can be traced through carbon cycle changes in the early Paleocene (Fig. 14A). The vertical (shallow-to-deep) $\delta^{13}C$ gradient in seawater DIC increased in two steps, corresponding to the two stages of ecosystem recovery (Coxall et al., 2006, Fig. 14A). The first step is marked by an increase in $\Delta^{13}C_{vert}$ from 0 to ~1‰ within 1 Myr of the crisis, and the second step by an increase to ~2‰ within 3 million years of the crisis. The latter value is similar to the $\Delta^{13}C_{vert}$ observed in modern marine systems and, thus, marks the re-establishment of an efficient biological pump by the late Danian, that is, less intense recycling of organic matter in the ocean-surface layer resulted in more export to the chemocline and deep ocean (D'Hondt et al., 1998; Coxall et al., 2006).

The Triassic–Jurassic (Tr–J) boundary mass extinction resulted in the demise of ~53% of marine genera (Sepkoski, 1996) and ~80% of species (Sepkoski, 1994). It eliminated conodonts and severely affected brachiopods and gastropods (McRoberts et al., 1997; Tomašových and Siblík, 2007), as well as ammonoids, bivalves, corals and ostracods (McRoberts and Newton, 1995; Kiessling, 2001, 2005; van de Schootbrugge et al., 2007; Mander and Twitchett, 2008; Fig. 14B). Eruption of the Central Atlantic magmatic province (CAMP) and the resulting global warming were the major causes of this mass extinction (Marzoli et al., 1999; McElwain et al., 1999; Hesselbo et al., 2002; van de Schootbrugge et al., 2009; Schoene et al., 2010; Ruhl et al., 2011).

Marine ecosystem recovery began rapidly in the Early Jurassic, within 120 k.y. (Ruhl et al., 2010) to 290 k.y. of the extinction event (Bartolini et al., 2012). Recovery was marked by increases in diversity during the earliest Hettangian among pelagic carbonate producers (radiolarians, calcareous nanofossils) (Clémence et al., 2010), molluscs (McRoberts et al., 1997), ammonoids (Hesselbo et al., 2002; Guex et al., 2012), and brachiopods (Tomašových and Siblík, 2007). This initial recovery (Fig. 14B) was followed by a second extinction event among ammonoids during the early Hettangian (Guex et al., 2004, 2012). A second, longer (~2–3-Myr) recovery phase (Fig. 14B) is evidenced by more diverse radiolarian assemblages in the mid to late Hettangian (Longridge et al., 2007), rediversification of ammonoids in the late Hettangian (Guex et al., 2012), and increases in the diverse of gastropod and coral faunas in the early Sinemurian (Seuß et al., 2005).

A large (~5‰), rapid negative carbon isotope excursion occurred at the end of Triassic (Korte et al., 2009; Schoene et al., 2010; Bartolini et al., 2012), and was followed a positive excursion (~3%) in the lower Hettangian (Williford et al., 2007; Korte et al., 2009; Schoene et al., 2010; Bartolini et al., 2012; Fig. 14B), suggesting an extreme carbon cycle disturbance at the T–J boundary. Paleobotanical data provide evidence of a rapid global warming at the T–J boundary (McElwain et al., 1999; Ruhl et al., 2011), and a subsequent cooling resulted from high marine productivity and enhanced organic matter burial (Korte et al., 2009). A long-term negative carbon isotope excursion during the early and middle Hettangian coincided with a greenhouse climate and widespread oceanic anoxia (Ruhl and Kürschner, 2011; Bartolini et al., 2012; Richoz et al., 2012), hindering the recovery of marine ecosystems until the Hettangian–Sinemurian boundary (Bartolini et al., 2012; van de Schootbrugge et al., 2013), when the carbon cycle stabilized (Bartolini et al., 2012; Guex et al., 2012). The initial recovery of pelagic and benthic

Please cite this article as: Wei, H., et al., Environmental controls on marine ecosystem recovery following mass extinctions, with an example from the Early Triassic, Earth-Sci. Rev. (2014), http://dx.doi.org/10.1016/j.earscirev.2014.10.007

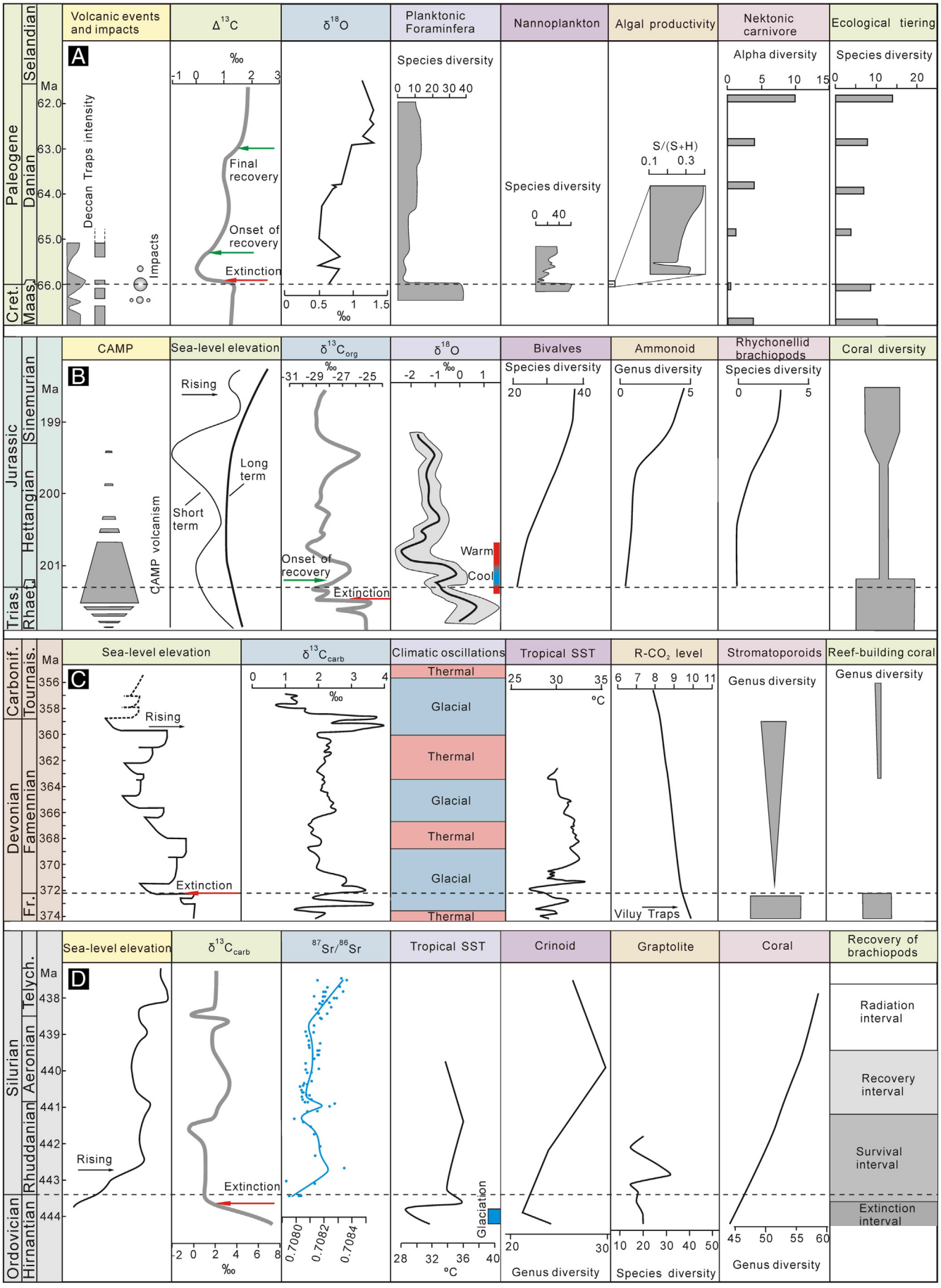

Please cite this article as: Wei, H., et al., Environmental controls on marine ecosystem recovery following mass extinctions, with an example from the Early Triassic, Earth-Sci. Rev. (2014), http://dx.doi.org/10.1016/j.earscirev.2014.10.007

organisms during the early Hettangian was impeded first by large climate fluctuations and then by a long-term global warming that resulted in marine environmental stresses including warming, seawater acidification, and anoxia (Richoz et al., 2012; van de Schootbrugge et al., 2013). These factors contributed to an extinction event among ammonoids in the mid-Hettangian and a protracted recovery among many elements of the marine nekton and benthon during the Hettangian (Guex et al., 2004, 2012). Falling atmospheric pCO_2 by the late Hettangian resulted in a cooler climate and ameliorated marine environmental conditions, leading to a second stage of recovery among plankton (Bartolini et al., 2012) and benthon (Seuß et al., 2005) during the Sinemurian stage. Thus, the Early Jurassic marine ecosystem recovery tracks contemporaneous environmental changes very well.

The Late Devonian mass extinction comprised a series of crises during an interval of ~20 Myr, of which the largest were at the Givetian–Frasnian (G–F), Frasnian–Famennian (F–F), and Devonian–Carboniferous (D–C) boundaries (Walliser, 1996; House, 2002; Morrow et al., 2011; Fig. 14C). Collectively, these crises killed ~50–60% of marine genera and ~82% of species (Jablonski, 1991; McGhee, 1996). Many clades of marine invertebrates suffered multiple declines, including brachiopods, trilobites, corals, and stromatoporoids (Copper, 1986; Stearn, 1987), and most colonial rugose corals went extinct at the F–F boundary (Fig. 14C, Copper, 2002; Shen and Webb, 2004). The F–F mass extinction evidenced a collapse of the metazoan reef ecosystem after the mid-late Devonian acme of metazoan reefs and a replacement by microbial reefs (Copper, 2002).

The immediate cause of the Late Devonian crisis appears to have been rapid changes in seawater temperatures and redox conditions (Joachimski et al., 2004; Chen et al., 2005a, 2005b). For example, the F–F cooling event severely affected the tropical-marine ecosystem, especially reef metazoans and, thus, is the probable cause of this mass extinction (Copper, 1986, 2002). However, the ultimate cause of the Late Devonian crisis is likely to have been the spread of higher land plants and consequent changes in nutrient cycling (Algeo et al., 1995, 2001; Algeo and Scheckler, 1998). A progressive expansion of terrestrial floras during the Devonian resulted in intensified chemical weathering of land areas, releasing more nutrients that stimulated algal blooms and a consequent expansion of anoxia in epicontinental seas. These paleobotanical developments resulted in a long-term decline in atmospheric pCO_2 owing to an increase in both organic carbon burial and silicate weathering, resulting in strong global climatic cooling (Algeo et al., 1995). The Late Devonian was a time of transition from the Middle Paleozoic greenhouse to the Late Paleozoic icehouse (Fig. 14C; Isaacson et al., 2008). Each of the Late Devonian crises coincided with a major global cooling event, the episodes at the F–F and D–C boundaries being particularly pronounced (Joachimski et al., 2004; Buggisch and Joachimski, 2006; Kaiser et al., 2006, 2008). It is not certain whether the spread of higher land plants was gradual and merely created background conditions for the development of episodic marine biocrises, or whether it actively triggered each crisis through pulses of expansion (Algeo and Scheckler, 2010).

Because of the multi-episode nature of the crisis, there was at least a partial recovery of marine ecosystems following each extinction event. For example, brachiopods and ostracods underwent a modest recovery during early Famennian, following the F–F boundary event, although they remained low in diversity (Casier and Lethiers, 1998; Baliński, 2002; Sokiran, 2002, Fig. 14C), and stromatoporoids began to recover during the early and middle Famennian but went extinct at the D–C boundary (Metherell and Workman, 1969; Stearn, 1987; Webb, 1998). A permanent recovery did not begin until after the D–C boundary crisis. Bryozoans recovered to their pre-extinction level of diversity during the Early Carboniferous (Bigey, 1989). Some corals (e.g., *Pseudouralinia*, *Siphonophyllia*) and brachiopods (e.g., *Eochoristites*, *Martiniella*) recovered in the middle Tournaisian of the Early Carboniferous (Liao, 2002). The extinction of colonial rugose corals at the F–F boundary resulted in replacement of metazoan reefs by small microbial patch reefs (Pickett and Wu, 1990; Webb, 1998; Morrow et al., 2011), with regrowth of large barrier reefs delayed until the Visean (Dix and James, 1987; Webb, 1998, 1999; Wahlmann, 2002; Fig. 14C). Loss of large metazoans during this crisis permitted the establishment of novel ecologies dominated by microbial communities (Wood, 2004). However, the final marine ecosystem recovery required the high-trophic-level ecosystem community establishment (e.g., Chen and Benton, 2012).

The Late Ordovician (Hirnantian) mass extinction (Fig. 14D) eliminated ~24% of families and 85% of species of marine invertebrates (Jablonski, 1991; Sepkoski, 1996; Brenchley et al., 2001; Sheehan, 2001). It was particularly severe among trilobites, brachiopods, molluscs (Sepkoski, 1984; Adrain et al., 2000; Harper and Rong, 2008), and graptolites and conodonts (Brenchley et al., 2001; Sheehan, 2001; Fan and Chen, 2007; Rasmussen and Harper, 2011a,b). The immediate cause of this extinction was the Hirnantian glaciation (Brenchley et al., 1995; Gibbs et al., 1997; Sheehan, 2001; Sutcliffe et al., 2006). A second extinction, ~1 Myr later, decimated the cool-adapted 'Hirnantian fauna' and was caused by a rapid termination of glaciation (Sheehan and Coorough, 1990). The Early Silurian (Llandovery epoch) was a transitional interval from the Late Ordovician icehouse to a middle Paleozoic greenhouse (Kaljo and Martma, 2000; Brand et al., 2006). Warming conditions, the killing factor in the second extinction, prevailed during the Llandovery, although interrupted by two brief glaciations during the Aeronian stage (Caputo, 1998; Azmy et al., 1998, 1999; Delabroye et al., 2011; Finnegan et al., 2011; Fig. 14D).

Marine ecosystems began to recover following the end-Ordovician extinctions, although climate fluctuations during the Aeronian stage complicated the recovery pattern. Microbialite resurgence in the immediate aftermath of the Late Ordovician extinction coincided with an interval of low-diversity megafaunal communities (Sheehan and Harris, 2004). Diversification of brachiopods and trilobites proceeded during the Rhuddanian, the first stage of the Early Silurian (Krug and Patzkowsky, 2004; Owen et al., 2008; Huang et al., 2012), representing the initial recovery of marine faunas (Fig. 14D). Crinoids and coral began to diversify from the Rhuddanian in the Early Silurian (Kaljo, 1996; Ausich and Deline, 2012). Climate fluctuations during the Llandovery resulted in a delay in the recovery of marine ecosystems (Copper, 2001; Gouldey et al., 2010). Full recovery of reef ecosystems took place by the mid-Aeronian stage, ~4 Myr after the end-Ordovician crisis (Copper, 2001).

Fig. 14. Patterns of environmental change and marine ecosystem recoveries following other major mass extinctions: (A) Cretaceous–Paleogene (K–Pg) boundary, (B) Triassic–Jurassic (Tr–J) boundary, (C) Late Devonian, and (D) Ordovician–Silurian (O–S) boundary. Data sources: (A) volcanism (Keller, 2003; Renne et al., 2013), impacts (Keller, 2003), $\delta^{13}C_{carb}$ (D'Hondt et al., 1998; Coxall et al., 2006), $\delta^{18}O$ (D'Hondt and Zachos, 1993; Norris, 1996; Birch et al., 2012), planktic foraminifera diversity (Keller, 2003; Coxall et al., 2006; Gallala et al., 2009), nanoplankton diversity (Hull et al., 2011), algal productivity (Sepúlveda et al., 2009; n.b., S/(S + H) = sterane/(sterane + hopane) ratio), nektonic carnivore alpha diversity (Sessa et al., 2012), ecological tiering at the sediment–water interface (Sessa et al., 2012); (B) CAMP volcanism (Olsen et al., 2002; Deene et al., 2010; Blackburn et al., 2013; Guex et al., 2012; Deenen et al., 2010; Ruhl et al., 2010), $\delta^{13}C_{org}$ (Williford et al., 2007; Ruhl et al., 2011; Bartolini et al., 2012), $\delta^{18}O$ (Korte et al., 2009), warm and cool intervals (Schoene et al., 2010), sea-level elevations (Haq et al., 1987), diversity of bivalves, ammonites, brachiopods, and reefs (Hallam, 1996); (C) sea-level elevations (Johnson et al., 1985; Algeo et al., 2007; Isaacson et al., 2008), $\delta^{13}C_{carb}$ (Buggisch and Joachimski, 2006), climatic oscillations (Isaacson et al., 2008), tropical sea surface temperatures (SSTs) (Joachimski et al., 2004), R-$CO_{2(atm)}$ (Berner, 1994; n.b., RCO_2 = ratio of atmospheric CO_2 in past to "modern" value of ~300 ppmv), stromatoporoid diversity (Stearn, 1987; Webb, 1998; Morrow et al., 2011), reef-building coral diversity (Webb, 1998); and (D) sea-level elevations (Johnson et al., 1991; Couto et al., 2013); $\delta^{13}C_{carb}$ (Finney et al., 1999; Kaljo and Martma, 2000; Gouldey et al., 2010; Cramer et al., 2011; Delabroye et al., 2011), $^{87}Sr/^{86}Sr$ (Azmy et al., 1999; Gouldey et al., 2010), tropical SSTs (Finnegan et al., 2011), glaciations (Azmy et al., 1998; Caputo, 1998; Delabroye et al., 2011), crinoid diversity (Ausich and Deline, 2012), graptolite diversity (Fan and Chen, 2007), coral diversity (Kaljo, 1996), brachiopod recovery stage (Rong and Harper, 1999).

Please cite this article as: Wei, H., et al., Environmental controls on marine ecosystem recovery following mass extinctions, with an example from the Early Triassic, Earth-Sci. Rev. (2014), http://dx.doi.org/10.1016/j.earscirev.2014.10.007

5.5. Evaluation of hypotheses regarding controls on marine ecosystem recovery

Three hypotheses have been advanced for the apparent delay in recovery of marine ecosystems following the end-Permian mass extinction, linking the duration of the recovery interval to: (1) the intensity of the mass extinction (Sepkoski, 1984; Solé et al., 2002), (2) the persistence of harsh environmental conditions (Hallam, 1991; Isozaki, 1997; Payne et al., 2004; Erwin, 2007), and (3) episodic occurrence of strong environmental disturbances during the recovery interval (Algeo et al., 2007, 2008; Orchard, 2007; Retallack et al., 2011; Fig. 1). Our analysis above of four Lower Triassic sections (Chaohu, Daxiakou, Zuodeng, and Mud) demonstrates unambiguously that there were large fluctuations in marine environmental conditions during the Early Triassic, and these disturbances were linked to transient biodiversity crises among coeval marine faunas and relapses in marine ecosystem complexity and integration. We conclude that episodic environmental disturbances were integral to the pattern and pace of marine ecosystem recovery during the Early Triassic.

Is it possible to draw general inferences about controls on marine ecosystem recovery following mass extinctions? With regard to duration, there is considerable variation among the recovery intervals following the "Big Five" Phanerozoic mass extinctions. If defined on the basis of (1) re-attainment of biodiversity equal to or exceeding pre-crisis levels, and (2) re-development of stable, well-integrated trophic systems, then the duration of the recovery interval was ~4 Myr for the end-Ordovician crisis, ~10 Myr for the F–F crisis, ~5 Myr for the end-Permian crisis, ~2.5 Myr for the end-Triassic crisis, and ~3 Myr for the end-Cretaceous crisis (Fig. 14). These durations are closely linked to the interval of disturbed environmental conditions that followed each extinction event. The shortest recovery interval, ~2.5 Myr after the end-Triassic crisis, was associated with rapid cooling with minimal climate fluctuations during the earliest Jurassic (Korte et al., 2009), suggesting that amelioration of marine environmental conditions proceeded quickly following the CAMP eruptions (Marzoli et al., 1999; McElwain et al., 1999; Hesselbo et al., 2002; Schoene et al., 2010; Ruhl et al., 2011). The ~3-Myr-long interval of recovery following the end-Cretaceous crisis was also associated with comparatively stable environmental conditions during the early Paleogene (Coxall et al., 2006). In contrast, the longest recovery interval, ~10 Myr after the F–F crisis, was interrupted by two glaciation episodes (Joachimski et al., 2004; Kaiser et al., 2006, 2008; Isaacson et al., 2008) during which environmental conditions deteriorated and marine ecosystem recovery was halted or reversed (Chen et al., 2005a,b). The second-longest recovery interval, ~5 Myr after the end-Permian crisis, was also associated with repeated environmental disturbances (Algeo et al., 2007, 2008; Retallack et al., 2011). Thus, unsettled environmental conditions following the main extinction crisis appear to be a strong control on the pattern and pace of marine ecosystem recovery.

Various types of environmental perturbations can contribute to destabilization of recovering marine ecosystems. First, temperature is clearly important, as most marine creatures are adapted to live within a relatively narrow temperature range (Brenchley and Harper, 1998). Extreme temperatures were a major factor in delayed ecosystem recovery during the Early Triassic (Sun et al., 2012; Romano et al., 2013), and strong climate fluctuations were important during other recovery intervals, e.g., the Late Devonian (Joachimski et al., 2004; Buggisch and Joachimski, 2006; Isaacson et al., 2008) and the Early Silurian (Finney et al., 1999; Gouldey et al., 2010; Finnegan et al., 2011, 2012). Second, nutrient inventories and patterns of nutrient cycling can be important. Changes related to shifts from eukaryotic to microbial primary production following the end-Cretaceous (D'Hondt et al., 1998) and end-Permian mass extinctions (Grice et al., 2005; Xie et al., 2010) probably influenced rebuilding of marine trophic systems (e.g., Chen and Benton, 2012). Third, ocean redox conditions, which are linked to temperature and nutrient cycling, influence the availability of ecospace for metazoans (e.g., Fig. 13). Development of reducing conditions leads to hypercapnia and hypoxemia, which are lethal to most marine invertebrates (Pörtner, 2001). Fourth, ocean acidification, which is commonly linked to elevated atmospheric pCO_2, impedes the growth of calcifying organisms. A possible transient increase in seawater acidity during the Early Triassic (Payne et al., 2010; Hinojosa et al., 2012) and early Paleocene (Alegret et al., 2012) are thought to have influenced the rate of recovery of some faunal components of marine ecosystems.

Other potential influences on rates of marine ecosystem recovery, i.e., persistently harsh environmental conditions (Hallam, 1991; Isozaki, 1997; Payne et al., 2004; Erwin, 2007) or magnitude of the extinction event (Sepkoski, 1984; Solé et al., 2002), may play a role as well. Although environmental conditions exhibit a tendency to fluctuate strongly following a biocrisis rather than remaining persistently harsh, at least some crises were followed by protracted intervals of generally inhospitable conditions. The best-documented example is the Early Triassic, during which tropical sea-surface temperatures remained persistently high (>32 °C) for at least 2 Myr following the end-Permian crisis (Sun et al., 2012; Romano et al., 2013). The Late Devonian may provide another example, owing to the persistence of strongly oxygen-depleted conditions in shallow-marine seas for intervals of millions of years following the G–F and F–F crises (Algeo et al., 1995). In both cases, conditions fluctuated during these extended intervals of environmental deterioration, yielding no distinct dividing line between persistently harsh conditions and recurrent environmental disturbances. With regard to the influence of magnitude of the extinction event, there appears to be no strong correlation with the duration of the recovery interval (e.g., Kirchner and Weil, 2000; Erwin, 2001). There are intrinsic limits to how quickly ecosystems are capable of recovery that depend on rates of biotic evolution and, thus, reoccupation of vacated ecological niches (Sepkoski, 1998; Kirchner and Weil, 2000). However, it appears that such rates are at least an order-of-magnitude faster than the durations of even the shorter marine ecosystem recoveries (Hairstone et al., 2008).

6. Conclusions

The overriding control on the pattern and pace of marine ecosystem recovery following a mass extinction event is environmental stability or lack thereof. An analysis of environmental variation following the end-Permian mass extinction demonstrates that the protracted (~5-Myr) interval of recovery of Early Triassic marine ecosystems was due to recurrent environmental perturbations. These perturbations were associated with high terrestrial weathering fluxes, elevated marine productivity, and more intensely reducing oceanic redox conditions, and they appear to have been triggered by episodes of strong climatic warming, possibly linked to stages of increased magmatism in the Siberian Traps Large Igneous Province. The main perturbations following the end-Permian extinction occurred during the early Griesbachian, late Griesbachian, mid-Smithian, and (more weakly) the mid-Spathian. These episodes were stronger and more temporally discrete in deepwater sections (Chaohu and Daxiakou) relative to shallow and intermediate sections (Zuodeng and Mud), probably because warming and attendant effects were felt most strongly in the oceanic thermocline region. The observed relationships between weathering and productivity fluxes imply that nutrient and energy flows were key influences on the pattern and pace of marine ecosystem recovery. Comparison with recovery patterns following the other four "Big Five" Phanerozoic mass extinctions suggests that marine ecosystem recovery in general depends on the stability of the post-crisis marine environment. Persistent environmental stresses may also play a role in the pace of ecosystem recovery, but there is no clear correlation to the magnitude of mass extinction event.

Please cite this article as: Wei, H., et al., Environmental controls on marine ecosystem recovery following mass extinctions, with an example from the Early Triassic, Earth-Sci. Rev. (2014), http://dx.doi.org/10.1016/j.earscirev.2014.10.007

Acknowledgments

Research by TJA is supported by the Sedimentary Geology and Paleobiology program of the U.S. National Science Foundation (No. EAR-1053449), the NASA Exobiology program, (No. NNX13AJ1IG) and the State Key Laboratory of Geological Processes and Mineral Resources, China University of Geosciences, Wuhan (Program: GPMR201301). This paper is a contribution to IGCP Projects 572 and 630.

Appendix A. Supplementary data

Supplementary data to this article can be found online at http://dx.doi.org/10.1016/j.earscirev.2014.10.007.

References

Adrain, J.M., Westrop, S.R., Chatterton, B.D.E., Ramsköld, L., 2000. Silurian trilobite alpha diversity and the end-Ordovician mass extinction. Paleobiology 26, 625–646.
Aguirre, J., Baceta, J.I., Braga, J.C., 2007. Recovery of marine primary producers after the Cretaceous–Tertiary mass extinction: Paleocene calcareous red algae from the Iberian Peninsula. Palaeogeogr. Palaeoclimatol. Palaeoecol. 249, 393–411.
Alegret, L., Thomas, E., 2009. Food supply to the seafloor in the Pacific Ocean after the Cretaceous/Paleogene boundary event. Mar. Micropaleontol. 73, 105–116.
Alegret, L., Thomas, E., Lohmann, K.C., 2012. End-Cretaceous marine mass extinction not caused by productivity collapse. Proc. Natl. Acad. Sci. U. S. A. 109, 728–732.
Algeo, T.J., Lyons, T.W., 2006. Mo-total organic carbon covariation in modern anoxic marine environments: implications for analysis of paleoredox and paleohydrographic conditions. Paleoceanography 21 PA1016.
Algeo, T.J., Maynard, J.B., 2004. Trace-element behavior and redox facies in core shales of Upper Pennsylvanian Kansas-type cyclothems. Chem. Geol. 206, 289–318.
Algeo, T.J., Scheckler, S.E., 1998. Terrestrial–marine teleconnections in the Devonian: links between the evolution of land plants, weathering processes, and marine anoxic events. Philos. Trans. R. Soc. B Biol. Sci. 353, 113–130.
Algeo, T.J., Scheckler, S.E., 2010. Land plant evolution and weathering rates changes in the Devonian. J. Earth Sci. 21, 75–78.
Algeo, T.J., Tribovillard, N., 2009. Environmental analysis of paleoceanographic systems based on molybdenum–uranium covariation. Chem. Geol. 268, 211–225.
Algeo, T.J., Twitchett, R.J., 2010. Anomalous Early Triassic sediment fluxes due to elevated weathering rates and their biological consequences. Geology 38, 1023–1026.
Algeo, T.J., Berner, R.A., Maynard, J.B., Scheckler, S.E., 1995. Late Devonian oceanic anoxic events and biotic crises: 'rooted' in the evolution of vascular land plants? GSA Today 5, 64–66.
Algeo, T.J., Scheckler, S.E., Maynard, J.B., 2001. Effects of the Middle to Late Devonian spread of vascular land plants on weathering regimes, marine biotas, and global climate. In: Gensel, P., Edwards, D. (Eds.), Plants Invade the Land: Evolutionary and Environmental Perspectives. Columbia University Press, New York, pp. 213–216.
Algeo, T.J., Ellwood, B.B., Nguyen, T.K.T., Rowe, H., Maynard, J.B., 2007. The Permian–Triassic boundary at Nhi Tao, Vietnam: evidence for recurrent influx of sulfidic watermasses to a shallow-marine carbonate platform. Palaeogeogr. Palaeoclimatol. Palaeoecol. 252, 304–327.
Algeo, T.J., Shen, Y., Zhang, T., Lyons, T.W., Bates, S.M., Rowe, H., Nguyen, T.K.T., 2008. Association of ^{34}S-depleted pyrite layers with negative carbonate $\delta^{13}C$ excursions at the Permian/Triassic boundary: evidence for upwelling of sulfidic deep-ocean watermasses. Geochem. Geophys. Geosyst. 9, 1–10.
Algeo, T.J., Chen, Z.Q., Fraiser, M.L., Twitchett, R.J., 2011a. Terrestrial–marine teleconnections in the collapse and rebuilding of Early Triassic marine ecosystems. Palaeogeogr. Palaeoclimatol. Palaeoecol. 308, 1–11.
Algeo, T.J., Kuwahara, K., Sano, H., Bates, S., Lyons, T., Elswick, E., Hinnov, L., Ellwood, B., Moser, J., Maynard, J.B., 2011b. Spatial variation in sediment fluxes, redox conditions, and productivity in the Permian–Triassic Panthalassic Ocean. Palaeogeogr. Palaeoclimatol. Palaeoecol. 308, 65–83.
Algeo, T.J., Henderson, C., Ellwood, B., Rowe, H., Elswick, E., Bates, S., Lyons, T., Hower, J.C., Smith, C., Maynard, J.B., Hays, L., Summons, R., Fulton, J., Freeman, K., 2012. Evidence for a diachronous Late Permian marine crisis from the Canadian Arctic region. Bull. Geol. Soc. Am. 124, 1424–1448.
Algeo, T.J., Henderson, C.M., Tong, J., Feng, Q., Yin, H., Tyson, R., 2013. Plankton and productivity during the Permian–Triassic boundary crisis: an analysis of organic carbon fluxes. Glob. Planet. Chang. 105, 52–67.
Alroy, J., Aberhan, M., Bottjer, D.J., Foote, M., Fürsich, F.T., Harries, P.J., Hendy, A.J.W., Holland, S.M., Ivany, L.C., Kiessling, W., Kosnik, M.A., Marshall, C.R., McGowan, A.J., Miller, A.I., Olszewski, T.D., Patzkowsky, M.E., Peters, S.E., Villier, L., Wagner, P.J., Bonuso, N., Borkow, P.S., Brenneis, B., Clapham, M.E., Fall, L.M., Ferguson, C.A., Hanson, V.L., Krug, A.Z., Layou, K.M., Leckey, E.H., Nürnberg, S., Powers, C.M., Sessa, J.A., Simpson, C., Tomašových, A., Visaggi, C.C., 2008. Phanerozoic trends in the global diversity of marine invertebrates. Science 321, 97–100.
Arenillas, I., Arz, J.A., Molina, E., Dupuis, C., 2000. The Cretaceous/Paleogene (K/P) boundary at Aïn Settara, Tunisia: sudden catastrophic mass extinction in planktic foraminifera. J. Foraminifer. Res. 30, 202–218.
Ausich, W.I., Deline, B., 2012. Macroevolutionary transition in crinoids following the Late Ordovician extinction event (Ordovician to Early Silurian). Palaeogeogr. Palaeoclimatol. Palaeoecol. 361–362, 38–48.
Azmy, K., Veizer, J., Bassett, M.G., Copper, P., 1998. Oxygen and carbon isotopic composition of Silurian brachiopods: implications for coeval seawater and glaciations. Geol. Soc. Am. Bull. 110, 1499–1512.
Azmy, K., Veizer, J., Wenzel, B., Bassett, M.G., Copper, P., 1999. Silurian strontium isotope stratigraphy. Bull. Geol. Soc. Am. 111, 475–483.
Baceta, J.I., Pujalte, V., Bernaola, G., 2005. Paleocene coralgal reefs of the western Pyrenean basin, northern Spain: new evidence supporting an earliest Paleogene recovery of reefal ecosystems. Palaeogeogr. Palaeoclimatol. Palaeoecol. 224, 117–143.
Baliński, A., 2002. Frasnian–Famennian brachiopod extinction and recovery in southern Poland. Acta Palaeontol. Pol. 47, 289–305.
Bambach, R.K., 1977. Species richness in marine benthic habitats through the Phanerozoic. Paleobiology 3, 152–167.
Bartolini, A., Guex, J., Spangenberg, J.E., Schoene, B., Taylor, D.G., Schaltegger, U., Atudorei, V., 2012. Disentangling the Hettangian carbon isotope record: implications for the aftermath of the end-Triassic mass extinction. Geochem. Geophys. Geosyst. 13. http://dx.doi.org/10.1029/2011GC003807 Q01007.
Baud, A., Richoz, S., Pruss, S., 2007. The lower Triassic anachronistic carbonate facies in space and time. Glob. Planet. Chang. 55, 81–89.
Baud, A., Nakrem, H.A., Beauchamp, B., Beatty, T., Embry, A.F., Henderson, C.M.B., 2008. Lower Triassic bryozoan beds from Ellesmere Island, High Arctic, Canada. Polar Res. 27, 428–440.
Beauchamp, B., Baud, A., 2002. Growth and demise of Permian biogenic chert along northwest Pangea: evidence for end-Permian collapse of thermohaline circulation. Palaeogeogr. Palaeoclimatol. Palaeoecol. 184, 37–63.
Benton, M.J., Twitchett, R.J., 2003. How to kill (almost) all life: the end-Permian extinction event. Trends Ecol. Evol. 18, 358–365.
Benton, M.J., Zhang, Q., Hu, S., Chen, Z.Q., Wen, W., Liu, J., Huang, J., Zhou, C., Xie, T., Tong, J., Choo, B., 2013. Exceptional vertebrate biotas from the Triassic of China, and the expansion of marine ecosystems after the Permo-Triassic mass extinction. Earth Sci. Rev. 125, 199–243.
Berner, R.A., 1994. Geocarb II: a revised model of atmospheric CO_2 over Phanerozoic time. Am. J. Sci. 294, 56–91.
Bhargava, O.N., Krystyn, L., Balini, M., Lein, R., Nicora, A., 2004. Revised litho- and sequence stratigraphy of the Spiti Triassic. Albertiana 30, 21–39.
Bigey, F.P., 1989. Devonian Bryozoan and global events: the Frasnian/Famennian extinction. In: McMillan, N.J., Embry, A.F., Glass, D.J. (Eds.), Devonian of the WorldPaleontology, Paleoecology, and Biostratigraphy III. Canadian Society of Petroleum Geologists Memoir, pp. 53–62 (14).
Birch, H.S., Coxall, H.K., Pearson, P.N., 2012. Evolutionary ecology of Early Paleocene planktonic foraminifera: size, depth habitat and symbiosis. Paleobiology 38, 374–390.
Black, B.A., Elkins-Tanton, L.T., Rowe, M.C., Peate, I.U., 2012. Magnitude and consequences of volatile release from the Siberian Traps. Earth Planet. Sci. Lett. 317–318, 363–373.
Blackburn, T.J., Olsen, P.E., Bowring, S.A., McLean, N.M., Kent, D.V., Puffer, J., McHone, G., Rasbury, E.T., Et-Touhami, M., 2013. Zircon U-Pb geochronology links the end-Triassic extinction with the Central Atlantic Magmatic Province. Science 340, 941–945.
Blätter, C.L., Jenkyns, H.C., Reynard, L.M., Henderson, G.M., 2011. Significant increases in global weathering during Oceanic Anoxic Events 1a amd 2 indicated by calcium isotopes. Earth Planet. Sci. Lett. 309, 77–88.
Bond, D.P.G., Wignall, P.B., 2010. Pyrite framboid study of marine Permo-Triassic boundary sections: a complex anoxic event and its relationship to contemporaneous mass extinction. Geol. Soc. Am. Bull. 122, 1265–1279.
Bottjer, D.J., Clapham, M.E., Fraiser, M.L., Powers, C.M., 2008. Understanding mechanisms for the end-Permian mass extinction and the protracted Early Triassic aftermath and recovery. GSA Today 18, 4–10.
Bown, P., 2005. Selective calcareous nannoplankton survivorship at the Cretaceous–Tertiary boundary. Geology 33, 653–656.
Brand, U., Azmy, K., Veizer, J., 2006. Evaluation of the Salinic I tectonic, Cancaniri glacial and Ireviken biotic events: biochemostratigraphy of the Lower Silurian succession in the Niagara Gorge area, Canada and U.S.A. Palaeogeogr. Palaeoclimatol. Palaeoecol. 241, 192–213.
Brayard, A., Bucher, H., Escarguel, G., Fluteau, F., Bourquin, S., Galfetti, T., 2006. The Early Triassic ammonoid recovery: paleoclimatic significance of diversity gradients. Palaeogeogr. Palaeoclimatol. Palaeoecol. 239, 374–395.
Brayard, A., Escarguel, G., Bucher, H., Monnet, C., Brühwiler, T., Goudemand, N., Galfetti, T., Guex, J., 2009. Good genes and good luck: ammonoid diversity and the end-Permian mass extinction. Science 325, 1118–1121.
Brayard, A., Vennin, E., Olivier, N., Bylund, K.G., Jenks, J., Stephen, D.A., Bucher, H., Hofman, R., Goudemand, N., Escarguel, G., 2011. Transient metazoan reefs in the aftermath of the end-Permian mass extinction. Nat. Geosci. 4, 693–697.
Brenchley, P.J., Harper, D.A.T., 1998. Palaeoecology: Ecosystems, Environments and Evolution. Thomson Science, Weinheim, Germany (402 pp.).
Brenchley, P.J., Carden, G.A.F., Marshall, J.D., 1995. Environmental changes associated with the "first strike" of the Late Ordovician mass extinction. Mod. Geol. 20, 69–82.
Brenchley, P.J., Marshall, J., Underwood, C.J., 2001. Do all mass extinctions represent an ecological crisis? Evidence from the Late Ordovician. Geol. J. 36, 329–340.
Brennecka, G.A., Herrmann, A.D., Algeo, T.J., Anbar, A.D., 2011. Rapid expansion of oceanic anoxia immediately before the end-Permian mass extinction. Proc. Natl. Acad. Sci. U. S. A. 108, 17631–17634.
Brinkhuis, H., Bujak, J.P., Smit, J., Versteegh, G.J.M., Visscher, H., 1998. Dinoflagellate-based sea surface temperature reconstructions across the Cretaceous–Tertiary boundary. Palaeogeogr. Palaeoclimatol. Palaeoecol. 141, 67–83.
Brühwiler, T., Ware, D., Bucher, H., Krystyn, L., Goudemand, N., 2010. New Early Triassic ammonoid faunas from the Dienerian/Smithian boundary beds at the Induan/

Olenekian GSSP candidate at Mud (Spiti, northern India). J. Asian Earth Sci. 39, 724–739.
Buggisch, W., Joachimski, M.M., 2006. Carbon isotope stratigraphy of the Devonian of Central and Southern Europe. Palaeogeogr. Palaeoclimatol. Palaeoecol. 240, 68–88.
Burgess, S.D., Bowring, S., Shen, S.Z., 2014. High-precision timeline for Earth's most severe extinction. http://dx.doi.org/10.1073/pnas.1317692111, (6 pp.).
Cai, J.X., Zhang, K.J., 2009. A new model for the Indochina and South China collision during the Late Permian to the Middle Triassic. Tectonophysics 467, 35–43.
Callaway, J.M., Brinkman, D.B., 1989. Ichthyosaurs (Reptilia, Ichthyosauria) from the Lower and Middle Triassic Sulphur Mountain Formation, Wapiti Lake area, British Columbia, Canada. Can. J. Earth Sci. 26, 1491–1500.
Calvert, S.E., Pedersen, T.F., 2007. Elemental proxies for palaeoclimatic and palaeoceanographic variability in marine sediments: Interpretation and application. In: Hillaire-Marcel, C., De Vernal, A. (Eds.), Proxies in Late Cenozoic PaleoceanographyDevelopments in Marine Geology 1. Elsevier, Amsterdam, pp. 567–644.
Campbell, I.H., Czamanske, G.K., Fedorenko, V.A., Hill, R.I., Stepanov, V., 1992. Synchronism of the Siberian traps and the Permian–Triassic boundary. Science 258, 1760–1763.
Cao, C., Love, G.D., Hays, L.E., Wang, W., Shen, S., Summons, R.E., 2009. Biogeochemical evidence for euxinic oceans and ecological disturbance presaging the end-Permian mass extinction event. Earth Planet. Sci. Lett. 281, 188–201.
Caputo, M.V., 1998. Ordovician–Silurian glaciations and global sea-level changes. In: Landing, E., Johnson, M.E. (Eds.), Silurian cycles: linkages of dynamic stratigraphy with atmospheric, oceanic and tectonic changes. New York State Museum Bulletin 491, pp. 15–25.
Casier, J.-G., Lethiers, F., 1998. The recovery of the ostracod fauna after the Late Devonian mass extinction: the Devils Gate Pass section example (Nevada, USA). Palaeontology 327, 501–507.
Chen, Z.Q., Benton, M.J., 2012. The timing and pattern of biotic recovery following the end-Permian mass extinction. Nat. Geosci. 5, 375–383.
Chen, Z.Q., McNamara, K.J., 2006. End-Permian extinction and subsequent recovery of Ophiuroidea (Echinodermata). Palaeogeography, Palaeoclimatology, Palaeoecology 236, 321–344.
Chen, D., Qing, H., Li, R., 2005a. The Late Devonian Frasnian–Famennian (F/F) biotic crisis: insights from $\delta^{13}C_{carb}$, $\delta^{13}C_{org}$ and $^{87}Sr/^{86}Sr$ isotopic systematics. Earth Planet. Sci. Lett. 235, 151–166.
Chen, Z.Q., Kaiho, K., George, A.D., 2005b. Early Triassic recovery of the brachiopod faunas from the end-Permian mass extinction: a global review. Palaeogeogr. Palaeoclimatol. Palaeoecol. 224, 270–290.
Chen, Z.Q., Tong, J., Fraiser, M.L., 2011. Trace fossils evidence for restoration of marine ecosystems following the end-Permian mass extinction in the Lower Yangtze region, South China. Palaeogeogr. Palaeoclimatol. Palaeoecol. 299, 449–474.
Chen, Y., Twitchett, R.J., Jiang, H., Richoz, S., Lai, X., Yan, C., Sun, Y., Liu, X., Wang, L., 2013. Size variation of conodonts during the Smithian–Spathian (Early Triassic) global warming event. Geology 41, 823–826.
Chenet, A.-L., Quidelleur, X., Fluteau, F., Courtillot, V., Bajpai, S., 2007. ^{40}K–^{40}Ar dating of the Main Deccan large igneous province: further evidence of KTB age and short duration. Earth Planet. Sci. Lett. 263, 1–15.
Clapham, M.E., Payne, J.L., 2011. Acidification, anoxia, and extinction: a multiple logistic regression analysis of extinction selectivity during the Middle and Late Permian. Geology 39, 1059–1062.
Clapham, M.E., Bottjer, D.J., Powers, C.M., Bonuso, N., Fraiser, M.L., Marenco, P.J., Dornbos, S.Q., Pruss, S.B., 2006. Assessing the ecological dominance of Phanerozoic marine invertebrates. Palaios 21, 431–441.
Clarkson, M.O., Richoz, S., Wood, R.A., Maurer, F., Krystyn, L., McGurty, D.J., Astratti, D., 2013. A new high-resolution $\delta^{13}C$ record for the Early Triassic: insights from the Arabian platform. Gondwana Res. 24, 233–242.
Clémence, M.E., Bartolini, A., Gardin, S., Paris, G., Beaumont, V., Page, K.N., 2010. Early Hettangian benthic–planktonic coupling at Doniford (SW England) palaeoenvironmental implications for the aftermath of the end-Triassic crisis. Palaeogeogr. Palaeoclimatol. Palaeoecol. 295, 102–115.
Coccioni, R., Luciani, V., 2006. *Guembelitria irregularies* bloom at the K–T boundary: morphological abnormalities induced by impact-related extreme environmental stress? In: Cockell, C., Koeberl, C., Gilmour, I. (Eds.), Biological Processes Associated With Impact Events. Springer, Berlin, pp. 179–196.
Copper, P., 1986. Frasnian–Famennian mass extinction and cold-water oceans. Geology 14, 835–839.
Copper, P., 2001. Reefs during the multiple crises towards the Ordovician–Silurian boundary: Anticostic Island, eastern Canada, and worldwide. Can. J. Earth Sci. 38, 153–171.
Copper, P., 2002. Reef development at the Frasnian/Famennian mass extinction boundary. Palaeogeogr. Palaeoclimatol. Palaeoecol. 181, 27–65.
Courtillot, V., Besse, J., Vandamme, D., Montigny, R., 1986. Deccan flood basalts at the Cretaceous/Tertiary boundary? Earth Planet. Sci. Lett. 80, 361–374.
Courtillot, V., Féraud, G., Maluski, H., Vandamme, D., Moreau, M.G., Besse, J., 1988. Deccan flood basalts and the Cretaceous/Tertiary boundary. Nature 333, 844–846.
Couto, H., Knight, J., Lourenço, A., 2013. Late Ordovician ice-marginal processes and sea-level change from the north Gondwana platform: Evidence from the Valongo Anticline (northern Portugal). Palaeogeography, Palaeoclimatology, Palaeoecology 375, 1–15.
Cox, C.B., Smith, D.G., 1973. A review of the Triassic vertebrate faunas of Svalbard. Geol. Mag. 110, 405–418.
Coxall, H.K., D'Hondt, S., Zachos, J.C., 2006. Pelagic evolution and environmental recovery after the Cretaceous–Paleogene mass extinction. Geology 34, 297–300.
Cramer, B.D., Brett, C.E., Melchin, M.A., Männik, P., Kleffner, M.A., McLaughlin, P.I., Loydell, D.K., Munnecke, A., Jeppson, L., Corradini, C., Brunton, F.R., Saltzman, M.R., 2011. Revised chronostratigraphic correlation of the Silurian System of North America with global and regional chronostratigraphic units and $\delta^{13}C_{carb}$ chemostratigraphy. Lethaia 44, 185–202.
Crasquin-Soleau, S.T., Galfetti, H., Bucher, H., Kershaw, S., Feng, Q., 2007. Ostracod recovery in the aftermath of the Permian–Triassic crisis: Palaeozoic–Mesozoic turnover. Hydrobiologia 585, 13–27.
D'Hondt, S., Zachos, J.C., 1993. On stable isotopic variation and earliest Palocene planktonic foraminifera. Paleoceanography 8, 527–547.
D'Hondt, S., Donaghay, P., Zachos, J.C., Luttenberg, D., Lindinger, M., 1998. Organic carbon fluxes and ecological recovery from the Cretaceous–Tertiary mass extinction. Science 282, 276–279.
Deene, M.H.L., Ruhl, M., Bonis, N.R., Krijgsman, W., Kuerschner, W.M., Reitsma, M., van Bergen, M.J., 2010. A new chronology for the end-Triassic mass extinction. Earth and Planetary Science Letters 291, 113–125.
De La Rocha, C.L., DePaolo, D.J., 2000. Isotopic evidence for variations in the marine calcium cycle over the Cenozoic. Science 289, 1176–1178.
Delabroye, A., Munnecke, A., Vecoli, M., Copper, P., Tribovillard, N., Joachimski, M.M., Desrochers, A., Servais, T., 2011. Phytoplankton dynamics across the Ordovician/Silurian boundary at low palaeolatitudes: correlations with carbon isotopic and glacial events. Palaeogeogr. Palaeoclimatol. Palaeoecol. 312, 79–97.
Devine, J.D., Sigurdsson, H., Havis, A.N., Self, S., 1984. Estimates of sulfur and chlorine yield to the atmosphere from volcanic eruptions and potential climatic effects. J. Geophys. Res. 89, 6309–6325.
Dix, G.R., James, J.P., 1987. Late Mississippian bryozoan/microbial build-ups on a drowned karst terrain, Port Au Port Peninsula, western Newfoundland. Sedimentology 34, 779–793.
Enos, P., Wei, J., Yan, Y., 1997. Facies distribution and retreat of Middle Triassic platform margin, Guizhou Province, south China. Sedimentology 44, 563–584.
Erwin, D.H., 1998. The end and the beginning: recoveries from mass extinctions. Trends Ecol. Evol. 13, 344–349.
Erwin, D.H., 2001. Lessons from the past: biotic recoveries from mass extinctions. Proc. Natl. Acad. Sci. U. S. A. 98, 5399–5403.
Erwin, D.H., 2005. Extinction: How Life on Earth Nearly Died 250 Millions Years Ago. Princeton University Press, Princeton, New Jersey, p. 306.
Erwin, D.H., 2007. Increasing returns, ecological feedback and the Early Triassic recovery. Palaeoworld 16, 9–15.
Erwin, D.H., 2008. Macroevolution of ecosystem engineering, niche construction and diversity. Trends Ecol. Evol. 23, 304–310.
Erwin, D.H., Pan, H., 1996. Recoveries and radiations: gastropods after the Permo-Triassic mass extinction. In: Hart, M.B. (Ed.), Biotic Recovery from Mass Extinction Events. Geological Society of London Special Publication 102, pp. 223–229.
Erwin, D.H., Bowring, S.A., Jin, Y.G., 2002. End-Permian mass-extinctions: a review. In: Koeberl, C., MacLeod, K.G. (Eds.), Catastrophic Events and Mass Extinctions: Impacts and Beyond. Geological Society of America Special Paper 356, pp. 353–383.
Fan, J., Chen, X., 2007. Preliminary report on the Late Ordovician graptolite extinction in the Yangtze region. Palaeogeogr. Palaeoclimatol. Palaeoecol. 245, 82–94.
Fantle, M.S., DePaolo, D.J., 2005. Variations in the marine Ca cycle over the past 20 million years. Earth Planet. Sci. Lett. 237, 102–117.
Fastovsky, D.E., Sheehan, P.M., 2005. The extinction of the dinosaurs in North America. GSA Today 15, 4–10.
Feng, Q., Algeo, T.J., 2014. Evolution of oceanic redox conditions during the Permo-Triassic: evidence from radiolarian deepwater facies. Earth Sci. Rev. 137, 34–51.
Finnegan, S., Bergmann, K., Eiler, J.M., Jones, D.S., Fike, D.A., Eisenman, I., Hughes, N.C., Tripati, A.K., Fischer, W.W., 2011. The magnitude and duration of Late Ordovician-Early Silurian glaciation. Science 331, 903–906.
Finnegan, S., Heim, N.A., Peters, S.E., Fischer, W.W., 2012. Climate change and the selective signature of the Late Ordovician mass extinction. Proc. Natl. Acad. Sci. U. S. A. 109, 6829–6834.
Finney, S.C., Berry, W.B.N., Cooper, J.D., Ripperdan, R.L., Sweet, W.C., Jacobson, S.R., Soufiane, A., Achab, A., Noble, P.J., 1999. Late Ordovician mass extinction: a new perspective from stratigraphic sections in central Nevada. Geology 27, 215–218.
Fischer, A.G., Bottjer, D.J., 1995. Oxygen-depleted waters: a lost biotope and its role in ammonite and bivalve evolution. Neues Jb. Geol. Paläontol. Abh. 195, 133–146.
Fraiser, M.L., 2011. Paleoecology of secondary tierers from Western Pangean tropical marine environments during the aftermath of the end-Permian mass extinction. Palaeogeogr. Palaeoclimatol. Palaeoecol. 308, 181–189.
Fraiser, M.L., Bottjer, D.J., 2004. The non-actualistic Early Triassic gastropod fauna: a case study of the Lower Triassic Sinbad Limestone member. Palaios 19, 259–275.
Fraiser, M.L., Twitchett, R.J., Bottjer, D.J., 2005. Unique microgastropod biofacies in the Early Triassic: indicator of long-term biotic stress and the pattern of biotic recovery after the end-Permian mass extinction. C. R. Palevol 4, 543–552.
Fuqua, L.M., Bralower, T.J., Arthur, M.A., Patzkowsky, M.E., 2008. Evolution of calcareous nannoplankton and the recovery of marine food webs after the Cretaceous–Paleocene mass extinction. Palaios 23, 185–194.
Galfetti, T., Hochuli, P.A., Brayard, A., Bucher, H., Weissert, H., Vigran, J.O., 2007a. Smithian–Spathian boundary event: evidence for global climatic change in the wake of the end-Permian biotic crisis. Geology 35, 291–294.
Galfetti, T., Bucher, H., Brayard, A., Hochuli, P.A., Weissert, H., Kuang, G., Atudorei, V., Guex, J., 2007b. Late Early Triassic climate change: insights from carbonate carbon isotopes, sedimentary evolution and ammonoid paleobiogeography. Palaeogeogr. Palaeoclimatol. Palaeoecol. 243, 394–411.
Gallala, N., Zaghbib-Turki, D., Arenillas, I., Arz, J.A., Molina, E., 2009. Catastrophic mass extinction and assemblage evolution in planktic foraminifera across the Cretaceous/Paleogene (K/Pg) boundary at Bidart (SW France). Marine Micropaleontology 72, 196–209.

Please cite this article as: Wei, H., et al., Environmental controls on marine ecosystem recovery following mass extinctions, with an example from the Early Triassic, Earth-Sci. Rev. (2014), http://dx.doi.org/10.1016/j.earscirev.2014.10.007

Ganino, C., Arndt, N.T., 2009. Climate changes caused by degassing of sediments during the emplacement of large igneous provinces. Geology 37, 323–326.

Garzanti, E., Angiolini, L., Sciunnach, D., 1996. The Mid-Carboniferous to lowermost Permian succession of Spiti (Po Group and Ganmachidam Formation, Tethys Himalaya, Northern India): Gondwana glaciation and rifting of Neo-Tethys. Geodin. Acta 9, 78–100.

Gibbs, M.T., Barron, E.J., Kump, L.R., 1997. An atmospheric pCO_2 threshold for glaciation in the Late Ordovician. Geology 25, 447–450.

Goto, M., 1994. Palaeozoic and early Mesozoic fish faunas of the Japanese islands. Island Arc 3, 247–254.

Gouldey, J.C., Saltzman, M.R., Young, S.A., Kaljo, D., 2010. Strontium and carbon isotope stratigraphy of the Llandovery (Early Silurian): implications for tectonics and weathering. Palaeogeogr. Palaeoclimatol. Palaeoecol. 296, 264–275.

Grasby, S.E., Beauchamp, B., Embry, A., Sanei, H., 2013. Recurrent Early Triassic ocean anoxia. Geology 41, 175–178.

Grice, K., Cao, C., Love, G.D., Bottcher, M.E., Twitchett, R.J., Grosjean, E., Summons, R.E., Turgeon, S.C., Dunning, W., Jin, Y., 2005. Photic zone euxinia during the Permian–Triassic superanoxic event. Science 307, 706–709.

Guex, J., Bartolini, A., Atudorei, V., Taylor, D., 2004. High-resolution ammonite and carbon isotope stratigraphy across the Triassic–Jurassic boundary at New York Canyon (Nevada). Earth Planet. Sci. Lett. 225, 29–41.

Guex, J., Schoene, B., Bartolini, A., Spangenberg, J., Schaltegger, U., O'Dogherty, L., Taylor, D., Bucher, H., Atudorei, V., 2012. Geochronological constraints on post-extinction recovery of the ammonoids and carbon cycle perturbations during the Early Jurassic. Palaeogeogr. Palaeoclimatol. Palaeoecol. 346–347, 1–11.

Guo, G., Tong, J., Zhang, S., Zhang, J., Bai, L., 2008. Cyclostratigraphy of the Induan (Early Triassic) in West Pingdingshan Section, Chaohu, Anhui Province. Sci. China Ser. D Earth Sci. 51, 22–29.

Hairstone, N.G., Ellner, S.P., Geber, M.A., Yoshida, T., Fox, J.A., 2008. Rapid evolution and the convergence of ecological and evolutionary time. Ecol. Lett. 8, 1114–1127.

Hallam, A., 1991. Why was there a delayed radiation after the end-Palaeozoic extinctions? Hist. Biol. 5, 257–262.

Hallam, A., 1996. Recovery of the marine fauna in Europe after the end-Triassic and early Toarcian mass extinction. In: Hart, M.B. (Ed.), Biotic Recovery from Mass Extinction Events. Geological Society Special Publication No 102, pp. 231–236.

Hallam, A., Wignall, P.B., 1999. Mass extinctions and sea-level changes. Earth Sci. Rev. 48, 217–250.

Haq, B.U., Schutter, S.R., 2008. A chronology of Paleozoic sea-level changes. Science 322, 64–68.

Haq, B.U., Hardenbol, J., Vail, P.R., 1987. Chronology of fluctuating sea level since the Triassic. Science 235, 1156–1167.

Harper, D.A.T., Rong, J., 2008. Completeness of the Hirnantian brachiopod record: spatial heterogeneity through the end Ordovician extinction event. Lethaia 41, 195–197.

Harries, P.J., Kauffman, E.J., 1990. Patterns of survival and recovery following Cenomanian–Turonian (Late Cretaceous) mass extinction in the western Interior Basin, United States. In: Kauffman, E.G., Walliser, O.H. (Eds.), Extinction Events in Earth History. Springer, Berlin, pp. 277–298.

Hautmann, M., Bucher, H., Brühwiler, T., Goudemand, N., Kaim, A., Nützel, A., 2011. An usually diverse mollusc fauna from the earliest Triassic of South China and its implications for benthic recovery after the end-Permian biotic crisis. Geobios 44, 71–85.

Hermann, E., Hochuli, P.A., Méhay, S., Bucher, H., Brühwiler, T., Ware, D., Hautmann, M., Roohi, G., ur-Rehman, K., Yaseen, A., 2011. Organic matter and palaeoenvironmental signals during the Early Triassic biotic recovery: the Salt Range and Surghar Range records. Sediment. Geol. 234, 19–41.

Hesselbo, S.P., Robinson, S.A., Surlyk, F., Piasecki, S., 2002. Terrestial and marine extinction at the Triassic–Jurassic boundary synchronized with major carbon-cycle perturbation: a link to initiation of massive volcanism? Geology 30, 251–254.

Hildebrand-Habel, T., Streng, M., 2003. Calcareous dinoflagellate associations and Maastrichtian–Tertiary climatic changes in a high latitude core (ODP Hole 689B, Maud Rise, Weddell Sea). Palaeogeogr. Palaeoclimatol. Palaeoecol. 197, 293–321.

Hilting, A.K., Kump, L.R., Bralower, T.J., 2008. Variations in the oceanic vertical carbon isotope gradient and their implications for the Paleocene–Eocene biological pump. Paleoceanography 23. http://dx.doi.org/10.1029/2007PA001458 PA3222.

Hinojosa, J.L., Brown, S.T., Chen, J., DePaolo, D.J., Paytan, A., Shen, S.Z., Payne, J.L., 2012. Evidence for end-Permian ocean acidification from calcium isotopes in biogenic apatite. Geology 40, 743–746.

Hofmann, R., Hautmann, M., Bucher, H., 2013. A new paleoecological look at the Dinwoody Formation (Lower Triassic, western US): intrinsic versus extrinsic controls on ecosystem recovery after the end-Permian mass extinction. J. Paleontol. 87, 854–880.

Hofmann, R., Hautmann, M., Brayard, A., Nützel, Bylund, K.G., Jenks, J.F., Vennin, E., Oliver, N., Bucher, H., 2014. Recovery of benthic marine communities from the end-Permian mass extinction at the low latitudes of eastern Panthalassa. Palaeontology 57, 547–589.

Hollis, C.J., Strong, C.P., Rodgers, K.A., Rogers, K.M., 2003. Paleoenvironmental changes across the Cretaceous/Tertiary boundary at Flaxbourne River and Woodside Creek, eastern Marlborough, New Zealand. N. Z. J. Geol. Geophys. 46, 177–197.

Horacek, M., Richoz, S., Brandner, R., Krystyn, L., Spötl, C., 2007. Evidence for recurrent changes in Lower Triassic oceanic circulation of the Tethys: the $\delta^{13}C$ record from marine sections in Iran. Palaeogeogr. Palaeoclimatol. Palaeoecol. 252, 355–369.

House, M.R., 2002. Strength, timing, setting and cause of mid-Paleozoic extinctions. Palaeogeogr. Palaeoclimatol. Palaeoecol. 181, 5–25.

Hu, S., Zhang, Q., Chen, Z., Zhou, C., Lü, T., Xie, T., Wen, W., Huang, J., Benton, M.J., 2011. The Luoping biota: exceptional preservation, and new evidence on the Triassic recovery from end-Permian mass extinction. Proc. R. Soc. B Biol. Sci. 278, 2274–2282.

Huang, B., Rong, J., Cocks, L.R.M., 2012. Global palaeobiogeographical patterns in brachiopods from survival to recovery after the end-Ordovician mass extinction. Palaeogeogr. Palaeoclimatol. Palaeoecol. 317–318, 196–205.

Hull, P.M., Norris, R.D., Bralower, T.J., Schueth, J.D., 2011. A role for chance in marine recovery from end-Cretaceous extinction. Nat. Geosci. 4, 856–860.

Ingall, E.D., van Cappellen, P., 1990. Relation between sedimentation rate and burial of organic phosphorus and organic carbon in marine sediments. Geochim. Cosmochim. Acta 54, 373–386.

Irmis, R.B., Whiteside, J.H., 2011. Delayed recovery of non-marine tetrapods after the end-Permian mass extinction tracks global carbon cycle. Proc. R. Soc. B Biol. Sci. http://dx.doi.org/10.1098/rspb.2011.1895 (9 pp.).

Isaacson, P.E., Díza-Martínez, E., Grader, G.W., Kalvoda, J., Babek, O., Devuyst, F.X., 2008. Late Devonian–earliest Mississippian glaciation in Gondwanaland and its biogeographic consequences. Palaeogeogr. Palaeoclimatol. Palaeoecol. 268, 126–142.

Isozaki, Y., 1997. Permo-Triassic boundary superanoxia and stratified superocean: Records from lost deep sea. Science 276, 235–238.

Jablonski, D., 1991. Extinctions: a paleontological perspective. Science 253, 754–757.

Jablonski, D., Chaloner, W.G., 1994. Extinctions in the fossil record. Philos. Trans. R. Soc. Lond. B Biol. Sci. 344, 11–16.

Jacobsen, N.D., Twitchett, R.J., Krystyn, L., 2011. Palaeoecological methods for assessing marine ecosystem recovery following the Late Permian mass extinction event. Palaeogeogr. Palaeoclimatol. Palaeoecol. 308, 200–212.

Jin, F., 2006. An overview of Triassic fishes from China. Vertebrata Palasiatica 44, 28–42.

Jin, Y.G., Wang, Y., Wang, W., Shang, Q.H., Cao, C.Q., Erwin, D.H., 2000. Pattern of marine mass extinction near the Permian–Triassic boundary in South China. Science 289, 432–436.

Joachimski, M.M., van Geldern, R., Breisig, S., Buggisch, W., Day, J., 2004. Oxygen isotope evolution of biogenic calcite and apatite during the Middle and Late Devonian. Int. J. Earth Sci. 93, 542–553.

Joachimski, M.M., Lai, X., Shen, S., Jiang, H., Luo, G., Chen, B., Chen, J., Sun, Y., 2012. Climate warming in the latest Permian and the Permian–Triassic mass extinction. Geology 40, 195–198.

Johnson, J.G., Klapper, G., Sandberg, C.A., 1985. Devonian eustatic fluctuations in Euramerica. Geological Society of America Bulletin 96, 567–587.

Johnson, M.E., Baarli, B.G., Nestor, H., Rubel, M., Worsley, D., 1991. Eustatic sea-level patterns from the Lower Silurian (Llandovery Series) of southern Norway Estonia. Geological Society of America Bulletin 103, 315–335.

Johnston, D.A., 1980. Volcanic contribution of chlorine to the stratosphere—more significant to ozone than previously estimated. Science 209, 491–493.

Jolley, D., Gilmour, I., Gurov, E., Kelley, S., Watson, J., 2010. Two large meteorite impacts at the Cretaceous–Paleogene boundary. Geology 38, 835–838.

Kaiser, S.I., Steuber, T., Becker, R.T., Joachimski, M.M., 2006. Geochemical evidence for major environmental change at the Devonian–Carboniferous boundary in the Carnic Alps and the Rhenish Massif. Palaeogeogr. Palaeoclimatol. Palaeoecol. 240, 146–160.

Kaiser, S.I., Steuber, T., Becker, R.T., 2008. Environmental change during the Late Famennian and Early Tournaisian (Late Devonian–Early Carboniferous): implications from stable isotopes and conodont biofacies in southern Europe. Geol. J. 43, 241–260.

Kakuwa, Y., 1996. Permian–Triassic mass extinction event recorded in bedded chert sequence in southwest Japan. Palaeogeogr. Palaeoclimatol. Palaeoecol. 121, 35–51.

Kakuwa, Y., 2008. Evaluation of palaeo-oxygenation of the ocean bottom across the Permian-Triassic boundary. Global and Planetary Change 63, 40–56.

Kaljo, D., 1996. Diachronous recovery patterns in Early Silurian corals, graptolites and acritarchs. In: Hart, M.B. (Ed.), Biotic Recovery from Mass Extinction Events. Geological Society of London Special Publication 102, pp. 127–133.

Kaljo, D., Martma, T., 2000. Carbon isotopic composition of Llandovery rocks (east Baltic Silurian) with environmental interpretation. Proceedings of the Estonian Academy of Sciences. 49, pp. 267–283.

Kamo, S.L., Czamanske, G.K., Amelin, Y., Fedorenko, V.A., Davis, D.W., Trofimov, V.R., 2003. Rapid eruption of Siberian flood-volcanic rocks and evidence for coincidence with the Permian–Triassic boundary and mass extinction at 251 Ma. Earth Planet. Sci. Lett. 214, 75–91.

Keller, G., 2003. Biotic effects of impacts and volcanism. Earth Planet. Sci. Lett. 215, 249–264.

Kershaw, S., Crasquin, S., Li, Y., Collin, P.Y., Forel, M.B., Mu, X., Baud, A., Wang, Y., Xie, S., Maurer, F., Guo, L., 2011. Microbialites and global environmental change across the Permian–Triassic boundary: a synthesis. Geobiology 10, 25–47.

Kershaw, S., Crasquin, S., Li, Y., Collin, P.-Y., Forel, M.-B., 2012. Ocean acidification and the end-Permian mass extinction: to what extent does evidence support hypothesis? Geosciences 2, 221–234. http://dx.doi.org/10.3390/geosciences2040221.

Kiessling, W., 2001. Paleoclimatic significance of Phanerozoic reefs. Geology 29, 751–754.

Kiessling, W., 2005. Long-term relationships between ecological stability and biodiversity in Phanerozoic reefs. Nature 433, 410–413.

Kiessling, W., Simpson, C., 2011. On the potential for ocean acidification to be a general cause of ancient reef crises. Glob. Chang. Biol. 17, 56–67.

Kirchner, J.W., Weil, A., 2000. Delayed biological recovery from extinctions throughout the fossil record. Nature 404, 177–180.

Knaust, D., 2007. Invertebrate trace fossils and ichnodiversity in shallow-marine carbonates of the German Middle Triassic (Muschelkalk). In: Bromley, R., Buatois, L.A., Mángano, M.G., Genise, J., Melchor, R. (Eds.), Sediment–Organism Interactions: A Multifaceted Ichnology. SEPM Special Publication 88, pp. 223–240.

Knoll, A.H., Bambach, R.K., Payne, J.L., Pruss, S., Fischer, W.W., 2007. Paleophysiology and end-Permian mass extinction. Earth Planet. Sci. Lett. 256, 295–313.

Korte, C., Hesselbo, S.P., Jenkyns, H.C., Rickaby, R.M., Spötl, C., 2009. Palaeoenvironmental significance of carbon- and oxygen-isotope stratigraphy of marine Triassic–Jurassic boundary sections in SW Britain. J. Geol. Soc. Lond. 166, 431–445.

Please cite this article as: Wei, H., et al., Environmental controls on marine ecosystem recovery following mass extinctions, with an example from the Early Triassic, Earth-Sci. Rev. (2014), http://dx.doi.org/10.1016/j.earscirev.2014.10.007

Korte, C., Pande, P., Kalia, P., Kozur, H.W., Joachimski, M.M., Oberhänsli, H., 2010. Massive volcanism at the Permian-Triassic boundary and its impact on the isotopic composition of the ocean and atmosphere. Journal of Asian Earth Sciences 37, 293–311.

Krug, A.Z., Patzkowsky, M.E., 2004. Rapid recovery from the Late Ordovician mass extinction. Proceedings of the National Academy of Sciences (U.S.A.) 101, 17605–17610.

Krystyn, L., Orchard, M., 1996. Lowermost Triassic ammonoids and conodont biostratigraphy of Spiti, India. Albertiana 17, 10–21.

Krystyn, L., Richoz, S., Baud, A., Twitchett, R.J., 2003. A unique Permian–Triassic boundary section from Oman. Palaeogeogr. Palaeoclimatol. Palaeoecol. 191, 329–344.

Krystyn, L., Bhargava, O.N., Richoz, S., 2007. A candidate GSSP for the base of the Olenekian Stage: Mud at Pin Valley, district Lahul & Spiti, Himachal Pradesh (Western Himalaya), India. Albertiana 35, 5–29.

Kump, L.R., Arthur, M.A., 1999. Interpreting carbon-isotope excursions: carbonates and organic matter. Chem. Geol. 161, 181–198.

Kuzmichev, A.B., Pease, V.L., 2007. Siberian trap magmatism on the New Siberian Islands: constraints for Arctic Mesozoic plate tectonic reconstructions. J. Geol. Soc. Lond. 164, 959–968.

Lehrmann, D.J., 1999. Early Triassic calcimicrobial mounds and biostromes of the Nanpanjiang basin, south China. Geology 27, 359–362.

Lehrmann, D.J., Ramezani, J., Bowring, S.A., Martin, M.W., Montgomery, P., Enos, P., Payne, J.L., Orchard, M.J., Wang, H., Wei, J., 2006. Timing of recovery from the end-Permian extinction: geochronologic and biostratigraphic constraints from south China. Geology 34, 1053–1056.

Lehrmann, D.J., Pei, D., Enos, P., Minzoni, M., Ellwood, B.B., Orchard, M.J., Zhang, J., Wei, J., Dillett, P., Koenig, J., Steffen, K., Druke, D., Druke, J., Kessel, B., Newkirk, T., 2007. Impact of differential tectonic subsidence on isolated carbonate-platform evolution: Triassic of the Nanpanjiang Basin, south China. Am. Assoc. Pet. Geol. Bull. 91, 287–320.

Li, J., 2001. Pattern and time of collision between the Sino-Korean and Yangtze Blocks: evolution of the Sinian–Jurassic sedimentary settings in the middle-lower reaches of the Yangtze River. Acta Geol. Sin. 75, 25–34 (in Chinese with English abstract).

Li, J., Liu, J., Li, C., Huang, Z., 2002. The horizon and age of the marine reptiles from Hubei Province, China. Vertebrata Palasiatica 40, 241–244.

Li, S., Tong, J., Liu, K., Wang, F., Huo, Y., 2007. The Lower Triassic cyclic deposition in Chaohu, Anhui Province, China. Palaeogeogr. Palaeoclimatol. Palaeoecol. 252, 188–199.

Li, H., Tong, J., Ren, J., Zhang, J., 2009. Early Triassic bivalve biostratigraphy and paleocommunities at Xiakou section in Xingshan, Hubei Province. Earth Science—Journal of China University of Geosciences 34, 733–742 (in Chinese with English abstract).

Liao, W.H., 2002. Biotic recovery from the Late Devonian F–F mass extinction event in China. Sci. China Ser. D Earth Sci. 45, 380–384.

Longridge, L.M., Carter, E.S., Smith, P.L., Tipper, H.W., 2007. Early Hettangian ammonites and radiolarians from the Queen Charlotte Islands, British Columbia and their bearing on the definition of the Triassic–Jurassic boundary. Palaeogeogr. Palaeoclimatol. Palaeoecol. 244, 142–169.

Looy, C.V., Brugman, W.A., Dilcher, D.L., Visscher, H., 1999. The delayed resurgence of equatorial forests after the Permian–Triassic ecological crisis. Proc. Natl. Acad. Sci. U. S. A. 96, 13857–13862.

Looy, C.V., Twitchett, R.J., Dilcher, D.L., van Konijnenburg-van Citter, J.H.A., Visscher, H., 2001. Life in the end-Permian dead zone. Proc. Natl. Acad. Sci. U. S. A. 98, 7879–7883.

Luo, G., Wang, Y., Algeo, T.J., Kump, L.R., Bai, X., Yang, H., Yao, L., Xie, S., 2011. Enhanced nitrogen fixation in the immediate aftermath of the latest Permian marine mass extinction. Geology 39, 647–650.

Luo, G.M., Algeo, T.J., Zhou, W.F., Wang, Y.B., Yang, H., Huang, J.H., Richoz, S., Xie, S.C., 2014. Vertical $\delta^{13}C_{org}$ gradients record changes in planktonic microbial community composition during the end-Permian mass extinction. Palaeogeogr. Palaeoclimatol. Palaeoecol. 396, 119–131.

Mander, L., Twitchett, R.J., 2008. Quality of the Triassic–Jurassic bivalve fossil record in northwest Europe. Palaeontology 51, 1213–1223.

Marshall, C.R., Ward, P.D., 1996. Sudden and gradual molluscan extinction in the latest Cretaceous of Western European Tethys. Science 274, 1360–1363.

Marzoli, A., Renne, P.R., Piccirillo, E.M., Ernesto, M., Bellieni, G., De Min, A., 1999. Extensive 200-million-year-old continental flood basalts of the central Atlantic magmatic province. Science 284, 616–618.

McElwain, J.C., Beerling, D.J., Woodward, F.I., 1999. Fossil plants and global warming at the Triassic–Jurassic boundary. Science 285, 1386–1390.

McGhee Jr., G.R., 1996. The Late Devonian Mass Extinction: The Frasnian/Famennian Crisis. Columbia University Press, New York (303 pp.).

McKinney, M., 1995. Extinction selectivity among lower taxa–gradational patterns and rarefaction error in extinction estimates. Paleobiology 21, 300–313.

McRoberts, C.A., Newton, C.R., 1995. Selective extinction among end-Triassic European bivalves. Geology 23, 102–104.

McRoberts, C.A., Furrer, H., Jones, D.S., 1997. Palaeoenvironmental interpretation of a Triassic–Jurassic boundary section from Western Austria based on palaeoecological and geochemical data. Palaeogeogr. Palaeoclimatol. Palaeoecol. 136, 79–95.

Metherell, R.G., Workman, L.E., 1969. Sedimentary features of the Crossfield Member. Bull. Can. Petrol. Geol. 17, 444–459.

Meyer, K.M., Yu, M., Jost, A.B., Kelley, B.M., Payne, J.L., 2011. $\delta^{13}C$ evidence that high primary productivity delayed recovery from end-Permian mass extinction. Earth Planet. Sci. Lett. 302, 378–384.

Morrow, J., Harries, P.J., Krivanek, J.G., 2011. Reef recovery following the Frasnian–Famennian (Late Devonian) mass extinction: evidence from the Dugway Range, west-central Utah. Palaios 26, 607–622.

Mundil, R., Ludwig, K.R., Metcalfe, I., Renne, P.R., 2004. Age and timing of the Permian mass extinctions: U/Pb dating of closed-system zircons. Science 305, 1760–1763.

Mutter, R.J., Neuman, A.G., 2006. An enigmatic chondrichthyan with Paleozoic affinities from the Lower Triassic of western Canada. Acta Palaeontol. Pol. 51, 271–282.

Norris, R.D., 1996. Symbiosis as an evolutionary innovation in the radiation of Paleocene planktic foraminifera. Paleobiology 22, 461–480.

Olsen, P.E., Kent, D.V., Sues, H.D., Koeberl, C., Huber, H., Montanari, A., Rainforth, E.C., Fowell, S.J., Szajna, M.J., Hartline, B.W., 2002. Ascent of dinosaurs linked to an iridium anomaly at the Triassic–Jurassic boundary. Science 296, 1305–1307.

Olsson, R.K., Hemleben, C., Berggren, W.A., Huber, B.T., 1999. Atlas of Paleocene Planktonic Foraminifera. Smithsonian Contributions to Paleobiology 85. Smithsonian Institution, Washington, D.C. (252 pp.).

Orchard, M.J., 2007. Conodont diversity and evolution through the latest Permian and Early Triassic upheavals. Palaeogeogr. Palaeoclimatol. Palaeoecol. 252, 93–117.

Ovtcharova, M., Bucher, H., Schaltegger, U., Galfetti, T., Brayard, A., Guex, J., 2006. New Early to Middle Triassic U–Pb ages from South China: calibration with ammonoid biochronozones and implications for the timing of the Triassic biotic recovery. Earth Planet. Sci. Lett. 243, 463–475.

Owen, A.W., Harper, D.A.T., Heath, R.A., 2008. A route to recovery: the early Silurian shallow-water shelly fauna in the northern Oslo basin. Lethaia 41, 173–184.

Payne, J.L., 2005. Evolutionary dynamics of gastropod size across the end-Permian extinction and through the Triassic recovery interval. Paleobiology 31, 269–290.

Payne, J.L., Lehrmann, D.J., Wei, J., Orchard, M.J., Schrag, D.P., Knoll, A.H., 2004. Large perturbations of the carbon cycle during recovery from the end-Permian extinction. Science 305, 506–509.

Payne, J.L., Lehrmann, D.J., Christensen, S., Wei, J., Knoll, A., 2006. Environmental and biological controls on the initiation and growth of a Middle Triassic (Anisian) reef complex on the Great Bank of Guizhou, Guizhou Province, China. Palaios 21, 325–343.

Payne, J.L., Turchyn, A.V., Paytan, A., DePaolo, D.J., Lehrmann, D.J., Yu, M., Wei, J., 2010. Calcium isotope constraints on the end-Permian mass extinction. Proc. Natl. Acad. Sci. U. S. A. 107, 8543–8548.

Payne, J.L., Summers, M., Rego, B.L., Altiner, D., Wei, J., Yu, M., Lehrmann, D.J., 2011. Early and Middle Triassic trends in diversity, evenness, and size of foraminifers on a carbonate platform in south China: implications for tempo and mode of biotic recovery from the end-Permian mass extinction. Paleobiology 37, 409–425.

Pedersen, T.F., Calvert, S.E., 1990. Anoxia vs. productivity: what controls the formation of organic-rich sediments and sedimentary rocks? Am. Assoc. Pet. Geol. Bull. 74, 454–466.

Pickett, J.W., Wu, W.S., 1990. The succession of Early Carboniferous coral faunas in eastern Australia and China. Alcheringa 14, 89–108.

Pörtner, H.O., 2001. Climate change and temperature-dependent biogeography: oxygen limitation of thermal tolerance in animals. Naturwissenschaften 88, 137–146.

Pospichal, J.J., 1994. Calcareous nannofossils at the K–T boundary, El Kef: no evidence for stepwise, gradual or sequential extinctions. Geology 22, 99–102.

Price, J.R., Velbel, M.A., 2003. Chemical weathering indices applied to weathering profiles developed on heterogeneous felsic metamorphic parent rocks. Chem. Geol. 202, 397–416.

Pruss, S.B., Bottjer, D.J., 2004. Early Triassic trace fossils of the Western United States and their implications for prolonged environmental stress from the end-Permian mass extinction. Palaios 19, 551–564.

Racki, G., Cordey, F., 2000. Radiolarian palaeoecology and radiolarites: is the present the key to the past? Earth-Science Reviews 52, 83–120.

Rampino, M.R., Adler, A.C., 1998. Evidence for abrupt latest Permian mass extinction of foraminifera: results of tests for the Signor-Lipps effect. Geology 26, 415–418.

Rasmussen, C.M.Ø., Harper, D.A.T., 2011a. Interrogation of distributional data for the end-Ordovician crisis interval: where did disaster strike? Geol. J. 46, 478–500.

Rasmussen, C.M.Ø., Harper, D.A.T., 2011b. Did the amalgamation of continents drive the end Ordovician mass extinction? Palaeogeogr. Palaeoclimatol. Palaeoecol. 311, 48–62.

Rego, B., Wang, S.C., Altiner, D., Payne, J.L., 2012. Within- and among-genus components of size evolution during mass extinction, recovery, and background intervals: a case study of Late Permian through Late Triassic foraminifera. Paleobiology 38, 627–643.

Reichow, M.K., Pringle, M.S., Al'Mukhamedov, A.I., Allen, M.B., Andreichev, V.L., Buslov, M.M., Davies, C.E., Fedoseev, G.S., Fitton, J.G., Inger, S., Medvedev, A.Ya., Mitchell, C., Puchkov, V.N., Safonova, I.Yu., Scott, R.A., Saunders, A.D., 2009. The timing and extent of the eruption of the Siberian Traps large igneous province: implications for the end-Permian environmental crisis. Earth Planet. Sci. Lett. 277, 9–20.

Renne, P.R., Zhang, Z., Richards, M.A., Black, M.T., Basu, A.R., 1995. Synchrony and causal relations between Permian–Triassic boundary crises and Siberian flood volcanism. Science 269, 1413–1416.

Renne, P.R., Deino, A.L., Hilgen, F.J., Kuiper, K.F., Mark, D.F., Mitchell III, W.S., Morgan, L.E., Mundil, R., Smit, J., 2013. Time scales of critical events around the Cretaceous–Paleogene boundary. Science 339, 684–687.

Retallack, G.J., Sheldon, N.D., Carr, P.F., Fanning, M., Thompson, C.A., Williams, M.L., Jones, B.G., Hutton, A., 2011. Multiple Early Triassic greenhouse crises impeded recovery from Late Permian mass extinction. Palaeogeogr. Palaeoclimatol. Palaeoecol. 308, 233–251.

Richoz, S., Krystyn, L., Baud, A., Brandner, R., Horacek, M., Mohtat-Aghai, P., 2010. Permian–Triassic boundary interval in Middle East (Iran and N. Oman): progressive environmental change from detailed carbonate carbon isotope marine curve and sedimentary evolution. J. Asian Earth Sci. 39, 236–253.

Richoz, S., van de Schootbrugge, B., Pross, J., Püttmann, W., Quan, T.M., Lindström, S., Heunisch, C., Fiebig, J., Maquil, R., Schouten, S., Hauzenberger, C.A., Wignall, P.B., 2012. Hydrogen sulphide poisoning of shallow seas following the end-Triassic extinction. Nat. Geosci. 5, 662–667.

Please cite this article as: Wei, H., et al., Environmental controls on marine ecosystem recovery following mass extinctions, with an example from the Early Triassic, Earth-Sci. Rev. (2014), http://dx.doi.org/10.1016/j.earscirev.2014.10.007

Romano, C., Brinkmann, W., 2010. A new specimen of the hybodont shark *Palaeobates polaris* with three-dimensionally preserved Meckel's cartilage from the Smithian (Early Triassic) of Spitsbergen. J. Vertebr. Paleontol. 30, 1673–1683.

Romano, C., Goudeman, N., Vennemann, T.W., Ware, D., Schneebeli-Hermann, E., Hochuli, P.A., Brühwiler, T., Brinkmann, W., Bucher, H., 2013. Climatic and biotic upheavals following the end-Permian mass extinction. Nat. Geosci. 6, 57–60.

Rong, J.Y., Harper, D.A., 1999. Brachiopod survival and recovery from the latest Ordovician mass extinctions in South China. Geological Journal 34, 321–348.

Ruhl, M., Kürschner, W.M., 2011. Multiple phases of carbon cycle disburbance from large igneous province formation at the Triassic–Jurassic transition. Geology 39, 431–434.

Ruhl, M., Deenen, M.H.L., Abels, H.A., Bonis, N.R., Krijgsman, W., Kürschner, W.M., 2010. Astronomical constraints on the duration of the early Jurassic Hettangian stage and recovery rates following the end-Triassic mass extinction (St Audrie's Bay/East Quantoxhead, UK). Earth Planet. Sci. Lett. 295, 262–276.

Ruhl, M., Bonis, N.R., Reichart, G.-J., Sinninghe Damsté, J.S., Kürschner, W.M., 2011. Atmospheric carbon injection linked to end-Triassic mass extinction. Science 333, 430–434.

Sageman, B.B., Rich, J., Arthur, M.A., Birchfield, G.E., Dean, W.E., 1997. Evidence for Milankovitch periodicities in Cenomanian–Turonian lithologic and geochemical cycles: Western Interior, U.S. J. Sediment. Res. 67, 286–301.

Sano, H., Kuwahara, K., Yao, A., Agematsu, S., 2010. Panthalassan seamount-associated Permian–Triassic boundary siliceous rocks, Mino Terrane, Central Japan. Paleontol. Res. 14, 293–314.

Scheaffer, B., Mangus, M., Laudon, L.R., 1976. An early Triassic fish assemblage from British Columbia. Bull. Am. Mus. Nat. Hist. 156, 517–563.

Schoene, B., Guex, J., Bartolini, A., Schaltegger, U., Blackburn, T.J., 2010. Correlating the end-Triassic mass extinction and flood basalt volcanism at the 100 ka level. Geology 38, 387–390.

Schoepfer, S.D., Shen, J., Wei, H., Tyson, R.V., Ingall, E., Algeo, T.J., 2014. TOC, organic P, and biogenic Ba accumulation rates as proxies for marine primary productivity and export flux. Earth Sci. Rev. in press (this volume).

Sephton, M.A., Looy, C.V., Brinkhuis, H., Wignall, P.B., de Leeuw, J.W., Visscher, H., 2005. Catastrophic soil erosion during the end-Permian biotic crisis. Geology 33, 941–944.

Sepkoski Jr., J.J., 1984. A kinetic model of Phanerozoic taxonomic diversity. III. Post Paleozoic families and mass extinctions. Paleobiology 10, 246–267.

Sepkoski Jr., J.J., 1986. Phanerozoic overview of mass extinction. In: Raup, D.M., Jablonski, D. (Eds.), Patterns and Processes in the History of Life. Springer-Verlag, Berlin, pp. 277–295.

Sepkoski Jr., J.J., 1994. Extinction and the fossil record. Geotimes 39, 15–17.

Sepkoski Jr., J.J., 1996. Patterns of Phanerozoic extinction: a perspective from global data bases. In: Walliser, O.H. (Ed.), Global Events and Event Stratigraphy in the Phanerozoic. Springer-Verlag, Berlin, pp. 35–51.

Sepkoski Jr., J.J., 1998. Rates of speciation in the fossil record. Philos. Trans. R. Soc. B Biol. Sci. 353, 315–326.

Sepúlveda, J., Wendler, J.E., Summons, R.E., Hinrichs, K., 2009. Rapid resurgence of marine productivity after the Cretaceous–Paleogene mass extinction. Science 326, 129–132.

Sessa, J.A., Bralower, T.J., Patzkowsky, M.E., Handley, J.C., Ivany, L.C., 2012. Environmental and biological controls on the diversity and ecology of Late Cretaceous through early Paleogene marine ecosystems in the U.S. Gulf Coastal Plain. Paleobiology 38, 218–239.

Seuß, B., Höfling, R., Nützel, A., 2005. Triassic/Jurassic carbonates from the Hochfelln Mountain (northern calcareous Alps)—its facies, silicified fauna and implications for the end-Triassic biotic crisis. Facies 51, 405–418.

Sheehan, P.M., 2001. The Late Ordovician mass extinction. Annu. Rev. Earth Planet. Sci. 29, 331–364.

Sheehan, P.M., Coorough, P.J., 1990. Brachiopod zoogeography across the Ordovician–Silurian extinction event. In: McKerrow, W.S., Scotese, C.R. (Eds.), Palaeozoic Palaeogeography and Biogeography. Geological Society of London Memoir 12, pp. 181–187.

Sheehan, P.M., Harris, M.T., 2004. Microbialite resurgence after the Late Ordovician extinction. Nature 430, 75–78.

Shen, J.W., Webb, G.E., 2004. Famennian (Upper Devonian) calcimicrobial (*Renalcis*) reef at Miaomen, Guilin, Guangxi, South China. Palaeogeogr. Palaeoclimatol. Palaeoecol. 204, 373–394.

Shen, S.Z., Crowley, J.L., Wang, Y., Bowring, S.A., Erwin, D.H., Sadler, P.M., Cao, C., Rothman, D.H., Henderson, C.M., Ramezani, J., Zhang, H., Shen, Y., Wang, X., Wang, W., Mu, L., Li, W., Tang, Y., Liu, X., Liu, L., Zeng, Y., Jiang, Y., Jin, Y., 2011a. Calibrating the end-Permian mass extinction. Science 334, 1367–1372.

Shen, Y., Farquhar, J., Zhang, H., Masterson, A., Zhang, T., Wing, B., 2011b. Multiple S-isotopic evidence for episodic shoaling of anoxic water during Late Permian mass extinction. Nat. Commun. 2. http://dx.doi.org/10.1038/ncomms1217 (no. 210).

Shen, J., Algeo, T.J., Hu, Q., Xu, G., Zhou, L., Feng, Q., 2013. Volcanism in South China during the Late Permian and its relationship to marine ecosystem and environmental changes. Glob. Planet. Chang. 105, 121–134.

Sigurdsson, H., D'Hondt, S., Carey, S., 1992. The impact of the Cretaceous/Tertiary bolide on evaporite terrane and generation of major sulfuric acid aerosol. Earth Planet. Sci. Lett. 109, 543–559.

Skulan, J., DePaolo, D.J., Owens, T.L., 1997. Biological control of calcium isotopic abundances in the global calcium cycle. Geochim. Cosmochim. Acta 61, 2505–2510.

Sobolev, S.V., Sobolev, A.V., Kuzmin, D.V., Krivolutskaya, N.A., Petrunin, A.G., Arndt, N.T., Radko, V.A., Vasiliev, Y.R., 2011. Linking mantle plumes, large igneous provinces and environmental catastrophes. Nature 477, 312–319.

Sokiran, E.V., 2002. Frasnian–Famennian extinction and recovery of rhychonellid brachiopods from the East European Platform. Acta Palaeontol. Pol. 47, 339–354.

Solé, R.V., Montoya, J.M., Erwin, D.H., 2002. Recovery from mass extinction: evolutionary assembly in large-scale biosphere dynamics. Philos. Trans. R. Soc. B Biol. Sci. 357, 697–707.

Song, H.J., Wignall, P.B., Chen, Z.-Q., Tong, J., Bond, D.P.G., Lai, X., Zhao, X., Jiang, H., Yan, C., Niu, Z., Chen, J., Yang, H., Wang, Y., 2011. Recovery tempo and pattern of marine ecosystems after the end-Permian mass extinction. Geology 39, 739–742.

Song, H.J., Wignall, P.B., Tong, J., Bond, D.P.G., Song, H., Lai, X., Zhang, K., Wang, H., Chen, Y., 2012. Geochemical evidence from bio-apatite for multiple oceanic anoxic events during Permian–Triassic transition and the link end-Permian extinction and recovery. Earth Planet. Sci. Lett. 353–354, 12–21.

Song, H.J., Wignall, P.B., Tong, J.N., Yin, H.F., 2013a. Two pulses of extinction during the Permian–Triassic crisis. Nat. Geosci. 6, 52–56.

Song, H.Y., Tong, J., Algeo, T.J., Horacek, M., Qiu, H., Song, H.J., Tian, L., Chen, Z., 2013b. Large vertical $\delta^{13}C_{DIC}$ gradients in Early Triassic seas of the South China craton: implications for oceanographic changes related to Siberian Traps volcanism. Glob. Planet. Chang. 105, 7–20.

Song, H.Y., Tong, J., Algeo, T.J., Song, H.J., Qiu, H., Zhu, Y., Tian, L., Bates, S., Lyons, T.W., Luo, G., Kump, L.R., 2014. Early Triassic seawater sulfate drawdown. Geochim. Cosmochim. Acta 128, 95–113.

Stampfli, G., Marcoux, J., Baud, A., 1991. Tethyan margins in space and time. Palaeogeogr. Palaeoclimatol. Palaeoecol. 87, 373–409.

Stanley, S.M., 2009. Evidence from ammonoids and conodonts for multiple Triassic mass extinctions. Proc. Natl. Acad. Sci. U. S. A. 106, 15264–15267.

Stearn, C.W., 1987. Effect of the Frasnian–Famennian extinction event on the stromatoporoids. Geology 15, 677–679.

Stemmerik, L., Bendix-Almgreen, S.E., Piasecki, S., 2001. The Permian–Triassic boundary in central East Greenland: past and present views. Bull. Geol. Soc. Den. 48, 159–167.

Sun, Y.D., Joachimski, M.M., Wignall, P.B., Yan, C.B., Chen, Y.L., Jiang, H.S., Wang, L.N., Lai, X.L., 2012. Lethally hot temperatures during the early Triassic greenhouse. Science 388, 366–370.

Sutcliffe, O.E., Dowdeswell, J.A., Whitington, R.J., Theron, J.N., Craig, J., 2006. Calibrating the Late Ordovician glaciation and mass extinction by the eccentricity cycles of Earth's orbit. Geology 28, 967–970.

Takemura, A., Sakai, M., Sakamoto, S., Aono, R., Takemura, S., Yamakita, S., 2007. Earliest Triassic radiolarians from the ARH and ARF sections on Arrow Rocks, Waipapa Terrane, Northland, New Zealand. In: Sporli, K.B., Takemura, A., Hori, R.S. (Eds.), The Oceanic Permian/Triassic Boundary Sequence at Arrow Rocks (Oruatemanu) Northland, New Zealand 24. GNS Science Monograph, Lower Hutt, New Zealand, pp. 97–107.

Tang, J., Kohler, S.J., Dietzel, M., 2008. Sr^{2+}/Ca^{2+} and $^{44}Ca/^{40}Ca$ fractionation during inorganic calcite formation: II. Ca isotopes. Geochim. Cosmochim. Acta 72, 3733–3745.

Timmreck, C., Graf, H.F., Lorenz, S.J., Niemeier, U., Zanchettin, D., Matei, D., Jungdaus, J.H., Crowley, T.J., 2010. Aerosol size confines climate response to volcanic supereruptions. Geophys. Res. Lett. 37. http://dx.doi.org/10.1029/2010GL045464 L24705.

Tomašových, A., Siblík, M., 2007. Evaluating compositional turnover of brachiopod communities during the end-Triassic mass extinction (Northern Calcareous Alps): removal of dominant groups, recovery and community reassembly. Palaeogeogr. Palaeoclimatol. Palaeoecol. 244, 170–200.

Tong, J., 1997. The ecosystem recovery after the end-Paleozoic mass extinction in South China. Earth Sci. J. China Univ. Geosci. 22, 373–376 (in Chinese with English abstract).

Tong, J., Yin, H., 2002. The Lower Triassic of South China. J. Asian Earth Sci. 20, 803–815.

Tong, J., Yin, H., Zhang, J., Zhao, L., 2001. Proposed new Lower Triassic stages in South China. Sci. China Ser. D Earth Sci. 44, 961–967.

Tong, J., Zakharov, Y.D., Orchard, M.J., Yin, H., Hansen, H.J., 2003. A candidate of the Induan–Olenekian boundary stratotype in the Tethyan region. Sci. China Ser. D Earth Sci. 46, 1182–1200.

Tong, J., Zhao, X., Erwin, D.H., Zuo, J., Zhao, L., 2006. Fossil fishes from the Lower Triassic of Majiashan, Chaohu, Anhui Province, China. J. Paleontol. 80, 146–161.

Tong, J., Zuo, J., Chen, Z.Q., 2007a. Early Triassic carbon isotope excursions from South China: Proxies for devastation and restoration of marine ecosystems following the end-Permian mass extinction. Geol. J. 42, 371–389.

Tong, J., Zhang, S., Zuo, J., Xiong, X., 2007b. Events during Early Triassic recovery from the end-Permian extinction. Glob. Planet. Chang. 55, 66–80.

Tribovillard, N., Algeo, T.J., Lyons, T., Riboulleau, A., 2006. Trace metals as paleoredox and paleoproductivity proxies: an update. Chem. Geol. 232, 12–32.

Twitchett, R.J., 1999. Palaeoenvironments and faunal recovery after the end-Permian mass extinction. Palaeogeogr. Palaeoclimatol. Palaeoecol. 154, 27–37.

Twitchett, R.J., 2007. The Lilliput effect in the aftermath of the end-Permian extinction event. Palaeogeogr. Palaeoclimatol. Palaeoecol. 252, 132–144.

Twitchett, R.J., Barras, C.G., 2004. Trace fossils in the aftermath of mass extinction events. In: McIlroy, D. (Ed.), Application of Ichnology to Palaeoenvironmental and Stratigraphic Analysis. Geological Society of London Special Publication 228, pp. 395–415.

Twitchett, R.J., Wignall, P.B., 1996. Trace fossils and the aftermath of the Permo-Triassic mass extinction: evidence from northern Italy. Palaeogeogr. Palaeoclimatol. Palaeoecol. 124, 137–151.

Twitchett, R.J., Krystyn, L., Baud, A., Wheeley, J.R., Richoz, S., 2004. Rapid marine recovery after the end-Permian extinction event. Geology 32, 805–808.

van de Schootbrugge, B., Tremolada, F., Bailey, T.R., Rosenthal, Y., Feist-Burkhardt, S., Brinkhuis, H., Pross, J., Kent, D.V., Falkowski, P.G., 2007. End-Triassic calcification crisis and blooms of organic-walled disaster species. Palaeogeogr. Palaeoclimatol. Palaeoecol. 244, 126–141.

van de Schootbrugge, B., Quan, T.M., Lindström, S., Püttmann, W., Heunisch, C., Pross, J., Fiebig, J., Petschick, R., Röhling, H.-G., Richoz, S., Rosenthal, Y., Falkowski, P.G., 2009. Floral changes across the Triassic/Jurassic boundary linked to flood basalt volcanism. Nat. Geosci. 2, 589–594.

Please cite this article as: Wei, H., et al., Environmental controls on marine ecosystem recovery following mass extinctions, with an example from the Early Triassic, Earth-Sci. Rev. (2014), http://dx.doi.org/10.1016/j.earscirev.2014.10.007

van de Schootbrugge, B., Bachan, A., Suan, G., Richoz, S., Payne, J.L., 2013. Microbes, mud and methane: cause and consequence of recurrent Early Jurassic anoxia following the end-Triassic mass extinction. Palaeontology 54, 685–709.
Wahlmann, G.P., 2002. Upper Carboniferous–Lower Permian (Bashkirian–Kungurian) mounds and reefs. In: Kiessling, W., Flügel, E., Golonka, J. (Eds.), Phanerozoic Reef Patterns. SEPM (Society of Sedimentary Geology) Special Publication 72, pp. 271–338.
Walliser, O.H., 1996. Global events in the Devonian and Carboniferous. In: Walliser, O.H. (Ed.), Global Events and Event Stratigraphy in the Phanerozoic. Springer-Verlag, Berlin, pp. 225–250.
Wang, N., Yang, S., Jin, F., Wang, W., 2001. Early Triassic Hybodontoidea from Tiandong of Guangxi, China—first report on the fish sequence study near the Permian–Triassic boundary in South China. Vertebrata Palasiatica 39, 237–250.
Wang, Y.B., Tong, J.N., Wang, J.S., Zhou, X., 2005. Calcimicrobialite after end-Permian mass extinction in South China and its paleoenvironmental significance. Chin. Sci. Bull. 50, 665–671.
Ward, P.D., Montgomery, D.R., Smith, R., 2000. Altered river morphology in South Africa related to the Permian–Triassic extinction. Science 289, 1740–1743.
Webb, G.E., 1998. Earliest known Carboniferous shallow-water reefs, Gudman Formation (Tn1b), Queensland, Australia: implications for Late Devonian reef collapse and recovery. Geology 26, 951–954.
Webb, G.E., 1999. Youngest Early Carboniferous (Late Visean) shallow-water patch reefs in eastern Australia (Rockhampton Group, Queensland): combining quantitative micro- and macro-scale data. Facies 41, 111–140.
White, R.V., Saunders, A.D., 2005. Volcanism, impact and mass extinctions: incredible or credible coincidences? Lithos 79, 299–316.
Wignall, P.B., 2001. Large igneous provinces and mass extinctions. Earth Sci. Rev. 53, 1–33.
Wignall, P.B., Twitchett, R.J., 1996. Oceanic anoxia and the end Permian mass extinction. Science 272, 1155–1158.
Wignall, P.B., Bond, D.P.G., Kuwahara, K., Kakuwa, Y., Newton, R.J., Poulton, S.W., 2010. An 80 million year oceanic redox history from Permian to Jurassic pelagic sediments of the Mino-Tamba terrane, SW Japan, and the origin of four mass extinctions. Global and Planetary Change 71, 109–123.
Williford, K.H., Ward, P.D., Garrison, G.H., Buick, R., 2007. An extended organic carbon-isotope record across the Triassic–Jurassic boundary in the Queen Charlotte Islands, British Columbia, Canada. Palaeogeogr. Palaeoclimatol. Palaeoecol. 244, 290–296.
Wood, R., 2004. Palaeoecology of a post-extinction reef: Famennian (Late Devonian) of the Canning Basin, north-western Australia. Palaeontology 47, 415–445.
Wu, H., Zhang, S., Feng, Q., Jiang, G., Li, H., Yang, T., 2012. Milankovitch and sub-Milankovitch cycles of the early Triassic Daye Formation, South China and their geochronological and paleoclimatic implications. Gondwana Res. 22, 748–759.
Xie, S., Pancost, R.D., Yin, H., Wang, H., Evershed, R., 2005. Two episodes of microbial change coupled with Permo/Triassic faunal mass extinction. Nature 434, 494–497.
Xie, S., Pancost, R.D., Huang, J., Wignall, P.B., Yu, J., Tang, X., Chen, L., Huang, X., Lai, X., 2007. Changes in the global carbon cycle occurred as two episodes during the Permian–Triassic crisis. Geology 35, 1083–1086.
Xie, S., Pancost, R.D., Wang, Y., Yang, H., Wignall, P.B., Luo, G., Jia, C., Chen, L., 2010. Cyanobacterial blooms tied to volcanism during the 5 m.y. Permo-Triassic biotic crisis. Geology 38, 447–450.
Yamamoto, S., Hasegawa, T., Tada, R., Goto, K., Rojas-Consuegra, R., Díaz-Otero, C., García-Delgado, D.E., Yamamoto, S., Sakuma, H., Matsui, T., 2010. Environmental and vegetational changes recorded in sedimentary leaf wax *n*-alkanes across the Cretaceous–Paleogene boundary at Loma Capiro, Central Cuba. Palaeogeogr. Palaeoclimatol. Palaeoecol. 295, 31–41.
Yang, S., Wang, X., Hao, W., 1986. New knowledge on the Lower Triassic of Zuodeng, Tiandong County, Guangxi. Acta Sci. Nat. Univ. Pekin. 4, 105–117.
Yin, H.F., Xie, S.C., Luo, G.M., Algeo, T.J., Zhang, K.X., 2012. Two episodes of environmental change at the Permian–Triassic boundary of the GSSP section Meishan. Earth Sci. Rev. 115, 163–172.
Young, G.M., Nesbitt, H.W., 1998. Processes controlling the distribution of Ti and Al in weathering profiles, siliciclastic sediments and sedimentary rocks. J. Sediment. Res. 68, 448–455.
Zakharov, Y.D., Abnavi, N.M., 2013. The ammonoid recovery after the end-Permian mass extinction: Evidence from the Iran-Transcaucasia Area, Siberia, Primorye, and Kazakhstan. Acta Palaeontologica Polonica 58, 127–147.
Zhang, Q., Zhou, C., Lu, T., Lou, X., Liu, W., Sun, Y., Huang, J., Zhao, L., 2009. A conodont-based Middle Triassic age assignment for the Luoping Biota of Yunnan, China. Sci. China Ser. D Earth Sci. 52, 1673–1678.
Zhang, Q., Zhou, C., Lü, T., Bai, J., 2010. Discovery of Middle Triassic Saurichthys in the Luoping area, Yunnan, China. Geol. Bull. China 29, 26–30.
Zhang, L., Zhao, L., Chen, Z.Q., Algeo, T.J., Chen, J., Wang, R., Chen, L., Hou, J., Yang, L., Qiu, H., Feng, X., Wang, X., 2014. Amelioration of marine environments at the Smithian–Spathian boundary, as recorded in the Shitouzhai section, Guizhou Province, South China. Biogeosci. Discuss. 11, 1–38.
Zhao, L., Lu, L., 2007. A new genus of Early Triassic perleidid fish from Changxing, Zhejiang, China. Acta Palaeontol. Sin. 46, 238–243.
Zhao, L., Xiong, X., Yang, F., Wang, Z., He, W., 2005. Conodonts from the Lower Triassic in the Nantuowan Section of Daxiakou, Xingshan County, Hubei Province. Albertiana 33, 113–114.
Zhao, L., Orchard, M.J., Tong, J., Sun, Z., Zuo, J., Zhang, S., Yun, A., 2007. Lower Triassic conodont sequence in Chaohu, Anhui Province, China and its global correlation. Palaeogeogr. Palaeoclimatol. Palaeoecol. 252, 24–38.
Zhao, L., Wang, L., Li, C., 2008. Studies of the Triassic marine reptiles of China: a review. Acta Palaeontol. Sin. 47, 232–239.
Zonneveld, J., Gingras, M.K., Beatty, T.W., 2010. Diverse ichnofossil assemblages following the P–Tr mass extinction, Lower Triassic, Alberta and British Columbia, Canada: evidence for shallow marine refugia on the northwestern coastal of Pangaea. Palaios 25, 368–392.

Please cite this article as: Wei, H., et al., Environmental controls on marine ecosystem recovery following mass extinctions, with an example from the Early Triassic, Earth-Sci. Rev. (2014), http://dx.doi.org/10.1016/j.earscirev.2014.10.007